Developing a Grassland Biomass Monitoring Tool Using a Time Series of Dual Polarimetric SAR and Optical Data

A Thesis Submitted to the College of Graduate Studies and Research in Partial Fulfillment of the Requirements for the Degree of Master of Science in the Department of Geography and Planning, University of Saskatchewan, Saskatoon.

By Carmen Finnigan

PERMISSION TO USE

This thesis is in partial fulfillment of the requirements for a Postgraduate degree from the University of Saskatchewan; I agree that the Libraries of this University may make it freely available for inspection. I further agree that permission for copying of this thesis in any manner, in whole or in part, for scholarly purposes may be granted by the professor who supervised my thesis work or, in their absence, by the Head of the Department or the Dean of the College of Geography and Planning where my thesis work was done. It is understood that any copying or publication or use of this thesis or parts thereof for financial gain shall not be allowed without my written permission. It is also understood that due recognition shall be given to me and to the University of Saskatchewan in any scholarly use which may be made of any material in my thesis.

Department Head
Department of Geography and Planning
University of Saskatchewan
9 Campus Drive
Saskatoon, Saskatchewan
S7N 5A5, Canada

Abstract

Grasslands are the most important ecosystem to humanity, as they are responsible for feeding that majority of the human population. These are also very large ecosystems; they cover approximately 40% of the surface of the earth (Loveland et al., 1998), making ground-based surveys for monitoring grassland health and productivity extremely time consuming. Remote sensing has the advantage of providing reliable and repeatable observations over large swaths of land; however, optical sensors exploiting the visible and near infrared regions of electromagnetic (EM) spectrum will be unable to collect information from the ground if clouds are present (Wang et al., 2009). Imaging radar sensors, the most common being synthetic aperture radar (SAR), have the advantage of being able to image the ground even during cloudy conditions. The longer wavelengths of EM energy used by the SAR sensor are able to penetrate clouds while shorter wavelength used by optical sensors are scattered. A grassland monitoring tool based on SAR imagery would have many advantages over an optical imagery system, especially when SAR data becomes widely available. To demonstrate the feasibility of grassland monitoring using SAR, this study experimented with a set of dual-polarimetric SAR imagery to extract several grassland biophysical parameters such as soil moisture, canopy moisture, and green grass biomass over the mixed grassland in southwestern Saskatchewan. Soil moisture was derived from these images using the simple Delta Index (Thoma et al., 2006) first developed for a sparsely vegetated landscape. The Delta Index was found to explain 80% of the variation in soil moisture, in this vegetated landscape. Canopy moisture was modeled using the water cloud model (Attema and Ulaby, 1978). This model has a similar explanatory power of $R^2 = 0.80$. This study found that only the photosynthesizing green grass biomass had a significant relationship with the canopy moisture model. However, only about 40% of the variation in green grass

biomass can be explained by canopy moisture alone. The cross-polarized ratio developed from the dual polarimetric images was found to reflect the plant form diversity of the grassland.

Biophysical parameters extracted from optical satellite imagery, Landsat-5 in the case of this study, were compared to those derived from the SAR images. This comparison revealed that the SAR images were superior in sensitivity to soil and canopy moisture. Optical imagery was found to be more sensitive to green canopy cover. An approach combining the results from both sensors showed an improvement in green grass biomass estimation (Adjusted $R^2 = 0.71$).

Acknowledgments
I would like to acknowledge my advisor Dr. Xulin Guo whose advice and encouragement was present at all stages of this research. Thank you, my committee members Dr. Bob Patrick, and Dr Mohammed Kamal for taking the time to read and comment on my proposal and thesis. Dr George Sofko kindly offered to serve as an external examiner for the thesis defense and gave much valuable feedback. Thank you so much.

This project could not have been completed without the RADARSAT-2 imagery that was provided by the SOAR-E program and ISTP Canada who supplied the funding for the ground information

The ground data collection took place in the Grassland National Park where staff members were extremely supportive and helpful. The team that collected the ground data included the author as well as Erica Keet, Meng Li, and Li Shen

Table of Contents

List of Acronyms and Glossary

ATSAVI Adjusted Transformed Soil Adjusted Vegetation Index. A vegetation index based on light reflected in the red and near infrared region. This index includes gain and offset value, which accounts for the presence of soil.

DEM Digital Elevation Model. This is model representation of the terrain in three dimensions.

DN Digital Number. The raw scaled pixel values in an image. This is a measure of relative brightness.

EM Electromagnetic. Refers to the oscillating electric and magnetic field that define a light wave.

GNP Grassland National Park. The only national park located in Canada that preserves a portion of the mixed grass prairie.

HH Horizontal transmit; horizontal receive. The co-polarization mode of SAR system. It transmits a horizontally polarized EM wave and it tuned to receive only a horizontally polarized wave.

HV Horizontal transmit; vertical receive. This is cross-polarization mode of the SAR sensor. It transmits a horizontally polarized EM wave and it tuned to receive only a vertically polarized wave.

LAI Leaf Area Index. LAI is the areal measure of the abundance of leaves within a plant canopy. This parameter is closely related to above ground biomass.

LFMC Live Fuel Moisture Content. LFMC is the proportion of moisture to dry material in vegetation

MIR Middle Infrared. An area within the infrared spectrum between 1.5 – 2.3 μm.

NDVI Normalized Difference Vegetation Index. This is commonly used vegetation index that uses the red and near infrared region of the EM spectrum. The index as the name suggests in normalized meaning it takes only values between -1 and 1. These values are correlated with the amount green biomass.

NDMI Normalized Difference Moisture Index. This index relies on reflected light from the near infrared and middle infrared portion of the EM spectrum. The middle infrared band lies near a water absorption feature.

NIR Near Infrared Region. The shorter wave portion of the infrared spectrum (0.7 – 1.1 μm).

SAR Synthetic Aperture Radar. An active imaging radar system that uses the motion of the sensor platform to synthesis a large antenna.

SATVI Soil Adjusted Total Vegetation Index. This index detects the total of both green and senescent vegetation. It used both the red and two middle infrared bands for its calculation.

SAVI Soil Adjusted Vegetation Index. This index is designed to be used in areas of low vegetation cover, where bare soil is exposed to the sensor.

SOAR-E Science and Operational Application Research for RADARSAT-2. Education. This program grants access to RADARSAT-2 imagery for research and development of new applications.

USGS United States Geological Survey

VCM Volumetric Canopy Moisture. The mass of moisture per unit volume that is present in the vegetation canopy.

A List of Figures

A List of Tables

CHAPTER ONE
INTRODUCTION: A GRASSLAND MONITORING TOOL

This thesis addresses the following question: can accurate information on grassland biomass, canopy moisture, soil moisture, and plant form diversity be derived from dual-polarimetric SAR imagery? This question is part of a broader question of whether SAR data can form a part of a grassland monitoring tool. The tool must be able to provide accurate, repeatable measurements over a large area. Such a tool could aid both researchers and governments to direct resources towards areas with low biomass production or low plant form diversity.

There are several advantages to using SAR imagery as the base of a grassland monitoring tool. SAR sensors are sensitive to moisture in both the canopy and the soil. A SAR based system, unlike an optical sensor, can image the earth through any intervening clouds. However, this all-weather capability of a SAR system comes with a loss of interpretability of the imagery. Other barriers to the uptake of SAR remote sensing technology are that the images often require specialized software. Although, innovations such as Google Earth have made great strides in bringing optical satellite images to the non-specialist who can then view these images on their home computer, such innovations are not available for SAR imagery. The cost of a SAR scene can be impractical for some users especially considering that many SAR based remote sensing application rely on multiple images. However, like some optical sensors, some providers (ESA, 2009) are planning to offer SAR imagery at no cost. When the United States Geological Survey (USGS) began to provide Landsat TM images, at no cost, they immediately reported a 45% increase in scenes acquired (Miller et al., 2011). If SAR data could be provided at no cost (as suggested by the ESA Sentinel Program) this will likely cause a similar increase in user uptake. A grassland-monitoring tool that depends on low cost or free satellite data, combined with the

all-weather capability of radar images, could reach and benefit more users.

Grasslands do not have the same levels of diversity as more complex ecosystems, rather the importance of a grassland lies in its ability to produce enough biomass to support large herds of herbivores.

Plant biomass is the base of any ecosystem; energy enters the system as sunlight and is converted to starches by plants to fuel their growth. The total biomass accumulated over the growing season is known as production. Grasslands with poor production cannot support the animals and humans that depend on it for food. Grasslands that are overused by livestock risk being damaged, this damage may become severe if the livestock damage continues to accumulate (Critchley et al., 2008). Grassland production is dependent on many factors, such as the availability of sunlight, moisture and nutrients. External forces, whether they are anthropogenic or climatic, have the potential to affect production in either a positive or negative manner. Resilient ecosystems are those ecosystems that can return to their previous state after a disturbance.

Diversity occurs at different scales within an ecosystem, from the level of the species to the ecosystem itself (Whittaker, 1972). Plant forms such as grasses and forbs are morphologically separate from one another and have different functions within an ecological system. Plant forms are also known as ecological function groups. A diversity of plant forms or functional groups can be used to infer ecological resistance to outside forcing (Tilman and Downing, 1994; Peterson et al., 1998).

The study area for this project is the West Block of the Grasslands National Park (GNP) located in southwestern Saskatchewan. This park preserves a portion of the mixed prairie grasslands in its natural state. External forces that can act on a grassland ecoregion, such as grazing and fire, are all carefully monitored, and controlled by human interactions.

1.1 Research Objectives

The main goal of this research is to evaluate the effectiveness of using dual polarimetric SAR imagery to measure biophysical parameters, such as biomass, soil and canopy moisture, and the complexity of various plant functional groups (*forbs*, *grasses*, *shrubs*). There are two research objectives.

1. The first and main objective is to extract those biophysical parameters from the dual polarimetric RADARSAT-2 imagery alone.
2. The second objective is to assess whether improvements in accuracy can be achieved by incorporating optical information.

Each type of sensor has its own strengths and limitations, and this research will explore whether the combination of the two sensors yields more information than each of the image types considered separately.

1.2 Thesis Organization

The thesis is organized into five chapters and references. Chapter 2, the literature review, is an introduction to the type of remotely sensed data that will be used throughout the analysis. A summary of the literature describing similar applications of SAR and optical data is found here as well. Chapter 3 introduces the study area, the ground data collection design, and the pre-processing that was required for both the SAR and optical images. Chapter 4 is split into three parts. Part 1 presents the data that was collected and summarizes the relationships among the different variables. Part 2 describes the applications of the various models to extract the biophysical parameters: canopy moisture, green biomass, and plant form diversity. Part 3 integrates the optical data into the results already obtained from the SAR imagery. Chapter 5

presents the conclusion and summarizes the contribution, limitation, and future directions. References are found at the end of this document. A list of the many acronyms used in this text is found immediately after the Table of Contents for ease of reference.

CHAPTER TWO

LITERATURE REVIEW

2.1 SAR Remote Sensing: Introduction

The RADARSAT-2 is an active sensor, meaning the satellite is the source of the microwave pulse that it uses to study the earth's surface. By contrast a passive system, like all optical satellites, uses the light emitted from the sun. Radar resolution depends on the antenna length, frequency and the distance to the target. Antenna length would be serious limitation to the practicality of either an airborne or spaceborne sensor, as the antenna lengths necessary would be extremely large. Certain properties of the radar pulse allow engineers to use the known details of the radar satellite's orbit to synthesize a much longer virtual antenna. This system is known as synthetic aperture radar (SAR); a SAR sensor will have a short physical antenna but will have the resolution capabilities as if it possessed an antenna several kilometers long. As the RADARSAT-2 is the only SAR sensor used in this study, the terms RADARSAT-2 and SAR are used interchangeably. RADARSAT-2 operates in the microwave region of the electromagnetic (EM) spectrum; more precisely it uses a wavelength of 5.6 cm in a region known as the C-band. The SAR sensor studies the energy that has scattered from the target back towards the sensor, the energy received by sensor after it sends out its initial pulse is known as backscatter. The long wavelengths of the microwave region are too large to scatter molecules in the same manner as short wave visible light (300 - 700 nm). The dominant features that determine the radar scattering process are surface roughness and the dielectric constant, a constant that describes the behavior of an electromagnetic wave within a target. While interpreting the interaction between the radar pulse and vegetation these two concepts must be kept in mind. A homogenous canopy

structure, of which cereals are an example, will appear "smooth" i.e. there is less energy backscattered towards the RADARSAT. In this context "smooth" means the surface roughness is on a scale smaller than the radar pulse wavelength (5.6 cm) (Peake and Oliver, 1971). Shrub canopies are heterogeneous; their branches have many orientations. This type of feature will appear "rough" and will scatter more of the microwave pulse back to the sensor (See Figure 2-1).

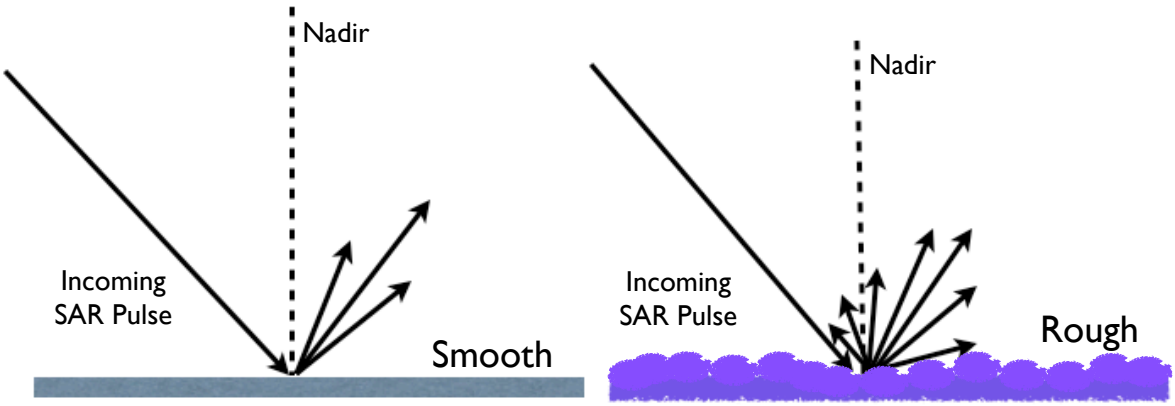

Figure 2-1 Relationship between backscatter and surface roughness; the smooth surface scatters most of the incoming energy away from the sensor, while the rough surface scatters some of the energy back to the sensor.

The dielectric properties of a medium mediate how an electromagnetic (EM) wave will interact with a target. What is of most importance here is that water has a high dielectric constant, meaning the radar sensor is very sensitive to the presence of water. A target that contains more moisture will appear brighter in SAR images than a dryer target. The RADARSAT has been used to retrieve biologically important parameters such as soil moisture (Moran et al., 2000), using empirical, semi-empirical, and physical models (Thoma et al., 2006).

Another important concept in radar remote sensing is the polarization. Polarization describes the orientation of the electric field oscillations of the electromagnetic wave. The microwave pulse

emitted by RADARSAT-2 toward the target is either horizontally oriented (H), or vertically oriented (V). The orientation of the electric field's oscillations is always perpendicular to the direction of travel. When the pulse scatters off the target, in general, it will have a polarization that is different from the transmitted polarization and one that has been influenced by the structure of the target. The satellite antenna can be tuned to receive only the portions of the returning microwave pulses that are in either a horizontal or vertical orientation (see Figure 2-2).

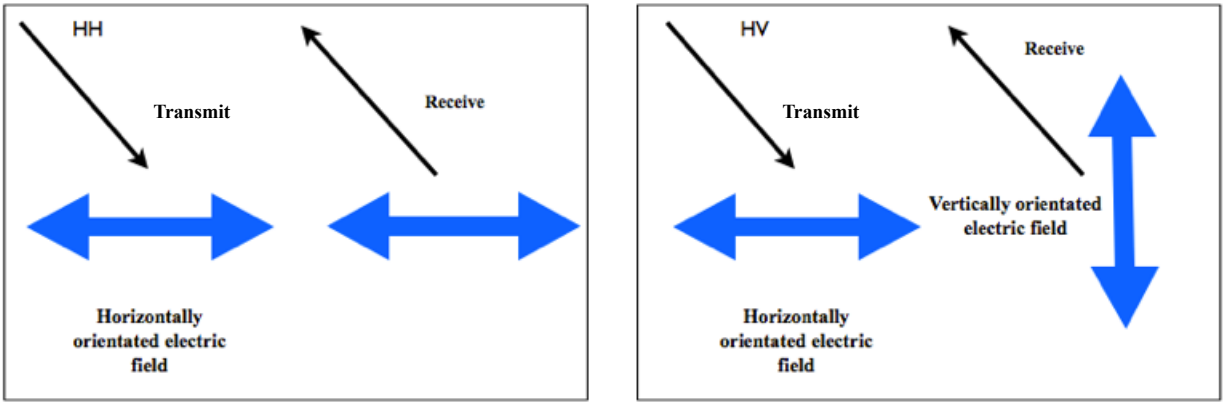

Figure 2-2 An illustration of the difference between the co-polarization HH and the cross polarization HV.

The dual polarization mode that was selected for this study was HH and HV. HH refers to for horizontal transmission, and horizontal receiving, i.e. the RADARSAT-2 is transmitting a horizontally oriented pulse and receiving only a horizontally polarized pulse in return. HV is the cross polarization mode because the sensor sends a horizontally polarized pulse and receives only the backscattered pulses that are vertically orientated. The combination of HH and HV can be used to distinguish surface (smooth) from volume scatterers (rough). In surface scattering most of the initial microwave pulse is scattered away from the sensor resulting in a low backscatter value in the co-polarized mode and an even lower backscatter value in the cross-polarized mode. In the case of volume scattering the microwave pulse undergoes multiple reflections from the target, which changes its polarization; a volume scatterer can produce high backscatter in both the co-polarized and

cross-polarized mode (Yonezawa et al., 2010; Gao et al., 2013). If the backscattered energy being returned to the sensor was completely un-polarized then the contributions from the HH and HV modes would be equal. Yonezawa et al. (2012) monitored rice fields using polarimetric RADARSAT-2 imagery during the time when the rice plants had just been transplanted; the paddies were characterized by mostly surface scattering. As the rice grew and the canopy became larger and more complex the scattering process shifted to more volume scattering. Gao et al., (2013) demonstrated that canopy parameters such as LAI were strongly related to volume scattering, and this could be measured by studying the cross polarization ratio.

2.2 SAR Remote Sensing: Water Cloud Model

The interaction of the SAR pulses with the vegetation canopy can be described using the semi-empirical water cloud model first defined by Attema and Ulaby (1978). They reasoned that the dielectric constant, which mediates the interaction between the incident EM beam and the target, is much greater for the moisture within the canopy than for the dry vegetation. The canopy volume is mainly occupied by air, which has a negligible dielectric constant. Given that the canopy is mostly air and the dielectric constant of the dry matter is negligible compared to moisture, the water cloud model treats the vegetation canopy as a Poisson distribution of identical spherical water droplets which act as scatterers.

The energy that scattered back to the sensor contains contributions from both the canopy and the soil. The contribution of each water droplets, bound within the canopy, to the vegetation backscatter must be summed while accounting for attenuation of the incident beam as it passes

through the canopy. The vegetation contribution to the backscatter is a function of incident angle, the optical path length, and the number of water droplets.

Soil moisture is known to have a linear relationship to SAR backscatter. This linear equation, which represents the contribution from soil moisture, is added incoherently to the vegetation contribution to produce the total backscatter σ. The final model is shown in Equation 1.

$$\sigma = A\cos\theta\left[1-\exp^{\left(\frac{-2\,BL}{\cos\theta}\right)}\right]+(C+Dm_s)\cdot\exp^{\left(\frac{-2BL}{\cos\theta}\right)} \quad (1)$$

where σ is the total backscatter returned from the target, θ in the incident angle of microwave pulse sent from the sensor, L is density of water droplet, and m_s is the soil moisture. The water cloud model has been employed in many applications with different definitions of the various parameters in the equation. The radar backscatter coefficient is defined as the radar cross-section per unit area therefore the units are represented as $\frac{m^2}{m^2}$. Soil moisture m_s may be represented as a ratio of two volumes or two masses, or occasionally as a mass per unit volume ($\frac{g}{m^3}$). The incident angle θ is measured in radians. The units for the canopy parameter *L* depend on which definition of *L* is being used. While researchers consistently interpret the water cloud model as a function of soil moisture, the canopy parameter L has variable interpretations (Graham & Harris, 2003). Attema and Ulaby conceived the water cloud model as measuring canopy moisture, more specifically as the number and density of the spherical scatterers, however others have interpreted the canopy parameter as leaf area index (LAI) or even biomass. The microwave pulse is far more sensitive to canopy moisture as a parameter, than LAI, which is related to biomass, or the Leaf Water Area Index (LWAI) (Dabrowska-Zielinska et al., 2007).

The model has four site-specific parameters: *A*, *B*, *C*, and *D*. From their position in Equation 1, *A* and *B* are vegetation parameters while *C* and *D* clearly represent soil parameters. Parameter *A* is sometimes defined as the backscatter from an area of complete canopy coverage and soil parameter *C* could be chosen from a lookup table (Graham and Harris, 2002), if the soil type is known. Of the four parameters only *B* and *D* must be derived from regression techniques.

There are two assumptions used in the water cloud model: one that the large-scale features of canopy are uniform, the distribution of the spherical droplet is still assumed to follow a random Poisson distribution. Two, the scattering mechanism is volumetric, and the most important variables are the canopy depth and density of the spherical scatterers.

2.3 SAR Remote Sensing: Soil Moisture

As discussed in the Section 2.1, SAR sensors are sensitive to the presence of moisture. The moisture contained within the soil can be orders of magnitudes greater than that found within the canopy. Soil moisture was known to have a linear relationship with SAR backscatter; this knowledge was exploited by Attema and Ulaby (1978) in their water cloud model (Section 2.2). The water cloud model (Equation 1) accounts for the contributions of both soil and vegetation canopy. If the water cloud model is to be used to study canopy moisture than the contribution by soil moisture must be accounted for. This requires an estimate of soil moisture over the entire image.

The first attempts to relate soil moisture took the form of a linear regression (Natali et al., 2009). While soil moisture is the dominant factor affecting backscatter in a grassland (Van der Velde and Su, 2009), it is not the only factor. Physical models, such as the Integral Equation Model, (IEM) (Oh, Y., 2004) models the interaction of the SAR microwave pulse and soil moisture while explicitly accounting for surface roughness (Moran et al., 2000, Oh, 2004).

Researchers such as Thoma et al. (2006) have noted that by calculating the image difference between a relatively wetter and dryer time of year can explain more of the variation in soil moisture than a single image alone. They created the Delta Index: the difference between a wet and dry SAR image divided by the dry image (Equation 2).

$$\Delta = \frac{\sigma_{wet} - \sigma_{dry}}{\sigma_{dry}} \quad (2)$$

Equation 2 manipulates the backscatter coefficients (σ) for two different SAR scenes; this coefficient is defined as the radar cross section per unit area, the units can be represented as $\frac{m^2}{m^2}$. Since the formulation of the Delta includes division the index itself is dimensionless. The subscripts wet and dry represent a relative difference in soil moisture content between the two scenes being analyzed. The exact quantitative differences in soil moisture that are required for the index to function were not specified by Thomas et al. (2006). This semi-empirical model is highly successful at explaining the variation within soil moisture. This empirical formula does not address surface roughness at all. Indeed, Thoma et al. postulate the differencing of the two images reduces the contribution of surface roughness to variation in backscatter.

2.4 Optical Remote Sensing: LAI and Biomass

Biomass is the dry weight of the plant material that defines both above ground and below ground biomass. For remote sensing applications, only the above ground biomass is considered since this is the only type of biomass that is visible to the sensor. The amount of vegetation biomass affects the maximum amount of food available for surface consumers, namely herbivores. Measuring this quantity from a remote sensing platform relies on the measuring vegetation indices that can be related to important parameters such as Leaf Area Index (LAI).

LAI is the area covered by flat leaves per area of ground surface and this measure is correlated

with biomass. LAI has been the focus of many investigations aiming to retrieve this parameter from optical imagery (He et al., 2009). Short-wave passive remote sensing systems, such as the Landsat, exploit the distinctive properties vegetation as it interacts with short wave visible and near infrared light. Chlorophyll, the molecule of photosynthesis, absorbs sunlight in the blue and red regions but reflects green light. The spongy cells that comprise the leaf are effective scatterers of near-infrared radiation (NIR). The combination of these absorption features of the blue and red bands and the high reflectance in the near infrared are a universal feature of green vegetation

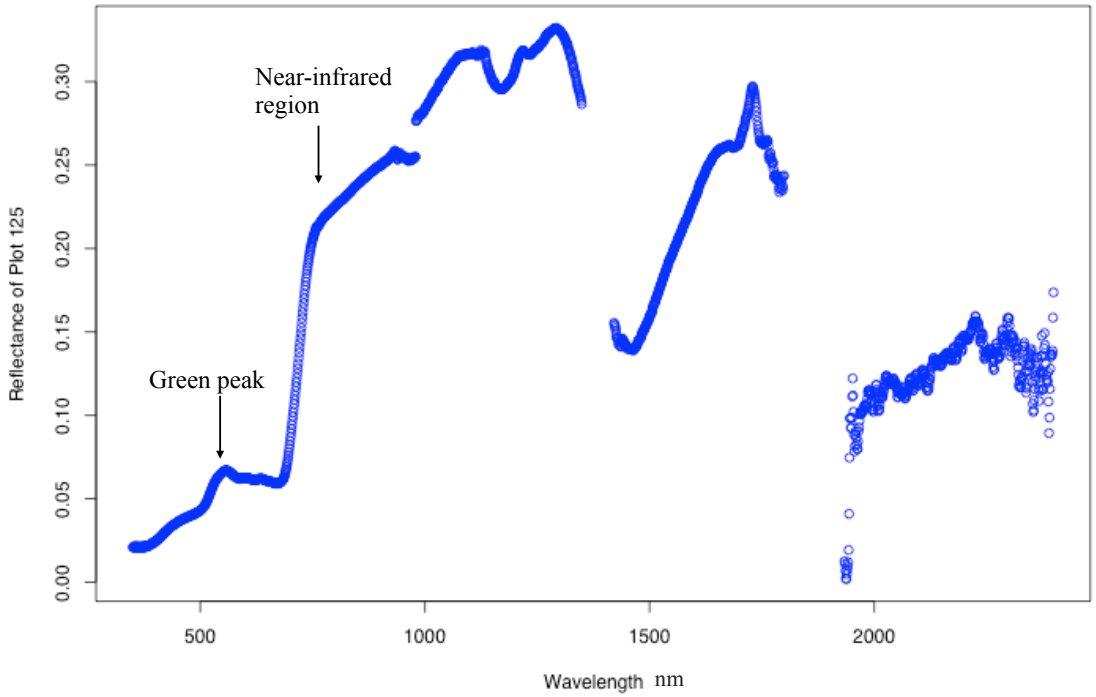

Figure 2-3 Typical Grasslands reflectance spectrum, collected in the GNP. The features that are typical of green vegetation are the green peak and the rapid increase in reflectance in the near-infrared region. There are breaks in the line due to noise present in the data. A prominent water absorption feature can be seen at 1500 nm. Spectra collected by Xioahui Yang from the Grasslands National Park.

(Figure 2-3). Remote sensing scientists have combined image bands in the near infrared and the red to create various vegetation indices. The most widely used vegetation index is the

Normalized Difference Vegetation Index or NDVI. NDVI produces values between -1 and 1 where values closer to one are greener vegetation. The NDVI is defined as follows (Equation 3):

$$NDVI = \frac{NIR-RED}{NIR+RED} \quad (3)$$

where NIR and RED represent the surface reflectance from the target vegetation in the near infrared and red bands respectively. Reflectance is defined as the percentage of the total incident radiation that was reflected from the target for a particular wavelength region; it is a dimensionless value.

Tucker and Seller (1986) described the importance of vegetation indices for the prediction of biomass production. They predicted a near linear relationship between satellite based vegetation indices and biophysical properties such as photosynthesis, the absorption of photosynthetic active radiation, and canopy conductance. Production, unlike biomass, is a cumulative measure and therefore includes time in its definition; the unit of production is expressed as g C/m^2/yr, (grams of Carbon per area per year). Biomass is approximately 50% Carbon by weight. This measure does not account for plant respiration and production is more accurately defined as the biomass accumulated per area per year minus the carbon lost to respiration. Researchers have been exploiting vegetation indices to derive biomass production even in difficult arid environments (Seaquist, J., 2003).

Tucker and Seller (1986), in their formulation of remote sensing of biomass production, did caution that soil and dead biomass would complicate the extraction of the biophysical properties of the canopy. It is understandable why this is the case; vegetation gains its unique spectral footprint because of the presence of chlorophyll; dead vegetation lacks that photosynthesizing molecule. In semiarid grasslands, such as the Canadian Prairies, dead biomass and soil brightness

cannot be ignored (He et al., 2006a). He et al. (2006b) demonstrated for grasslands that modifications of the NDVI can be correlated with LAI and are suitable for productivity models in an area with considerable amounts of dead biomass. Considering the information presented above, Landsat data is expected to be suitable for analysis of grassland production and biomass estimation.

2.5 SAR Remote Sensing: Biomass

Vegetation biophysical parameters have been explored with SAR imagery, however much of the work has concentrated on forests and agriculture. Some of the agriculture applications have been yield estimations (Chen et al., 2011), crop typing and tillage monitoring (McNairn and Brisco, 2004).

SAR biomass applications in grasslands are not as numerous. Hill and Vickery (1999), using SAR imagery, classified grasslands vegetation into various classes using such biophysical parameter as canopy height and water content. Svoray and Shoshany (2002) derived biomass in a difficult semiarid grassland region. This is a significant achievement since, as previously discussed, even optical sensors can underestimate biomass when soil brightness and dormant biomass dominate.

Since optical and radar remote sensing gather information by exploiting different types of interactions with EM radiation, the combination of both sensors has the potential for even greater information content. Hill et al. (2005) combined multi-frequency radar data with optical imagery to create a classification map that included canopy height measured from the radar, and vegetation greenness from the optical sensors. Svoray and Shoshany (2003) also combined SAR and Landsat data to successfully map biomass in a heterogeneous semiarid grassland region. They used Landsat data to determine the fractional vegetation coverage of the different types of

plant forms plus bare soil, which was then used to modify the water cloud model to account for the presence of different canopy types. Combinations of optical and SAR sensor have been applied successfully to annual crops estimation (Shang et al., 2008; McNairn et al., 2009).

An earlier study by Price et al. (2002) failed to demonstrate any improvement in grasslands mapping in Kansas using a combination of Landsat and SAR. However, Chust et al. (2004) had success with a SAR time series and optical data in the Mediterranean. Since the study by Price failed using a single date SAR image and the study by Chust et al. (2004) succeeded with SAR time series and optical images, this strongly suggests that using a combination of SAR and optical time series is a more effective approach.

2.6 Remote Sensing: Plant Form Diversity

Much of Saskatchewan's native grasslands were lost in the conversion to agriculture. The diverse grasses of the native prairies were plowed and replaced with a monoculture of tame grasses, such as the introduced crested wheatgrass (*Agropyron cristatum*). Quantifying this loss by means of remote sensing has faced serious challenges, namely, with the exception of some trees; remote sensing imagery resolutions are far too coarse to directly identify species. Measurements of diversity must rely on indirect methods.

Duro et al. (2007) identified four key components of a potential remote sensing based diversity monitoring program: productivity, disturbance, topography, and land cover. Productivity, as discussed in Section 2.4, is a measure of the amount of biomass accumulated per unit area per time. Disturbances can be anthropogenic or environmental, examples of anthropogenic disturbances would be the introduction of invasive species, fire suppression, or plowing the land. Examples of natural disturbance are prolonged drought, heat or cold, fire or grazing. Hawkins et al., (2003) identified climate conditions as a major driver for biodiversity. Disturbed areas should

appear as low diversity in any diversity map.

Topography is a description of the shape of the landscape. Topography, due to its connection with surface roughness, will be highlighted by the SAR imagery. By using the cross polarization ratio, several of Duro et al. (2007) parameters may be derived from a single image. Land cover is describing what is on the earth surface. Examples would be bare soil, grasses, trees, asphalt, anthropogenic structures, etc. The biodiversity framework developed by Duro et al. (2007) could be applied here to the diversity of plant forms.

Previous remote sensing studies of diversity have focused on the Landsat series of satellites as they have the longest continuous archive. Land-cover assessment and classification with the Landsat sensor was explored by McDermid et al. (2005) along with Franklin (2010) as an important tool in understanding wildlife diversity. This study played an important role in efforts to understand and conserve Grizzly Bear habitat in the Foothills of Alberta. Debinski et al. (1999) explored vegetation cover and diversity and reached a similar conclusion that land cover data derived from satellites was an important tool for understanding diversity. The 30 m spatial resolution of the Landsat sensor does not appear to be an issue in coarse biodiversity studies. Griffiths and Lee (2000) noted that Landsat spatial resolution was better than the resolution of their database of plant locations. They were able to resolve the resolution differences between the two data sets for their analysis. The planned SAR sensors will have resolutions very similar to Landsat; it is encouraging to learn that other researchers have found moderate spatial resolutions are not a limiting factor in inferring diversity.

Plant diversity studies using SAR data have predominantly focused on forested landscapes using texture and multi-temporal and multi-frequency SAR (Evans et al., 2010). Zhang et al. (2006) attempted to relate radar images to grassland diversity in the Grasslands National Park. This

research sought species richness rather than the coarser diversity measure of plant forms. The results were mixed, but encouraging.

CHAPTER THREE

STUDY AREA AND METHODS

3.1 Study Area

The study area was located in the west block of the Grasslands National Park (GNP) and nearby community pastures. The park itself is located in the extreme south of central Saskatchewan (Figure 3-1), and is situated within the Mixed Grassland ecological region; the driest region of the province. Grasses are predominantly wheat grass (*Pascopyrum smithii*) and needle and thread grass of the genus *Stipa*. Shrubs can grow wherever adequate moisture is present, and this occurs primarily in riparian areas. The west block is traversed by the Frenchman River, which creates an environment hospitable to the shrub plant form. The cumulative annual rainfall amounts to 262 mm, with the majority falling in May and June. Average temperatures range from 18 C to -13 C.

This is a productive ecosystem, home to cattle, bison, antelope, deer, and coyote, along with raptors, grouse, shrikes and many other species including the reintroduced black-footed ferret. Livestock have not grazed the GNP for a period from 1984 to 2002. In 2002, park managers decided to reopen the park to grazing. Bison were introduced to the park in 2006 and certain areas were designated for cattle grazing. (Parks Canada, 2010)

3.2 Field Design and Data

The Grasslands National Park has been the site of active grasslands research since its inception in 2001. Park researchers have previously established biophysical monitoring sites both within and outside the park, and these were incorporated into the field design for this study (Parks Canada, 2010).

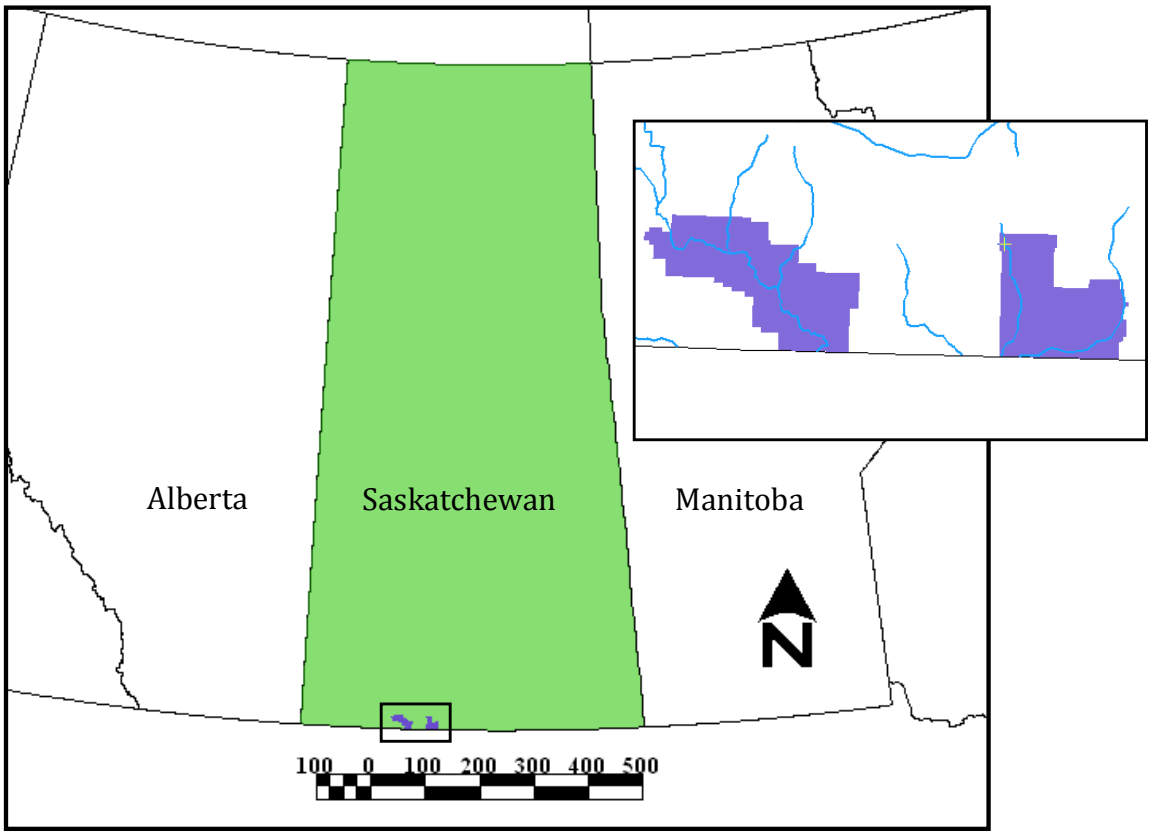

Figure 3-1 The west block of the Grasslands National Park is located in extreme south of Saskatchewan.

Ten of these monitoring sites were selected in advance and two non-monitored sites were added in the field (Figure 3-2). The two additional sites were added due to the difficulty of accessing the planned sites. Roads were flooded out or simply impassable. There was a real concern at the time that not all sites will be reached. Fortunately dryer weather eventually allowed for access. The existing biophysical sites represented two different grazing levels; they are either grazed by cattle or were within the park boundary and were considered ungrazed. The sites are labeled with a U or G depending on whether they are ungrazed or grazed. The grazed sites were labeled as G0, G1, G2, G3, and G4. The ungrazed sites correspondingly were labeled as U0, U1, U2, U3, and U4. These historical names were kept for this analysis. The sites added in the eventuality that the planned sites could not be reached were referred to as Site 01 and 02. Figure 3-2 illustrates

the distribution of the sites using a multipolarimetric SAR image as background. Note that one site never overlaps the RADARSAT-2 imagery (G2) as this reduces the original 12 sites to 11. Site G2 will not be a part of any subsequent analysis. The study sites were chosen before the imagery was acquired. The SAR acquisition plan must have included a small error that caused that one site to missed.

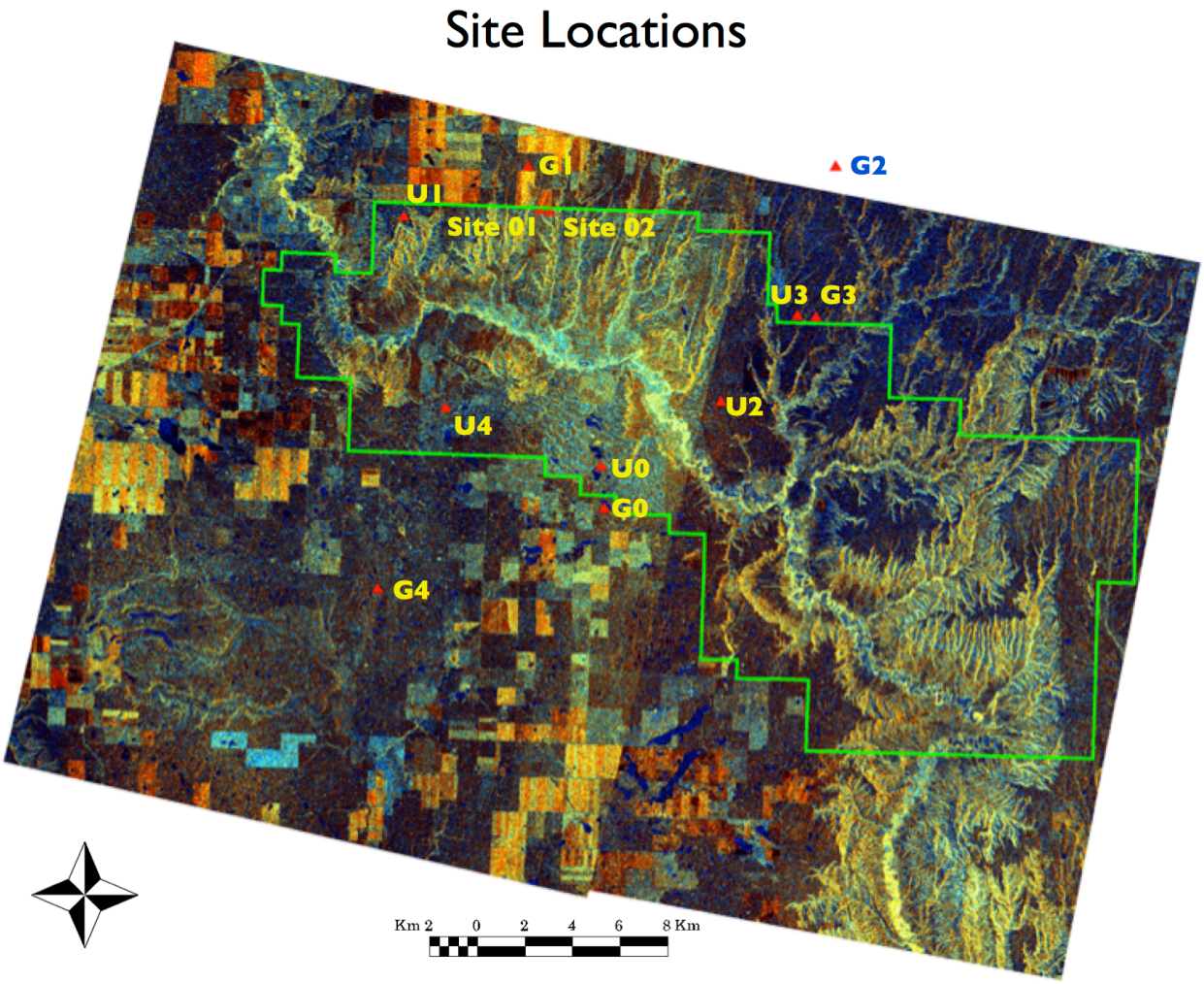

Figure 3-2 Ground information sites (red triangle) within the west block of the GNP: This false color image was created usingtwo polarization modes. RADARSAT-2 Image: Red: HH, Green: HV: Blue: Ratio of Cross Polarized band and the co-polarized band $\frac{HV^2}{HH^2}$.

At each site, two 100 m transects were laid out, crossing at midpoint and at a right angle; one is orientated north south while the other is orientated east west, this configuration will be referred hereafter as a "Transect Cross" (Figure 3-3). Along each arm three 50 x 50 cm^2 quadrants were used to collect non-invasive biophysical measurements, with one quadrant per arm being set aside for biomass clipping. The quadrants were placed at 10 m, 30 m and at 50 meters from the central point. Measurements were recorded in the same order for each site, moving clockwise around the Transect Cross starting with the north direction; motion along the transects always began with the center point and moved outwards. This was done in order to relate each measurement to the correct quadrant. As long as the same order of data collection was consistently followed this could be done.

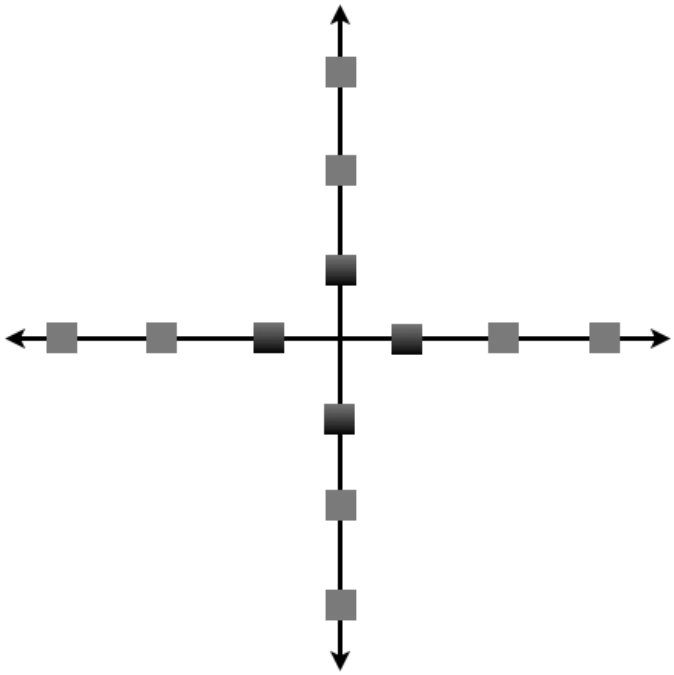

Figure 3-3 Site Layout: the dark boxes represent the quadrants set aside for biomass sampling.

The ground data collection campaign occurred in June of 2011. The park was unusually wet in

2011; this delayed the peak green of the vegetation to July rather than June. The peak green of the grasslands did not coincide at all with the ground data campaign.

At each 50 x 50 cm^2 quadrant the following data was collected: soil moisture and temperature, LAI, and the percent canopy coverage of the different plant forms for example: *grasses*, *forbs*, *standing dead*, *litter*, *moss*, along with non-vegetative covers such as *rock*, and *bare ground*. Soil moisture was measured with a short probe that penetrated approximately 5 cm into the soil. The LAI was measured with the Li-Cor LAI 2000 instrument (Figure ii in Appendix A). This instrument has been used in previous ground campaigns, therefore the calibration and operation of the probe has been well verified (He and Guo, 2006b). The probe recorded one above canopy measurement and six below canopy measurements; this configuration was deemed accurate by previous experience with the instrument. Estimation of canopy cover percentage was done by visually estimating the percentages of each canopy cover type, if present. For consistency only one observer made the majority of the observations.

On each arm of the Transact Cross a smaller quadrant (20 x 50 cm^2) was used for biomass clipping (See Figure i in Appendix A). All standing material was clipped leaving only moss, litter and other debris. The clipped sample was placed unsorted into a bag and weighed immediately. The scale used for weighing in the field was not sensitive enough to detect the weight of the bag alone, therefore the weight of the bag was assumed to be insignificant compared to the mass of the plant material. This measurement will be known as the "wet weight" since it includes the weight of the plant material and the moisture within the canopy.

3.2.1 Volumetric Canopy Moisture

The biomass sample once removed from the field was sorted into the following categories: *green grass*, *forbs*, *shrubs*, and *dead biomass*. These were dried in an oven for 48 hours in order to

evaporate the remaining moisture, giving the dry weight. Drying temperatures are at about 100 ^{o}C, which is hot enough to evaporate the water, while not breaking down the remaining plant material. Small samples can dry overnight, but some of the biomass samples collected were larger and required more time. The difference between the wet and dry weight is the mass of the moisture evaporated by the oven. The scale used to determine the dry weight was far more sensitive than the field scale, meaning the weight of the paper bag was subtracted from the dry weight. Canopy moisture can be represented by grams per unit area, however, as the water cloud model requires a measure of water droplet density, units of grams per unit volume is more appropriate in this case. Average canopy height was recorded in the field; the canopy height and the clipped area (20 x 50 cm) were used to calculate a volume; the volumetric canopy moisture (VCM) is reported in units of g/m^{3}. This volumetric canopy moisture calculation assumes the moisture is distributed evenly throughout the volume. This is not strictly true, in either the canopy or the water cloud model, however the variation in the moisture density is far below the detection limits of the sensors used in this research. Results from all quadrants were averaged together to represent each site.

3.2.2 Soil Moisture

Soil moisture was measured near the surface using a ProCheck soil moisture probe (Figure iii in Appendix A). The results from each quadrant were averaged creating a single value that would represent the entire site. The soil moisture probe collects measurements as a ratio of two volumes (water to soil); however, to be comparable with the volumetric canopy moisture this ratio must be converted to grams per cubic meter. The water volume can be expressed in grams by using the known density of water while noting that this quantity does vary with temperature. Soil temperature was measured simultaneously along with soil moisture. The density of water for a

given soil temperature was retrieved from a look up table. The moisture available in the soil, when converted to the same unit as the VCM is easily several orders of magnitude greater than the moisture bound within the canopy.

3.3 List of Images

A list of images used in this research is as follows (See Table 3-1 and 3-2). Since each RADARSAT-2 image covers half of the park there should be two images per month. June is the only exception, and an unfortunate one, as Chapter 4 Section 2 will illustrate.

Table 3-1 List of RADARSAT-2 Images used in this research.

Date	Polarization	Beam Mode
May 14, 2011	HH, VV, HV, VH	Standard Quad 24
May 17, 2011	HH, VV, HV, VH	Standard Quad 12
Jun 24, 2011	HH, VV, HV, VH	Standard Quad 21
July 18, 2011	HH, VV, HV, VH	Standard Quad 20
July 21, 2011	HH, VV, HV, VH	Standard Quad 08
August 18, 2011	HH, VV, HV, VH	Standard Quad 24
August 21, 2011	HH, VV, HV, VH	Standard Quad 12

Table 3-2 List of Landsat-5 images used in this research.

Path/Row	Date
37/26	May 12, 2011
37/26	June 13, 2011
37/26	July 15, 2011
37/26	August 11, 2011

All Landsat-5 images were obtained from the online USGS archive. This archive stores orthorectified Landsat-5 that may be retrieved at no cost. The orthorectification corrects the satellite image to a ground coordinates while accounting for variations in elevation.

3.4 Image Processing

3.4.1 Sigma Nought

All RADARSAT-2 images were converted to sigma nought $\sigma_\circ$: the radar backscatter coefficient or the radar cross-section per unit area $\left(\frac{m^2}{m^2}\right)$. PCI Geomatica automatically performs this conversion on opening the raw imagery. The sigma nought images are output as backscatter amplitude, however these values can be converted to decibels using the following formula (Equation 4):

$$R_{db} = 10 * \log (R_a^2) \quad (4)$$

where R_{db} is the backscatter as decibels and R_a is the backscatter represented as amplitude.

3.4.2 Median Filter

Radar speckle is an inherent feature of SAR imagery; it can only be reduced by filtering and never eliminated (Porcello et al., 1976). The median filter operates by means of a moving window consisting of an odd number of pixels, for example 3 x 3, 5 x 5, 7 x 7, etc. The filter replaces the center pixel of the moving window with the median value of the surrounding pixels. This results in a smoother appearance of the SAR imagery. Variation among the backscatter amplitude pixels within the 100 m x 100 m sample begins decreasing as the median filter is applied. The variation continues to decrease with each increase in moving window size. The decrease in variation eventually leveled off, and any subsequent increases in the moving window size produced inconsequential decreases in variation (See Figure 3-4). This occurred at a moving window size of 9 x 9; the earlier dramatic drop in variation was attributed to the removal of noise from the scene. A median filter of moving window size 9 x 9 was applied to all SAR images.

At this point in the image preprocessing process a geometric correction is normally done. This

correction ties the SAR image to ground map coordinates. However, the geometric accuracy of the RADARSAT-2 imagery as is was accurate enough to match the orthorectified Landsat-5 imagery and all existing GIS layers, therefore further geocorrection was not necessary.

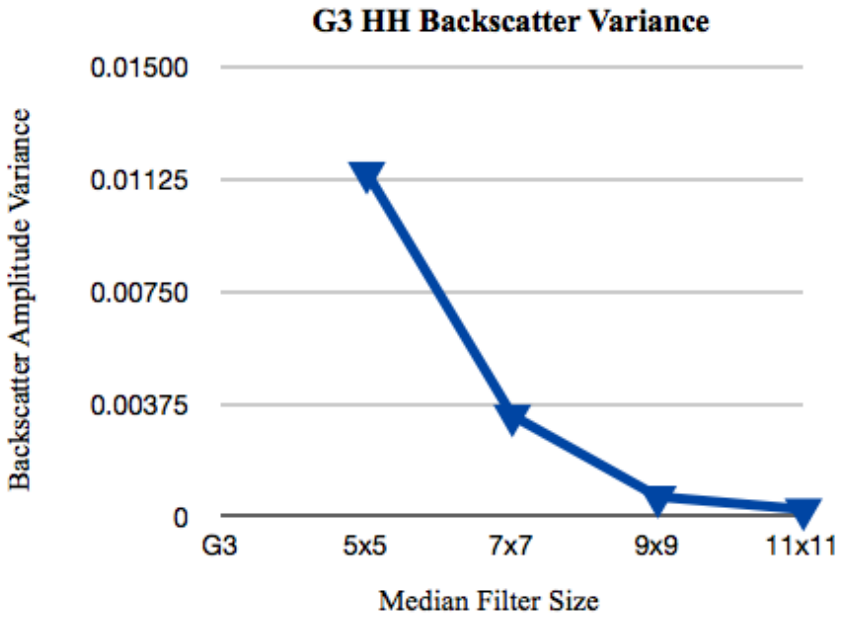

Figure 3-4 The relationship between variance and median filter size. The variance rapidly drops as noise is filtered out.

3.4.3 Cross Polarization Ratio

The cross polarization ratio was calculated using the following formula (Jensen, 2007) (Equation 5):

$$\frac{HV^2}{HH^2} \tag{5}$$

Equation 5 was applied to the filtered images, however the remaining noise within the image was amplified by this calculation. As a result the cross polarization ratio band is extremely noisy (See Figure 3-5). However it does contain information that is invariant with soil moisture (Oh, 2004), meaning the variation in the cross polarization ratio is most likely related to canopy or surface

roughness; recall that backscatter is a function of the dielectric constant, i.e. moisture, and surface roughness.

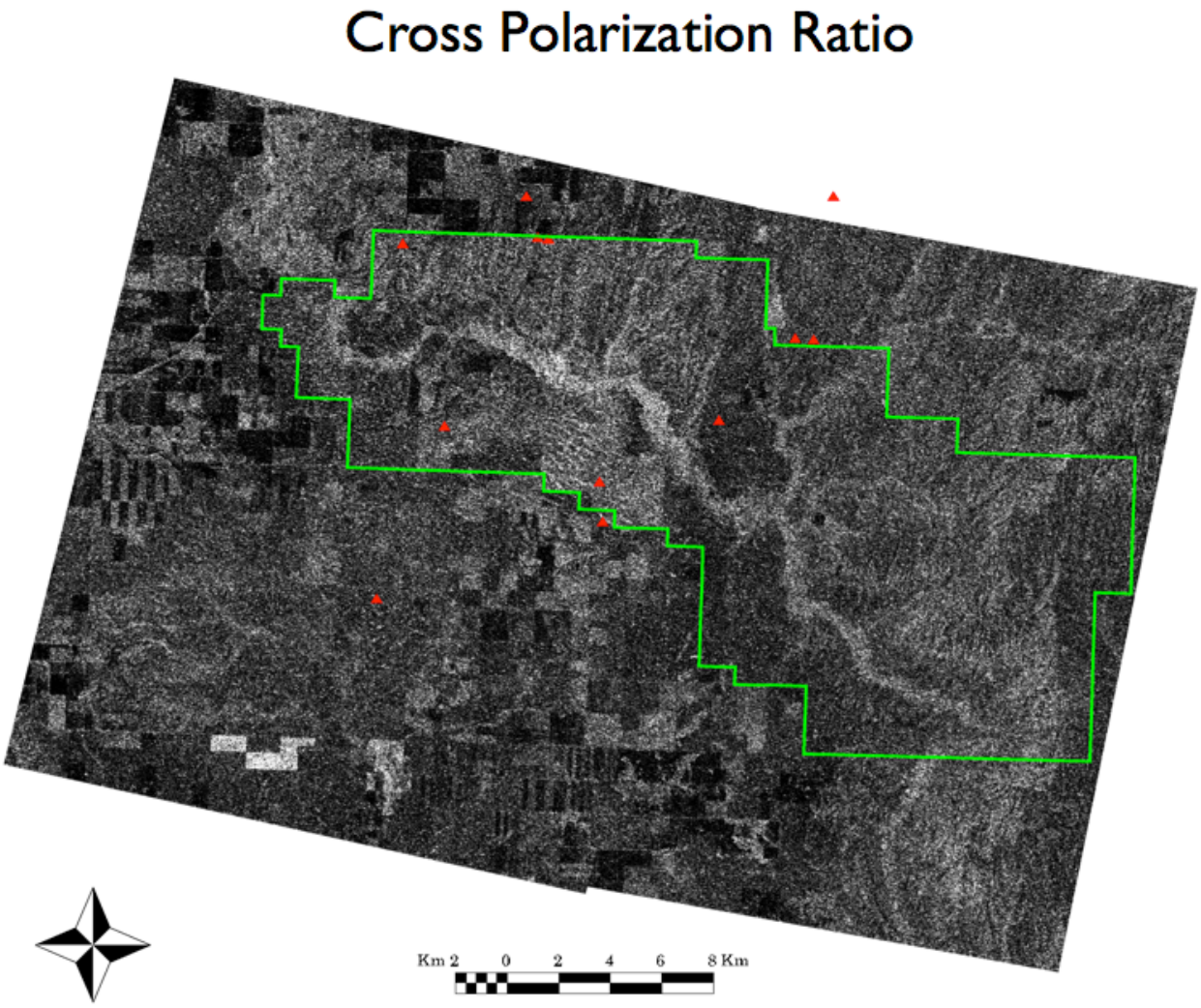

Figure 3-5 The Cross Polarization Ratio. The tone correlates to the type of scattering process present. The darker the tone the more surface scattering, conversely the brighter the tone the more volume scattering.

3.4.4 RADARSAT-2 Mosaicking

The RADARSAT-2 images are standard quad images with a spatial resolution, the area on the ground that is represented by one pixel, of 8 x 3 m; one standard quad image does not cover all sites. To capture all sites, it is necessary to mosaic the two scenes acquired for each month. A

significant difference in backscatter amplitude exists between acquisitions. The contrast matching option of many image-processing software alters the digital numbers (DN) of the pixels of one image to match a reference image. The user does not always know the exact nature of the conversion. The DNs are of great significance to this analysis, and if they are to be altered it should be in an understandable manner.

Matching images for mosaicking required selecting one of the images to be the reference. The June 24th image is the closest match in time to the ground data collection period; therefore it was the ideal choice for the reference image. The next image collected was on July 13th; this image was to be matched to the reference. This is the only image pair that has such a long period between acquisitions; all other images were temporally closer together. Both images have been converted to sigma nought, therefore sensor and incident angle effects have already been accounted for. To match the July 13th image to the June 24th image the Empirical Line Calibration was employed. This technique requires samples from low and high digital number areas from both images. Low digital number areas are often water bodies, which were relatively stable from image to image. The open water presents a smooth surface that reflects most of the initial radar pulse away from the sensor. High digital number areas represented either vegetation or topographical effects. Slopes facing toward the RADARSAT-2 would return a higher amount of backscatter than slopes facing away from the sensor. High backscatter vegetation is mainly related to moisture, rather than surface roughness. There are only a handful of trees in the park that could produce a strong backscatter from their complex surfaces. The moisture and vegetation interaction is time sensitive, and will not remain stable between images. Topographical effects (slopes facing the sensor) are the result of the viewing geometry, which is also not consistent from image to image. Wherever possible, vegetative targets were sampled

rather than topographical features. As a result, a plot of the high and low digital numbers from the two images had significant variation among the high digital numbers (Figure 3-6).

The linear equation derived from the scatterplot was applied to the July 13th image and used to predict the backscatter amplitude of the June 24th image. This analysis was repeated for the May, July and August pairs of images. Since these pairs were closer together in time they tended to have less mosaicking artifacts.

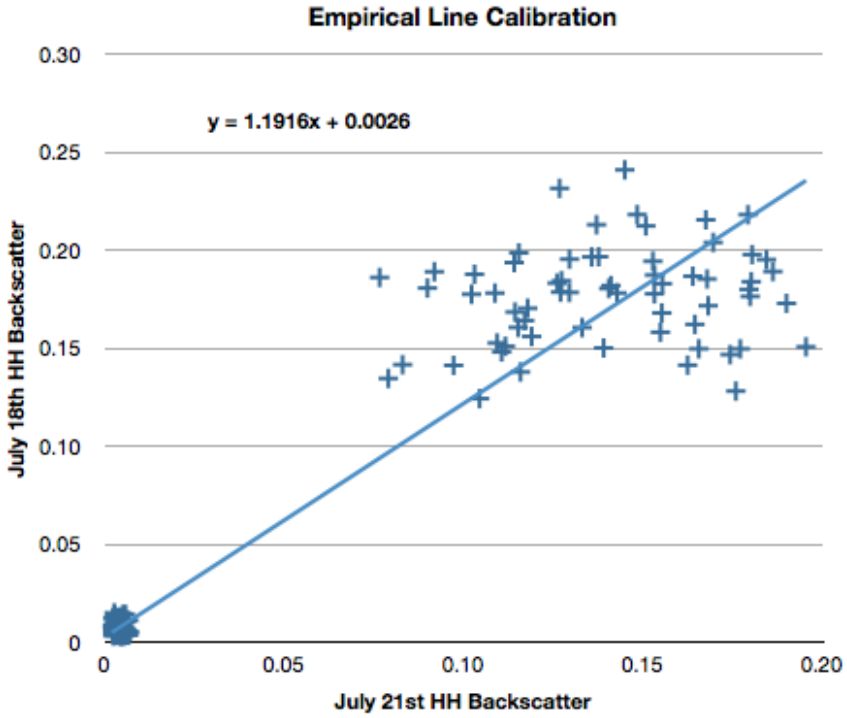

Figure 3-6 Empirical Line Calibration between two images acquired in July: HH backscatter amplitude.

This technique did not produce a perfect match between the two images for the reasons described above. This will have consequences later in the analysis.

3.4.5 Topographical Correction of SAR Data

Topographical correction is often necessary as SAR backscatter can increase or decrease over

similar land cover types depending on the incident angle. The incident angles reported in the image metadata assume the terrain is completely flat. If the terrain slopes towards or away from the SAR sensor, the backscatter will be affected by either increasing or decreasing the energy returned to the sensor. The relationship between the radar backscatter and topographical effects is described in the following equation (6) from Hinse et al. 1988:

$$\sigma = m*\cos I + b \quad (6)$$

where in σ is the SAR backscatter, and m, and b are fitted parameters and I is the local incident angle in radians. The calculation of the local incident angle requires knowledge of the terrain and the geometry of the RADARSAT-2. Information on the RADARSAT-2 was available in the metadata file; the terrain information was to come from a digital elevation model or DEM. The higher the quality of the DEM the better estimate of local incident angle. The local incident angle is defined as follows (Equation 7), again from Hinse et al. 1988

$$\cos I = cos\theta cosP + sin\theta sinP(Az - Ac) \quad (7)$$

Where I is the local incident angle in radians, θ is the flat terrain SAR incident angle in radians, P is the slope value, (measured as a percentage) of a single pixel, Az is the aspect, the direction towards which a slope faces, of the pixel, and Ac is the azimuth of the RADARSAT beam. If the local incident angle differed significantly from the flat terrain SAR incident angle then topographical correction would be necessary. To test this hypothesis the local incident angle was calculated for the study area.

A quality DEM was necessary, and the ASTER 15 m DEM (Fujisada, et al., 2005) was chosen to represent the terrain. Using the internal tools provided with the PCI Geomatica software, slope and aspect were calculated. RADARSAT-2 azimuth was calculated from the information given

in the metadata. The satellite's elevation and position were recorded in the metadata, and online tools were used convert this x, y, z coordinate into an azimuth. The local incident angle calculation was completed in the EASI modeler in PCI. While the local incidence angle did vary within each site (+/- 2^{o}) the average angle was no different than the SAR incident angle (See Table 3-3). Therefore topographical effects are not important for the 11 sites, as each site is represented by the average of the pixels within 100 x 100 m area rather than the individual pixels themselves. The Frenchman river valley is located within the park and the local incident angle does vary significantly within this feature, however no data was collected on those slopes. If these areas were to be included into the analysis, both additional ground data and topographical correction would be required.

Table 3-3 Local Incident Angle versus the flat terrain SAR incident angle. Areas where the local incident angle exceeded the flat terrain SAR incident angle are highlighted in grey

Site	Mean Local Incident Angle	SAR Incident Angle
Site 01	41.4	40.2 - 41.6
Site 02	42.1	40.2 - 41.6
U0	41.5	40.2 - 41.6
U1	41.7	40.2 - 41.6
U4	42.9	40.2 - 41.6
G0	40.4	40.2 - 41.6
G1	41.6	40.2 - 41.6
G4	42.2	40.2 - 41.6

3.4.6 Atmospheric and Radiometric Correction for Landsat-5 Images.

Unlike the SAR images, images from optical sensors, such as the Landsat-5, require atmospheric correction. No atmospheric parameters were collected during the study, therefore only correction

algorithms with a pre-defined atmospheric model can be applied. One such algorithm is the ATCOR-2 correction in PCI Geomatica. The ATCOR correction was implemented without using a DEM, meaning the terrain was assumed to be flat. The gain and offset calibration coefficients, that are necessary for the correction, were derived from metadata file attached to each Landsat-5 image. Applying the gain and offset to original dimensionless DNs will convert the raw data to units of radiance.

Gain and offset were derived as follows in equation 8:

$$Gain = \frac{Lmax - Lmin}{255}$$

$$Offset = Lmin \quad (8)$$

where *Lmax* is the spectral radiance in units of watts per square meter per steradian per wavelength (W/m^2 sr μm) scaled to the maximum digital number (DN), and *Lmin* is the spectral radiance (W/m^2 sr μm) scaled to the minimum DN (Chander et al., 2007).

After entering the date, gain and offset, and solar angle information the program was run with one of its pre-defined atmospheric models.

Normally at this point the images would be geocorrected, however the data in the USGS archive had already been orthorectified. It was not necessary to re-do this process.

CHAPTER FOUR

RESULTS AND DISCUSSION

4.1 Relationships among Biophysical Properties and RADARSAT-2 Backscatter

4.1.1 Weather

The summer of 2011 was wetter than the norm; 88 mm of precipitation was recorded at the Val Marie weather station in the month of May, compared to the 30 year average (1971-2000) of 48 mm. The cumulative precipitation per month dropped steadily over the growing season while still remaining above average. The majority of growing season's precipitation occurred in May and June. Mean daily temperatures reached their peak in July (See Figure 4-1).

4.1.2 SAR Backscatter

SAR backscatter amplitude for all sites was at its maximum in June, increasing slightly from the May acquisition, and steadily decreasing throughout the growing seasons; reversals in this trend occurred only when precipitation fell on the site. The steady decrease in backscatter mirrored a trend in the precipitation data. The backscatter time series described a sinusoidal curve similar to vegetation index time series calculated from optical data. The vegetation index curve is known follow plant phenology. However, the SAR curve is out of phase with plant phenology time series curve; it reached a peak in June, while the peak green of the grasslands occurred in July. The SAR backscatter is sensitive to ground features other than grass phenology. The work of Van Der Velde and Su (2009) argues that SAR backscatter variation is highly correlated with soil moisture.

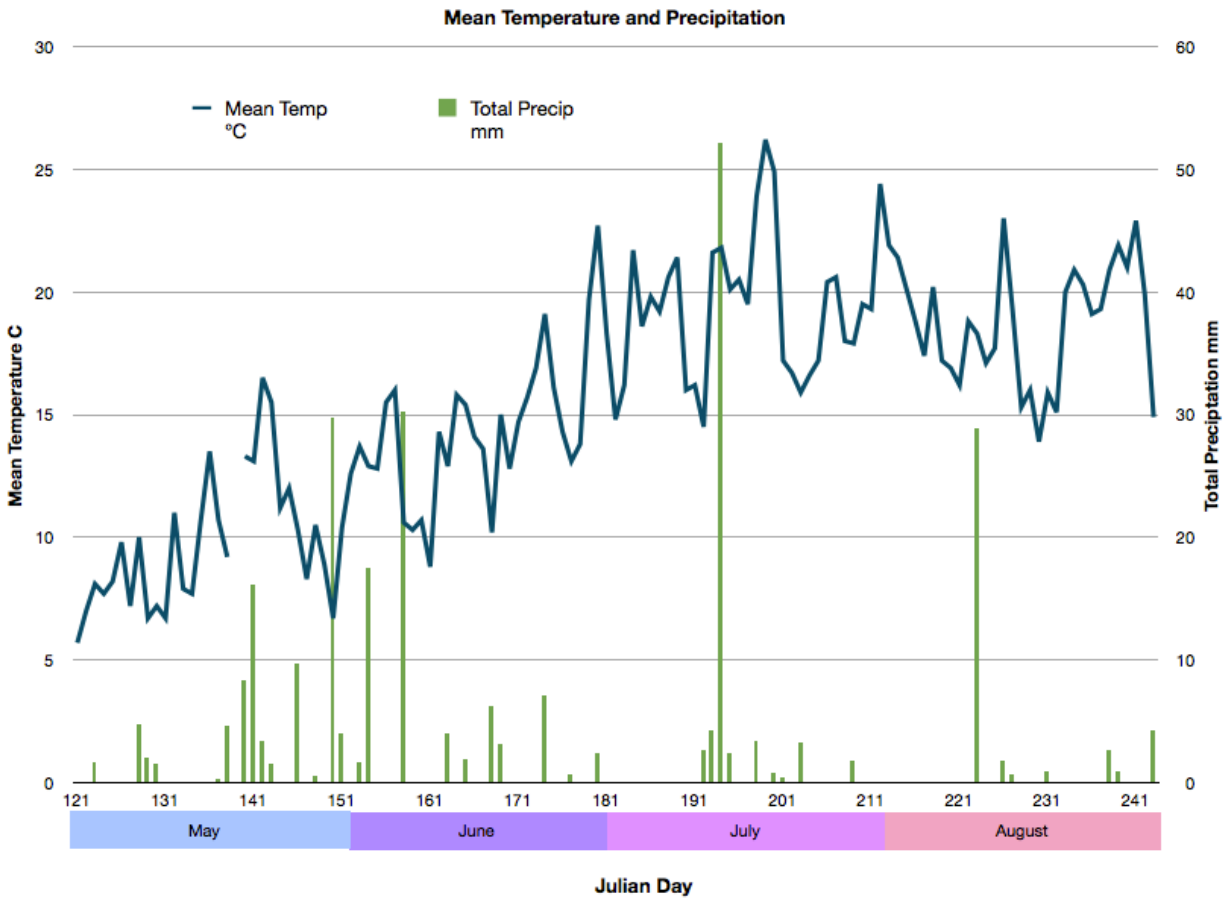

Figure 4-1 Mean daily temperature and precipitation recorded at the Val Marie weather station.

Therefore the arc of the SAR curve likely represents the moisture available within the near surface soil. This was partially confirmed by the ground data collected in June. Near surface soil moisture could explain a large portion of the variation in SAR backscatter. Two images could explain even more (see next section). There is a clear lag between the maximum near surface soil moisture and the green peak of the vegetation.

A precipitation event was captured by the August 11 acquisition (Figure 4-2). The rain footprint is clearly visible in the multi-polarimetric image (Red HH, Green, HV, and Blue in the cross polarization band). The large bright area is the rain footprint.

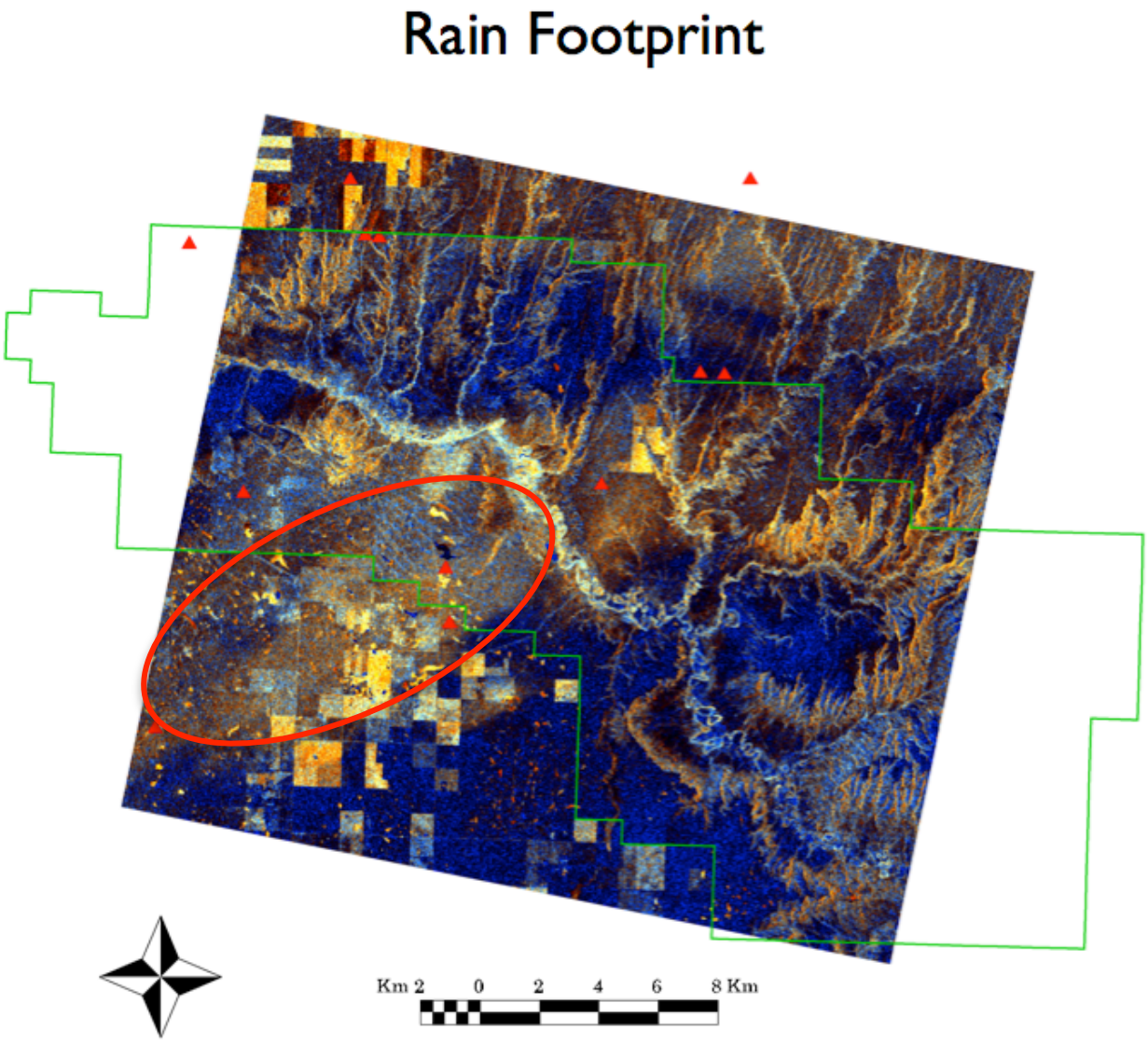

Figure 4-2 August 11th False colour Multipolarimetric SAR image. The rain footprint can be seen in the southwest as brighter area. The footprint has been circled in red.

The SAR time series are presented in Figure 4-3. For context the SAR backscatter was plotted along with the precipitation data. The rain event is the green spike near Julian day 220. It is the fourth largest spike in precipitation during the study period.

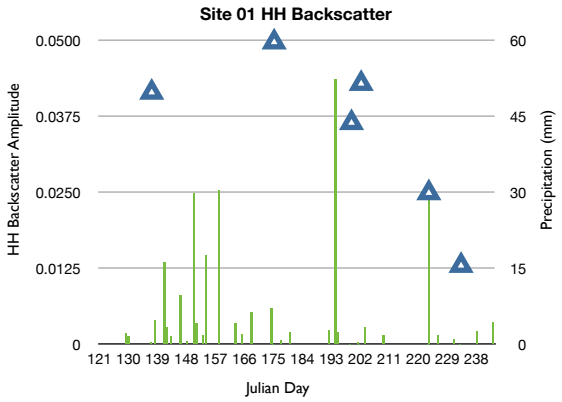
Site 01 HH Backscatter
HH Backscatter Amplitude
0.0500
0.0375
0.0250
0.0125
0
Precipitation (mm)
60
45
30
15
0
121 130 139 148 157 166 175 184 193 202 211 220 229 238
Julian Day

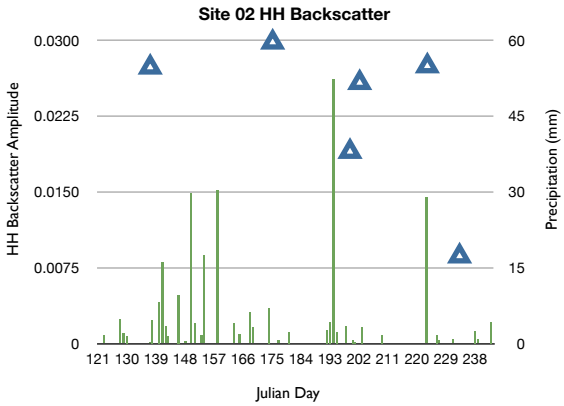
Site 02 HH Backscatter
HH Backscatter Amplitude
0.0300
0.0225
0.0150
0.0075
0
Precipitation (mm)
60
45
30
15
0
121 130 139 148 157 166 175 184 193 202 211 220 229 238
Julian Day

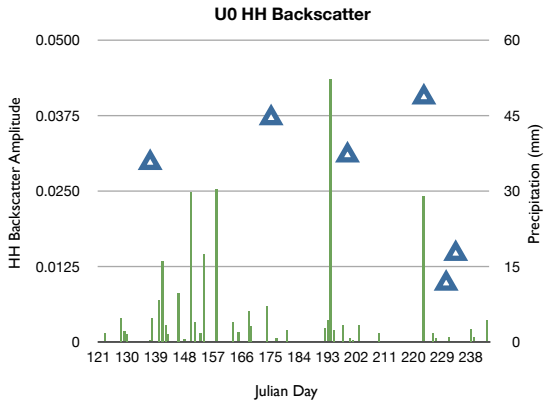
U0 HH Backscatter
HH Backscatter Amplitude
0.0500
0.0375
0.0250
0.0125
0
Precipitation (mm)
60
45
30
15
0
121 130 139 148 157 166 175 184 193 202 211 220 229 238
Julian Day

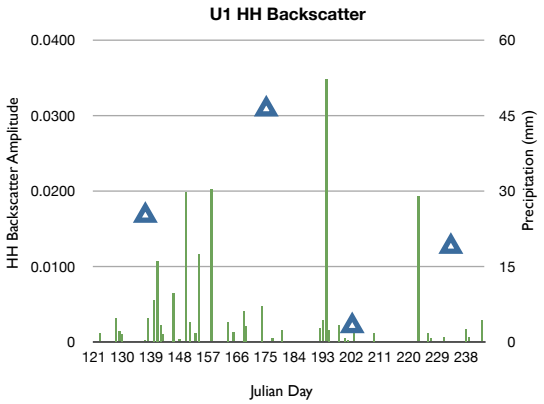
U1 HH Backscatter
HH Backscatter Amplitude
0.0400
0.0300
0.0200
0.0100
0
Precipitation (mm)
60
45
30
15
0
121 130 139 148 157 166 175 184 193 202 211 220 229 238
Julian Day

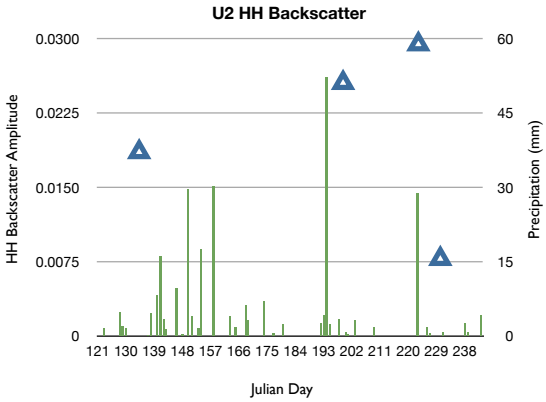
U2 HH Backscatter
HH Backscatter Amplitude
0.0300
0.0225
0.0150
0.0075
0
Precipitation (mm)
60
45
30
15
0
121 130 139 148 157 166 175 184 193 202 211 220 229 238
Julian Day

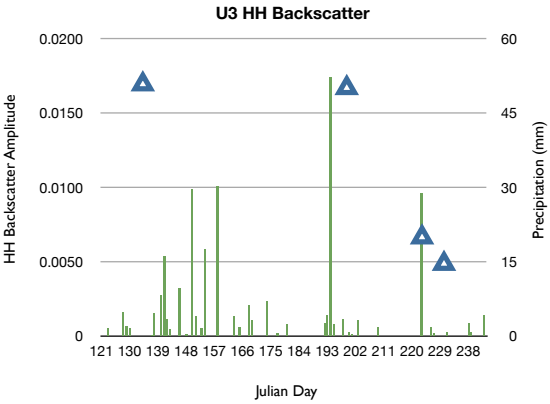
U3 HH Backscatter
HH Backscatter Amplitude
0.0200
0.0150
0.0100
0.0050
0
Precipitation (mm)
60
45
30
15
0
121 130 139 148 157 166 175 184 193 202 211 220 229 238
Julian Day

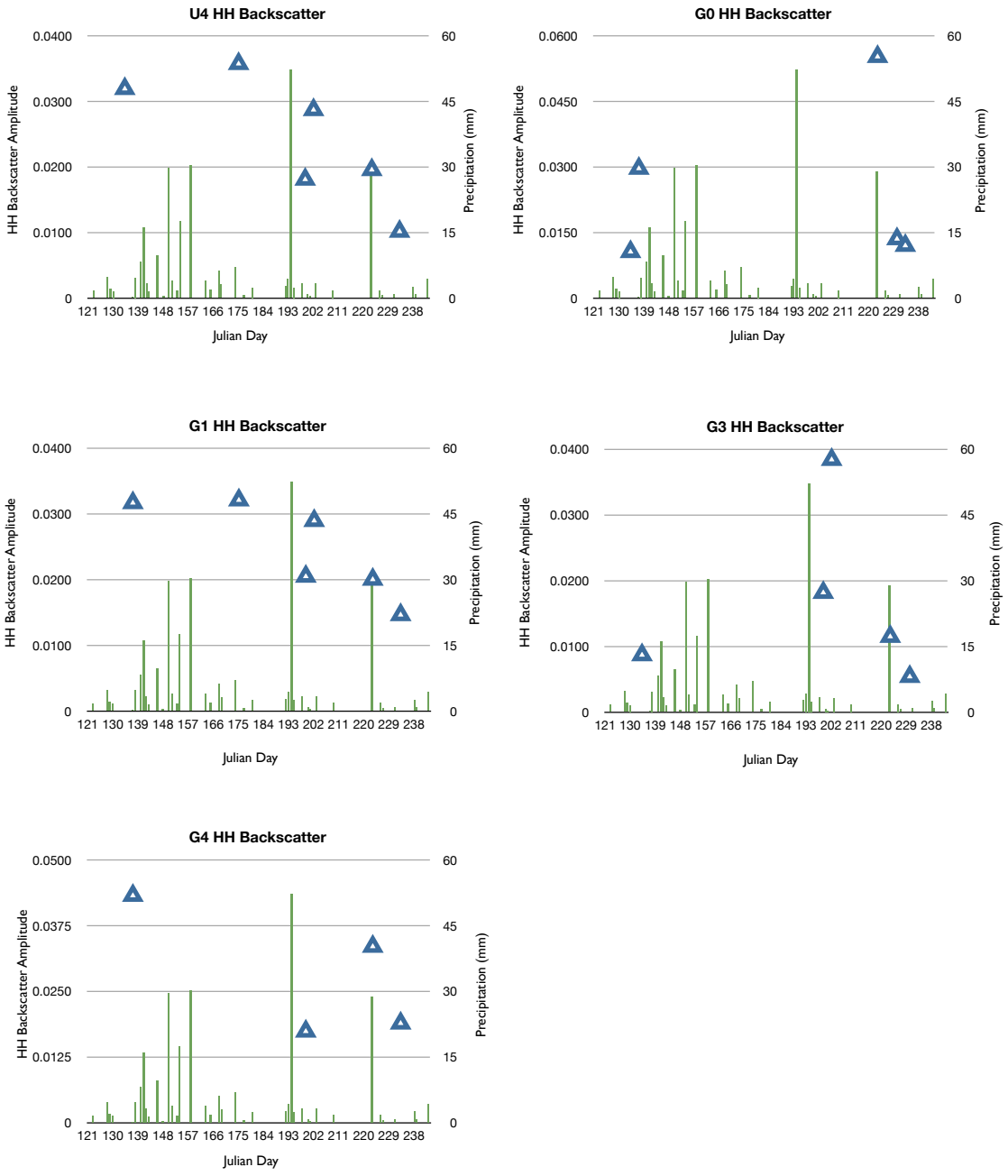

Figure 4-3 Backscatter amplitude over time: Given the strong relationship with moisture, the HH backscatter (blue triangle) has been plotted along with the precipitation (green bar). The effects of the rain footprint are visible in sites: U1, U2, G0, and G4. Backscatter is highest in May and June (Julian Day 121 – 181) afterwards it begins to decrease. The decrease in soil moisture is thought to be responsible for most of the decrease in backscatter. There are other factors that can affect backscatter other than moisture. Exactly what other factors are in play is unknown as the sites were only visited once. Had they

been visited at every acquisition more would be known.

4.1.3 NDVI Time Series

The NDVI values were derived from the Landsat-5 imagery, and since this satellite has a revisit time of 16 days, only four images were captured over the period of May to August. The above average precipitation levels were apparent in the May imagery, as the landscape contained multiple ponds. The image acquired in May held the lowest NDVI values. Normally the peak green or peak NDVI occurs in June, however the above average precipitation levels at the park delayed the peak green to July in the year of 2011, after which the NDVI values began to fall (Figure 4-4). This pattern represented the phenological changes expected of a grassland in a higher latitude. The growing warmth of spring allows for the perennial grasses to leave their dormant stage and begin producing green leaves. This stage is known as greening up. The grasses will continue to grow and increase biomass production until the plants shifts from growth to reproduction. At this stage the grass will stop using energy to create more biomass and will shift to creating reproductive structures such as flowers and seeds. This point in the grasses' life cycle is known as peak green. After the peak green the plant is producing no more biomass. The hotter and dry months of July and August can send the grasses back into dormancy, meaning they stop active photosynthesis. If the grass is an annual, this senescence marks the end of its life cycle. The result is a steady decrease of NDVI as fall approaches and more grasses become dormant or dead.

The temporal resolution of the Landsat-5 data was far too coarse to compare with the climate data in any great detail (Figures 4-4, 4-5, and 4-6).

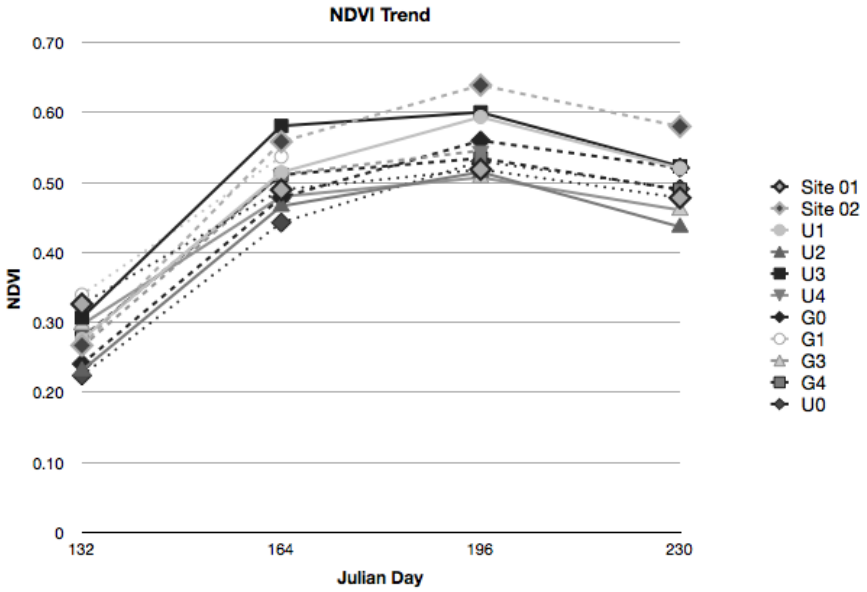

Figure 4-4 NDVI Trend for the months of May, June, July, and August. Note that peak green occurs in July.

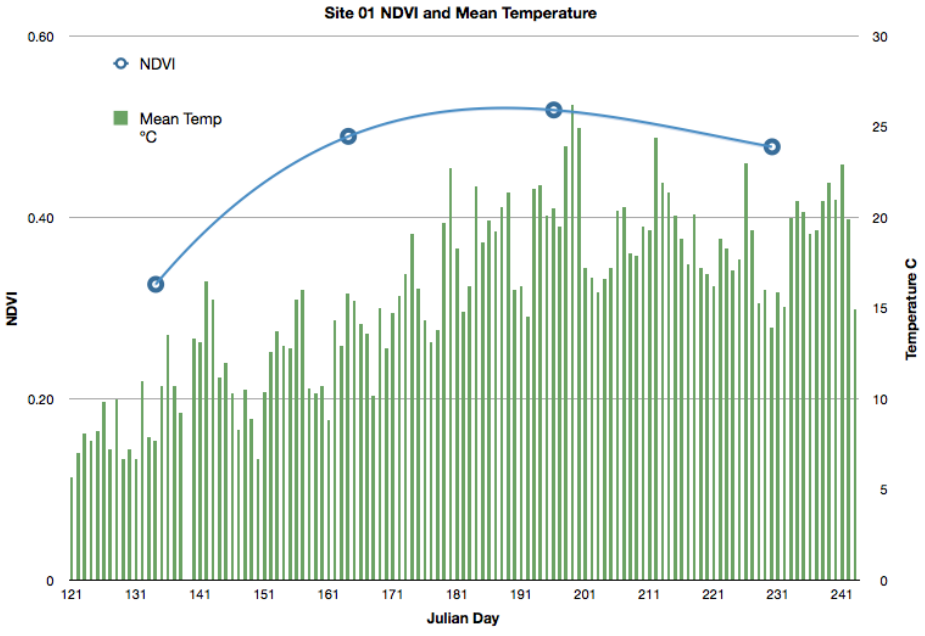

Figure 4-5 NDVI Trend in blue and mean daily temperature is represented in green.

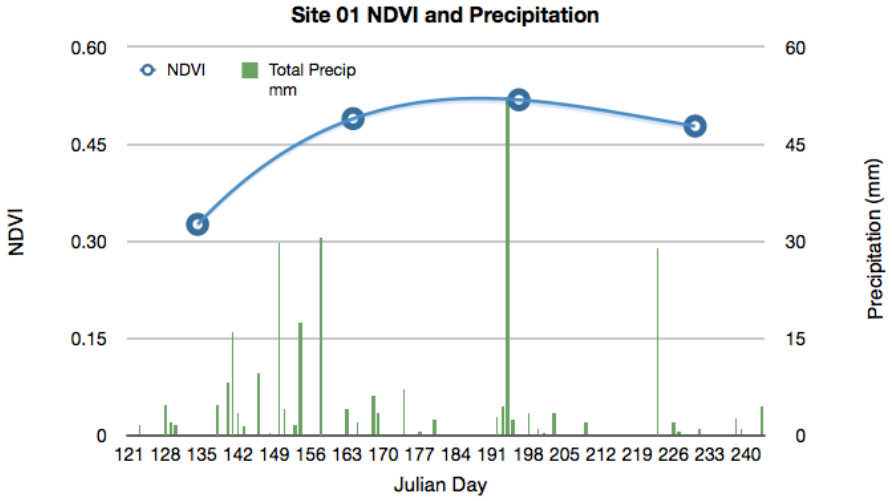

Figure 4-6 NDVI Trend and daily precipitation for Site 01.

There is no rise and fall of NDVI values that is linked with the precipitation information (See Figure 4-6). Since the temporal resolution of the climate data is far greater than the temporal resolution of the Landsat – 5 NDVI images, this makes comparison of the two data sets extremely difficult. As the mean temperature rises so do the NDVI values (Figure 4-5). This is still a coarse correlation as the temporal resolution of the two data sets is so different.

4.1.4 Volumetric canopy moisture (VCM) and biomass

Plant materials collected from the field were sorted into *green grass*, *forbs* and *dead materials*. The water cloud model as defined by Attema and Ulaby (1978) models the canopy as a mist of water droplets. In order to relate canopy water content to other biophysical parameters, it is instructive to explore the relationship VCM has with biomass.

Table 4-1 Results of the linear regression between biomass type and VCM.

Biomass g/m^2	Slope	p-value	Intercept	p-value	R^2
Dead .	-23.3	0.084	3341	0.002	0.30
Forbs	2.27	0.79	1749	0.02	0.01
Green Grass *	38	0.04	1069	0.03	0.38
Total Green Biomass (grass + forbs)	0.02	0.31	53	0.16	0.12

In table 4-1 a "." indicates the relationship is significant to the $p < 0.1$ level and a "*" is significant at $p < 0.05$. R^2 is the coefficient of determination of the linear regression. The table reports that green grass biomass is positively correlated to VCM, while dead biomass is negatively related to canopy moisture. Since grasses were plentiful in the study area, it is to be expected that the more live green grass contained in the sample the greater the VCM. Dead biomass has ceased photosynthesis and has largely desiccated. Forb biomass had no relationship with volumetric canopy moisture; one possible reason for this is that forbs were poorly represented in the study area. Total green biomass, that is the sum of green grass and forbs, was also not significant; this is most likely the result of the poor relationship between forbs and VCM.

4.1.5 Soil Moisture and SAR Backscatter

The SAR time series displayed a decreasing trend throughout the growing season. There are several possible interpretations for this trend. Surface roughness and moisture content are the two parameters responsible for the majority of the variation in backscatter. A decrease in soil moisture throughout the summer seems more likely than a decrease in surface roughness.

There is a positive correlation between soil moisture and the backscatter amplitude as would be predicted by the literature (Figures 4-7 and 4-8). The charts plot backscatter and soil moisture for the June 24th image only. Not all sites were represented by this image, however the noise caused

by the mosaicking process is absent in these charts.

There is a positive correlation between backscatter and soil moisture with R^2 values of 0.41 and 0.37 for the HH and HV images respectively. The HH image has a larger backscatter amplitude than the HV image. For this reason all subsequent modeling is performed on the HH image. However this relationship reported here is not significant; other researchers (Natalie et al., 2009, Van der Velde and Su, 2009, Thoma et al., 2006) have reported a similar correlation between the backscatter of a single image and soil moisture that was statistically significant.

Thoma et al (2006) developed an indicator known as the Delta Index, which they used to predict near surface moisture. The index is computationally simple; see Equation 2 in Chapter 2. The index relies on a comparison between a relatively wet and dry image. The driest SAR image would have the lowest backscatter values in Figure 4-3.

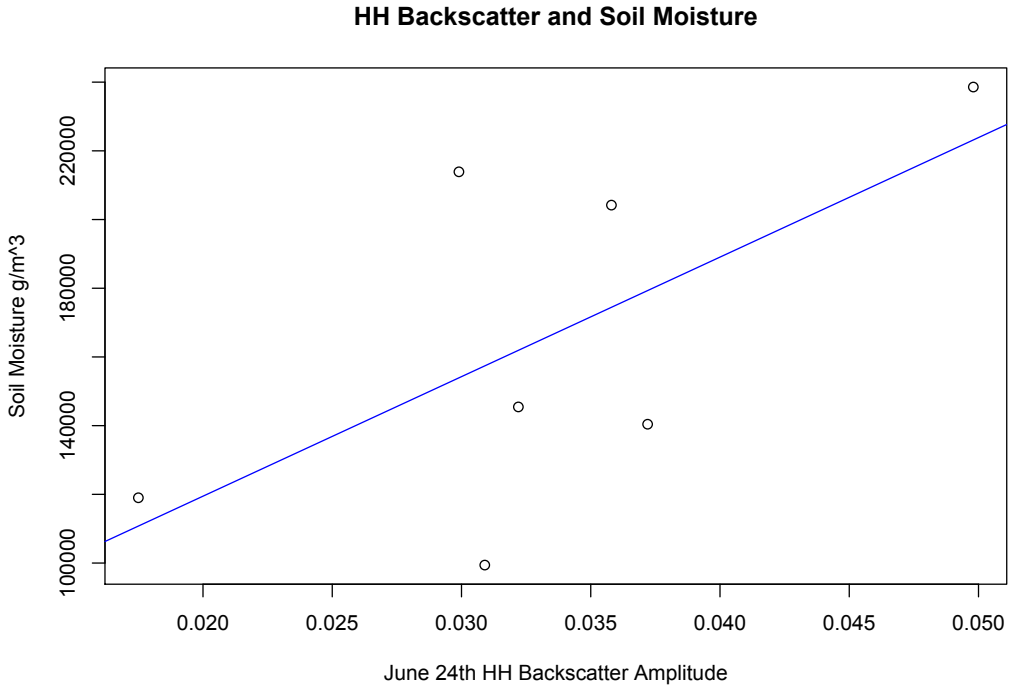

Figure 4-7 A simple linear regression between soil moisture and HH backscatter amplitude.

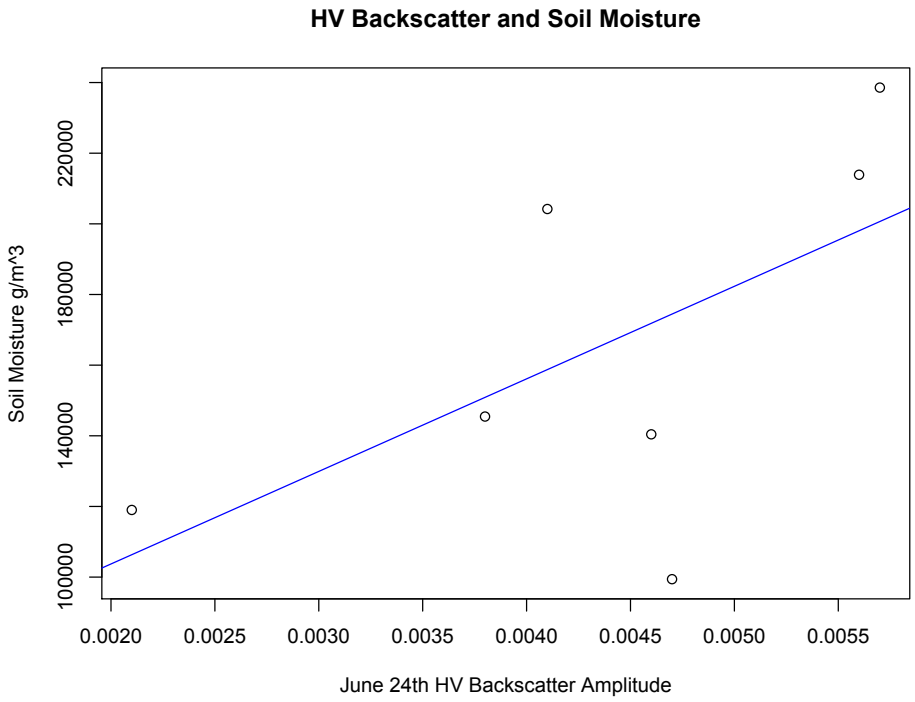

Figure 4-8 A simple linear regression between soil moisture and HV backscatter amplitude.

The lowest backscatter images were the August 18th and 21st mosaic and this was designated as the dry image. The June 24th and July 18th mosaic was chosen as the wet image. This image was chosen because it corresponds with the ground data acquisition, it is also likely the wettest image in the time series for two reasons. One, the climate station in Val Marie recorded the majority of the precipitation falling in May and June (See Figure 4-1) and two, the June/July mosaic had the highest backscatter values of the entire time series.

Figures 4-7 and 4-8 suggest that a higher backscatter amplitude is associated with greater level of soil moisture. By subtracting a dry image from the wet image variations in surface roughness are subtracted out leaving the soil moisture information. The Delta Index observed here does not have as high R^2 that has been reported in Thoma et al. (2006). This analysis used mosaicked images and the matching of digital numbers between the June and July images was not without

problems. The mosaicking processing added unexplained variation in the backscatter values. The Delta Index from the mosaicked images had a R^2 of 0.60 and was significant at the $p < 0.001$ level (Figure 4-9).

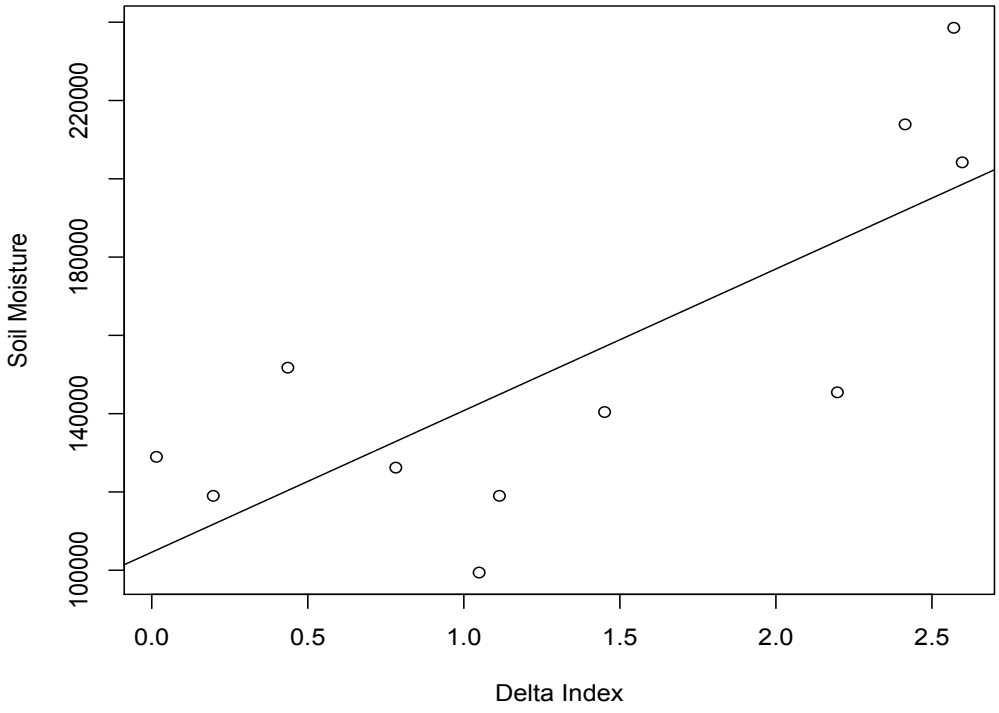

Figure 4-9 Delta Index and Soil Moisture, a stronger correlation than a single image backscatter.

Soil Moisture = 36181g/m^3*Delta Index + 104600g/m^3 (9)

Equation 9 is the derived relationship between Delta Index and soil moisture. Soil moisture is represented in units of g/m^3 and the Delta Index is dimensionless. The slope and intercept were fitted using general linear regression.

The Delta index can be calculated for the months of May, June, and July, using the August mosaic as the dry image. When comparing the Delta Index calculated in these other months to the soil moisture data collected in June, there is a correlation. However the correlation was not as strong as the one for the June image. The coefficient of determination was strongest in June and

weakest in July. This could explain why the June/July mosaicked image did not have the strong correlation reported in by Thoma et al (2006). If only the June 24th image is used, i.e. not using the July image, the coefficient of determination R^2 rises to 0.80 and remains significant at $p < 0.01$, even though not all sites could be included (Figure 4-10).

Still, the Delta Index can be used to represent soil moisture in the study area even if a mosaic is used. However the two scenes to be mosaicked should be much closer together in time. Two images from the same month are preferred, since the correlation was always weaker for other months.

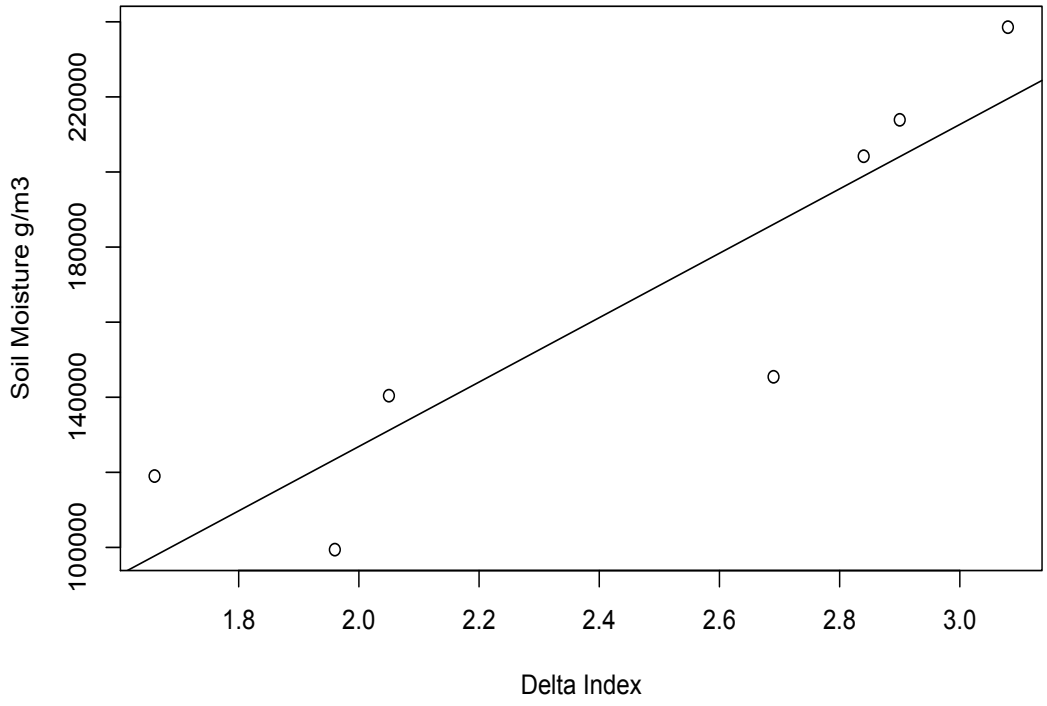

Figure 4-10 Delta Index and soil moisture from a single RADARSAT-2 scene. There are fewer points, however the correction is far stronger.

The soil moisture image was grouped into classes representing different values of soil moisture (Figure 4-11). The intervals between classes were smallest in the more common soil moisture

regimes and coarser for the extremes. The difference between the western and eastern portions of the west block is immediately apparent. This image is a fusion of four different images. The eastern portion had to be mosaicked, for both the wet (June and July) and dry (August) images. The errors resulting from both processes have cumulated, causing the discontinuity. For clarity the results from a single (unmosaicked) image are presented here as well (Figure 4-12). This image contains only the June 24 (wet) and August 21 (dry) images and contains only seven data points.

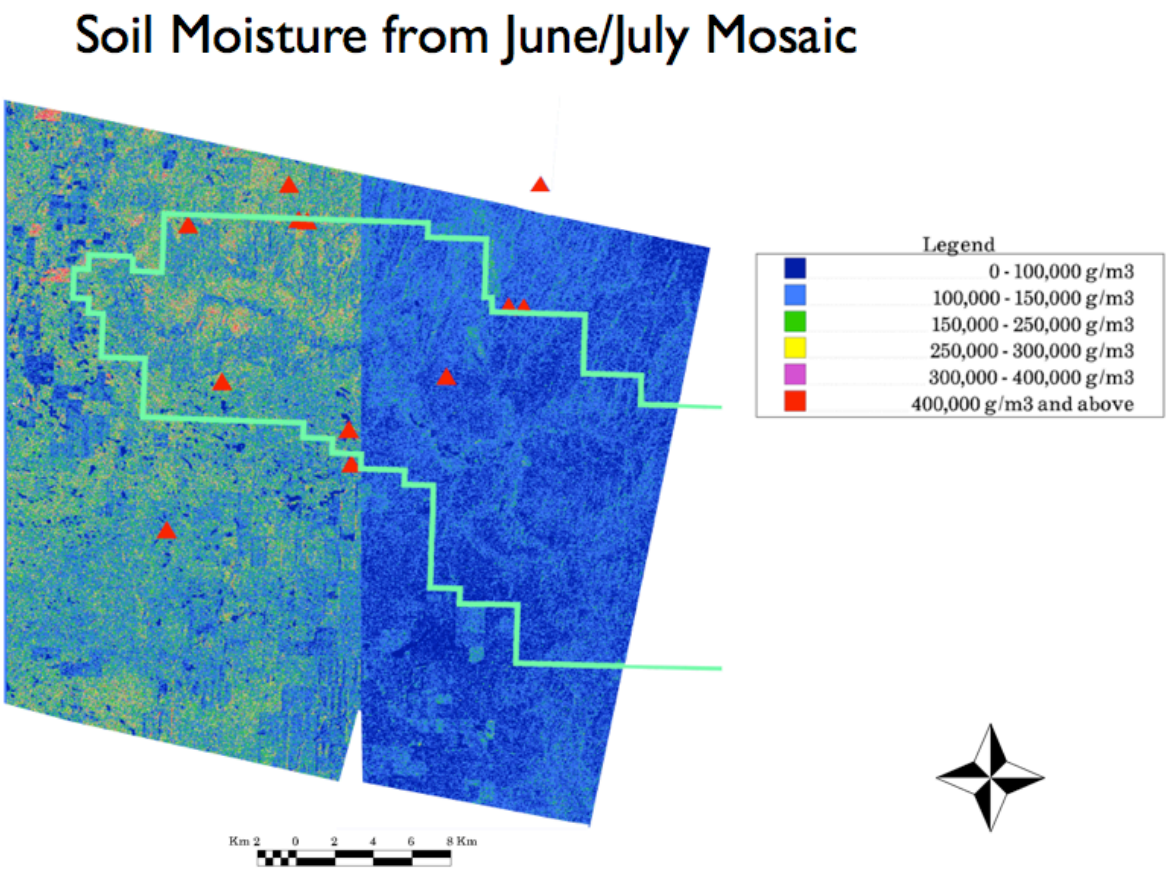

Figure 4-11 Mosaicked soil moisture image. The darker half is the dryer July imagery.

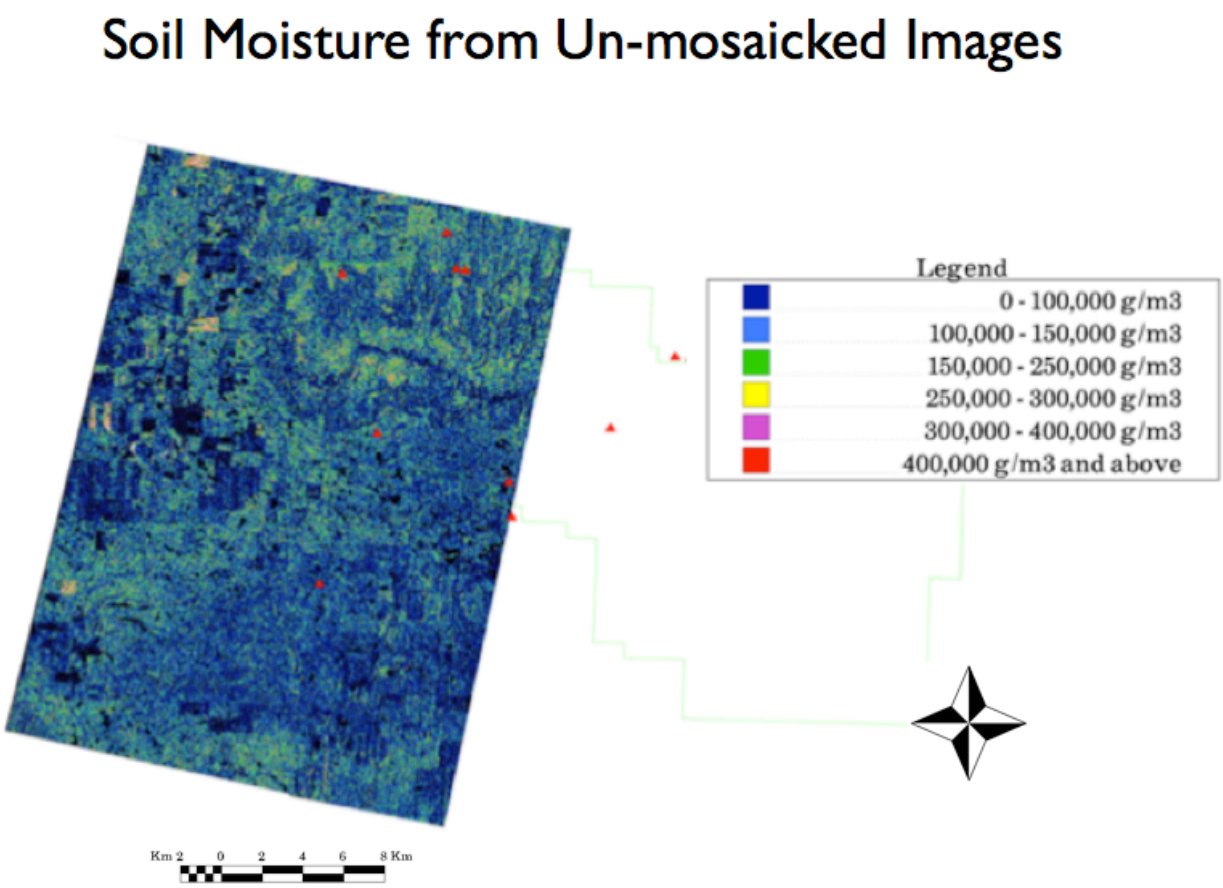

Figure 4-12 The June 24th soil moisture image.

4.1.6 Cross Polarization Ratio and Plant Form Diversity

The cross polarization ratio is the ratio of the cross-polarimetric mode HV to the co-polarization mode HH (Equation 5) squared. This ratio is sensitive to the different kinds of scattering processes that may occur when the incident beam interacts with the target.

In the study area the grass dominated area represented a smoother surface (surface scattering), which returned a low amplitude backscatter in the co-polarized mode (HH), and even lower amplitude in the cross-polarized mode (HV). Only in the shrubs dominated areas surrounding the Frenchman river did the cross-polarized mode have an equivalent or greater amplitude than the

co-polarized mode, due to the shrubs being volume scatterers. For shrubs, the incident radar beam undergoes multiple scattering off the leaves and branches before being returned to the sensor. Higher amplitudes in the cross polarization (HV) mode are indicative of a volume scatterer.

Calculating the cross-polarimetric ratio is simple, however the output is extremely noisy even with the 9 x 9 median filter applied to the original HH and HV images. Immediately apparent in the cross-polarimetric ratio image (Figure 3.5) are the shrubs surrounding the Frenchman river.

To study the relationship between the cross-polarimetric ratio and the diversity of plant forms, diversity must be quantified using a metric. The Simpson Index is defined as the probability that two samples drawn at random will represent the same type (Simpson, 1949). For this study, it will be defined as the probability that two plant forms drawn at random will represent the same form. The Simpson's Index is defined as follows (Equation 10):

$$\lambda = \sum_{i=1}^{j} p_i^2 \qquad (10)$$

where j is the total number of plant forms and p_i is the proportion of the ith plant form. In this study, proportion is defined as the fraction of the total canopy cover that is occupied by the ith plant form.

The Shannon Index is another diversity index; unlike the Simpson Index it measures entropy. Entropy in this context is a measure of information content, or the difficulty in predicting the identity of a sample drawn at random. This index was not developed for ecology; rather it was conceived as a means to measure information in a string of text (Shannon, 1948). If a site contained nothing but the grass plant form, it would have a very low entropy, and little information content as it would be trivial to predict the identity of the next sample drawn from

the site. As the number of plant forms present increases, the entropy increases, and the uncertainty in predicting the identity of the sample grows as well. The site is at maximum entropy if the proportions, i.e. fraction of the total canopy cover, of each plant form are equal and the uncertainty in the identity of the next sample is at its greatest. Shannon's Index is derived from the following formula (Equation 11):

$$H' = -\sum_{i=1}^{j} p_i log p_i \quad (11)$$

where j is the total number of types, and p_i is proportion of type i.

There are multiple ways to interpret the data returned from the field. There are four plant forms within the park: *grasses*, *forbs*, *moss*, and *shrubs*. There are also dead materials such as the standing dead grass, and the litter layer. While the standing dead grass is still a grass plant form, its moisture content is different than the living biomass (See Section 4.4). There are other cover types in the study area that are not plant forms but could also impact backscatter amplitude, such as bare soil. Given the small percentage coverage of rock and bare soil they are unlikely to make a significant contribution.

The percentage canopy coverage for all cover types are summarized in Table 4-2. While data had been collected for site G2, the RADARSAT-2 mosaics do not overlap this site. As it plays no role in the analysis it has therefore been omitted from these tables.

Table 4-2 Percentage Canopy Cover for all sites.

Site	Grass	Forb	Shrub	Standing Dead	Lichen	Moss	Litter	Rock	Bare Soil	Total
Site 01	28	6	0	12	0	10	33	4	5	100
Site 02	29	13	0	26	0	4	28	0	0	100
U0	24	13	0	32	0	11	16	2	3	100
U1	36	12	0	21	0	11	19	0	0	100
U2	28	7	0	31	0	9	23	0	2	100
U3	30	14	0	9	0	7	38	0	1	100
U4	21	11	0	26	0	18	23	0	0	100
G0	20	15	0	23	0	9	31	2	1	100
G1	29	8	0	18	0	19	26	0	1	100
G3	17	18	0	4	4	16	41	1	0	100
G4	23	10	2	13	0	14	35	3	0	100

Both the Shannon and Simpson indices were calculated from this full dataset. Since Shannon's Index measures entropy, if there is a relationship between the Cross-Polarization ratio and entropy this correlation will be positive. Simpson's Index is a measure of probability of two samples drawn at would be of the same type, as the entropy increases that probability will decrease. Therefore a negative trend is expected.

Using all the cover classes in Table 4-2 the expected relationships are not apparent (See Figures 4-13 and 4-14).

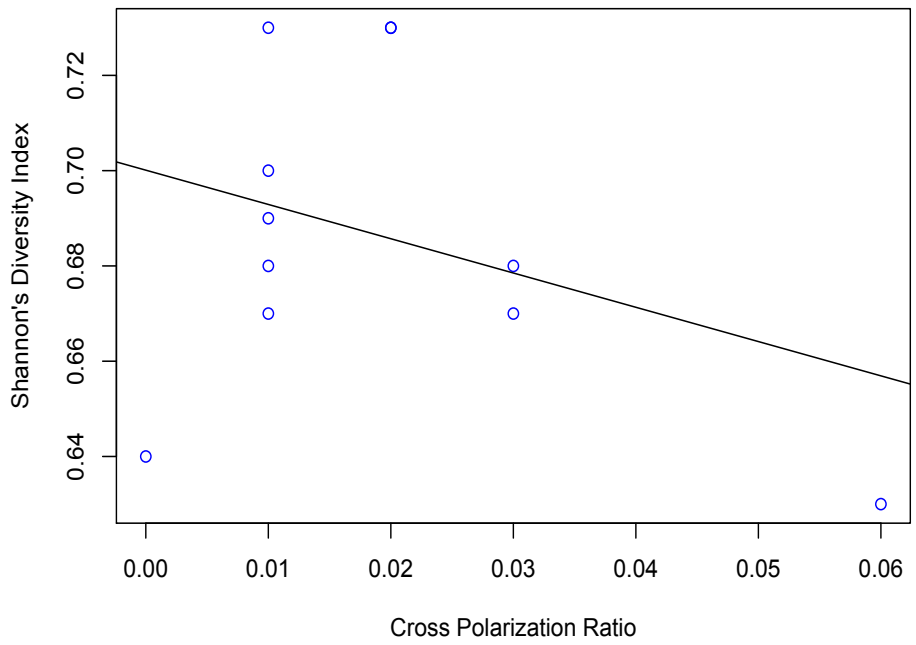

Figure 4-13 An unexpected negative trend between Shannon's Index and the cross polarization ratio.

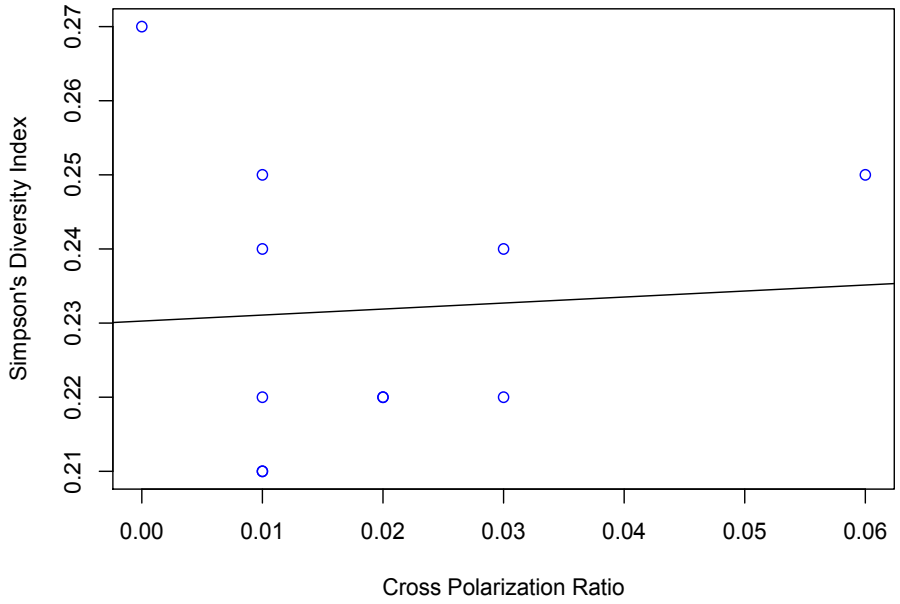

Figure 4-14 An unexpected positive trend between the Cross Polarization Ratio and Simpson's Diversity Index.

The actual trends are opposite to expectation. There is considerable variation is both plots; had the expected relationship existed, the model would have been of little use.

Restricting the data set to just the plant forms, i.e. removing such cover types as rock and bare soil, the two indices can be recalculated. When plotted against the cross-polarization the expected trends appear. The plant forms do represent most of the cover present in the study area (Table 4-3). Dead biomass is still being considered separate from living biomass due to the different moisture levels.

Table 4-3 Percentage of Canopy Cover for plant-form-only.

Site	Grass	Forb	Shrub	Standing Dead	Moss	Litter	Total
Site 01	31	7	0.3	14	12	36	100
Site 02	29	13	0.0	26	4	28	100
U0	25	13	0.0	34	11	17	100
U1	36	12	0.4	21	11	19	100
U2	29	7	0.0	31	9	24	100
U3	31	15	0.0	9	7	38	100
U4	21	11	0.0	26	18	24	100
G0	21	15	0.0	24	9	32	100
G1	29	8	0.0	18	19	27	100
G3	18	19	0.0	4	17	43	100
G4	24	10	2	14	14	36	100

In this plant-form-only analysis the expected relationships appear. However the model diagnostic tool available in the R statistical software revealed that one point had undue leverage on the result. It was removed and linear model was improved (See Figure 4-15 and 4-16).

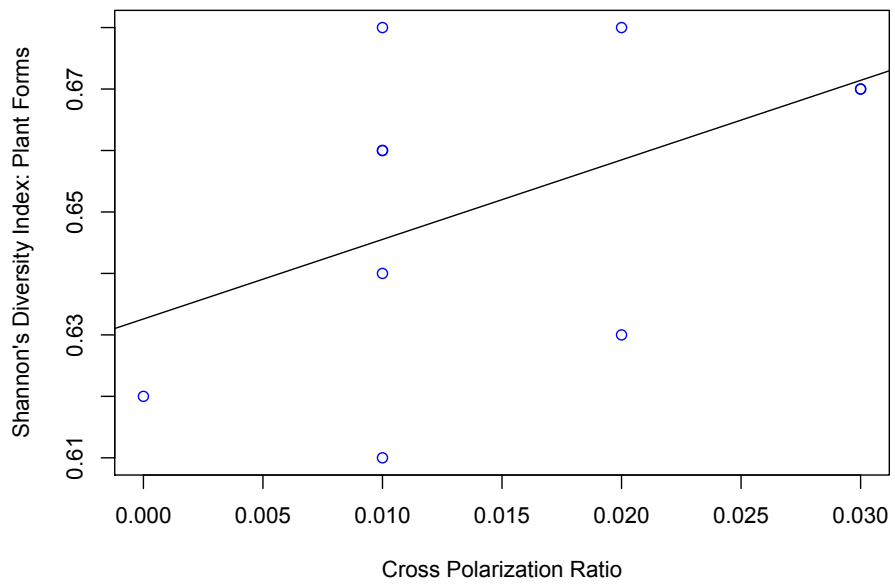

Figure 4-15 A positive trend is apparent between Shannon's Index and Cross Polarization Ratio.

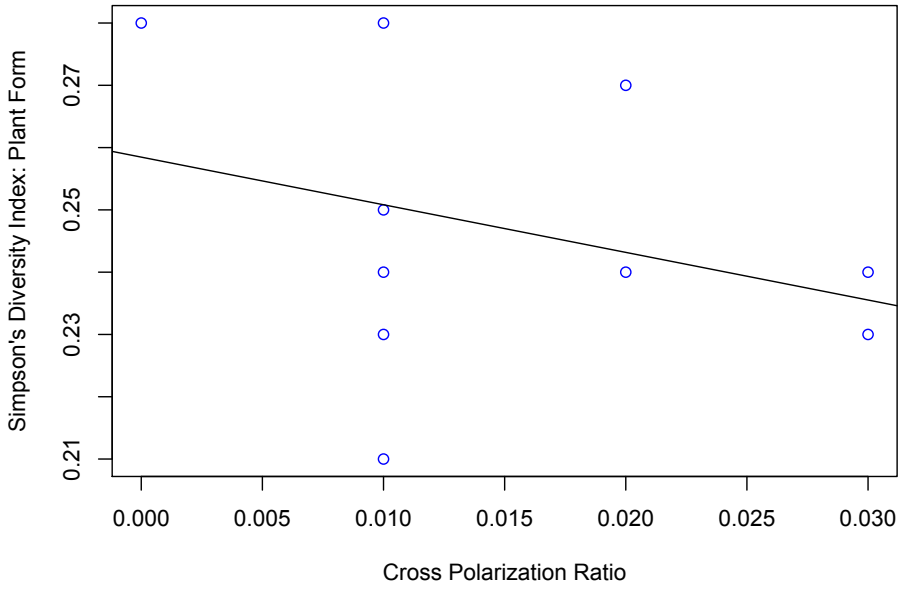

Figure 4-16 The expected trend between the Simpson's Index and the Cross Polarization Ratio.

The cross polarization ratio did have the expected relationship with the two diversity indices, however that relationship was noisy and subtle.

Both the Simpson and Shannon index had very small ranges between 0.21 and 0.28 for the Simpson Index, and 0.61 to 0.68 for Shannon Index. All of the ground samples were dominated

by grasses, live and dead, and in this one environment the relationships behaved as predicted by the definition of the indices. In a different environment, such as a shrub-dominated environment, the cross polarization ratio will be much higher and the relationship discovered here would not remain valid.

It is worth exploring texture measures of the cross-polarization ratio, as these are measures of variation. Measures of variation as a predictor of entropy may be more stable across different environments. This hypothesis cannot be tested with the ground data collected since all samples are in grass-dominated environments.

PCI Geomatica has several texture filters including entropy, homogeneity, standard deviation and others. The texture filters operate using a moving window, the size of which is chosen by the user. In this study the window size was chosen to be 11 x 11. The reason for this choice is that this window size was the closest to the site size of 100 m x 100 m. Four texture parameters were studied: homogeneity, contrast, standard deviation, and entropy. Homogeneity is a measure of the uniformity within the 11 x 11 moving window, the more similar the DNs within the window the higher the homogeneity. From this definition we can predict that homogeneity would be positively correlated with the Simpson Index, and negatively correlated with Shannon Index. Contrast is the opposite measure of homogeneity as it is a measure of variation. Therefore one can predict that contrast will be negatively correlated with the Simpson Index and positively correlated with the Shannon Index. Standard Deviation is a straightforward measure of variation and the same predictions that applied for contrast applies here as well. Entropy, in this case, is applied to the DN of the pixels within the moving window. Entropy here has its more classical definition of the logarithm of the number of microstates that have identical macro-states. If the pixels within the moving window are uniform the entropy will be very low. Entropy as measured

by the Shannon Index has a maximum value when the fractions of the total canopy cover of all plant forms are equal. The maximum entropy measured from the DN is constrained only by the radiometric resolution of the imagery. Therefore, this definition will allow values much higher than those allowed by the Shannon Index. It is clear that entropy measured by the texture filter should be positively correlated with the Shannon Index and negatively correlated with Simpson Index.

Using the diversity indices calculated from the full dataset, i.e. the values in Table 4-1, correlation values were derived for all indices (Table 4-4).

Table 4-4 Correlation Coefficient (R) between the texture variables and the two diversity indices.

Texture Measure	Simpson's Index	Shannon's Index
Homogeneity	0.04	-0.36
Contrast	-0.77**	0.71*
Standard Deviation	-0.61*	0.74**
Entropy	-0.08	0.41

where a '*' is significant at the $p < 0.05$ level, and a '**' significant at $p < 0.005$.

All texture measures have the expected sign in their coefficients, however only Contrast and Standard Deviation are significant (See Figure 4-17 and 4-18).

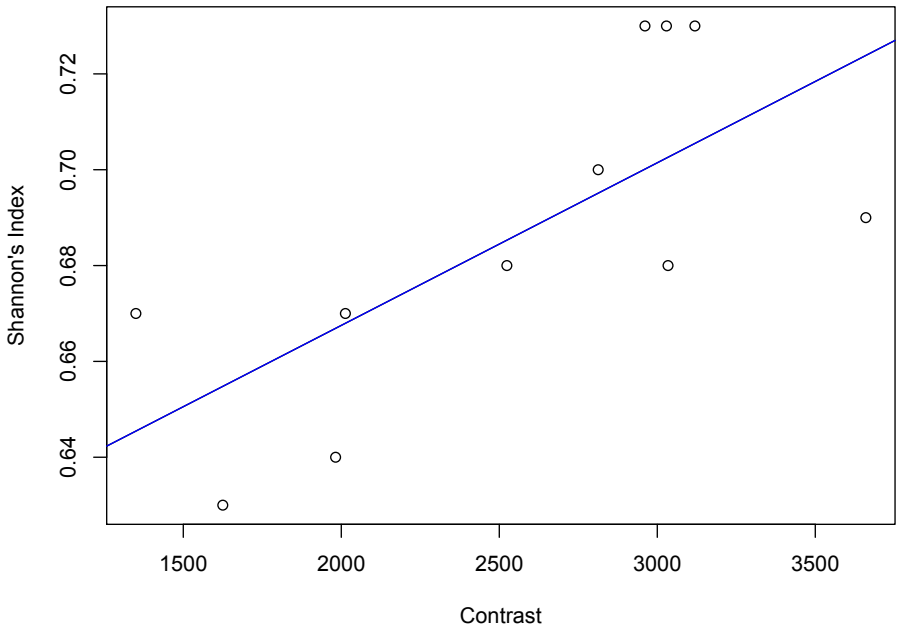

Figure 4-17 The relationship between Contrast and Shannon's Index. The positive trend is as expected from the definition of Shannon's Index.

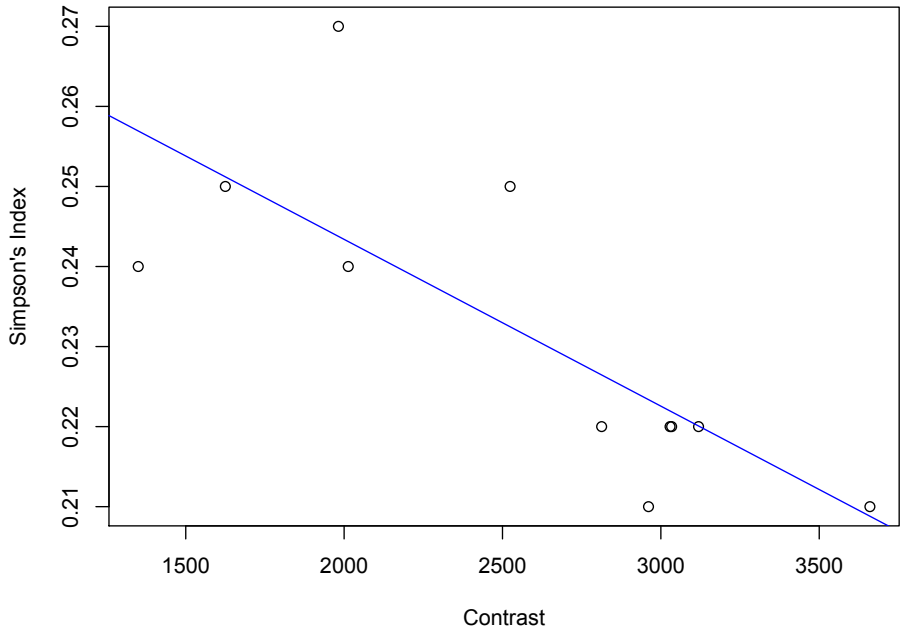

Figure 4-18. The relationship between Simpson's Index and Contrast. The negative trend is as expected from the definition of Simpson's Index.

Adjusting that definition of the Simpson and Shannon Indices for plant forms only creates a problem. The texture measures Homogeneity and Entropy no longer have the sign expected by definition (Table 4-5)

Table 4-5 Correlation Coefficient (R) for texture measures and plant form only diversity indices.

Texture Measure	Simpson's Index	Shannon's Index
Homogeneity	-0.22	0.15
Contrast	-0.44	0.51
Standard Deviation	-0.21	0.34
Entropy	0.20	-0.11

None of the correlation coefficients reported here are significant. Only Contrast and Standard Deviation take the expected sign. These two textures parameter had the strongest relationship with the diversity indices in the full dataset and remained reasonable with this restricted diversity dataset.

4.2 Extracting Biomass And Plant Form Diversity From Radarsat-2

4.2.1 Applying the Water Cloud Model

The water cloud model predicts radar backscatter given that certain properties of the vegetation canopy and soil are known. The model treats the vegetation canopy as consisting of mainly empty space with a random distribution of water droplets throughout. The VCM was measured using the procedure described in Section 3.2.1, and this measurement was to become the canopy parameter *L* in the water cloud equation (See Equation 1). *L* was interpreted as volumetric canopy moisture in the original Attema and Ulaby (1978) paper, however other researchers have interpreted L as leaf-area index (LAI) (Graham and Harris, 2003). Interpreting *L* as biomass as Svoray and Shoshany (2003) have done, is not appropriate in this environment as most of the biomass collected was non-photosynthesizing, i.e. dead biomass. As demonstrated in the previous chapter there is a relationship between volumetric canopy moisture and certain types of biomass, such as, green grass biomass. However the presence of dead biomass in the study area means that the relationship between green grass biomass and VCM is not a simple one; VCM and biomass are not interchangeable in the water cloud model. This research presents the canopy parameter *L* as representing canopy moisture, to do otherwise would violate the main assumptions of the model, namely, the assumption that the dielectric coefficient of dry vegetation matter is negligible. Biomass collected from the park did contain considerable amounts of dead materials. Non-photosynthesizing biomass has mostly desiccated and contains much less moisture than living plants. Attema and Ulaby (1978) when defining their water cloud model ignored the contribution of the dry vegetation to the scattering model.

Four site-specific parameters needed to be derived, see Equation 1. Given the backscatter, volumetric canopy moisture and the soil moisture the four parameters were fit using least-

squares non-linear regression. Once fitted the model could be employed to predict backscatter, however the parameter of interest is the canopy moisture parameter L. Therefore, the Equation 1 must be inverted (Equation 12).

$$L = -\frac{cos\Theta}{2B}\ln\frac{\sigma - Acos\Theta}{C + D(m_S - Acos\Theta)} \quad (12)$$

where L is the canopy parameter taken to mean volumetric canopy moisture in units of $\frac{g}{m^3}$, σ is the backscatter amplitude in units of $\frac{m^2}{m^2}$ or dimensionless, and m_s represents soil moisture also represented in units of $\frac{g}{m^3}$.

This new equation by necessity contains a natural logarithm, meaning the numerator and denominator must produce a value greater than zero; else the equation will be undefined. For the numerator that condition is satisfied if $\sigma > Acos\theta$. As m_s is a large number and $Acos\theta$ is a small number, the denominator tends to remain positive. The parameter A is crucial, as it will be subtracted from the backscatter amplitude. The value derived for A, in some applications of the water cloud model, represents a canopy with complete vegetation coverage (Graham and Harris, 2003). In this application such as definition for A does not apply. Bare soil was an extremely rare cover type and most sites had complete canopy coverage. Using the value fitted for A by the non-linear regression resulted in much of the grass dominated areas being undefined in the inverted model. If A were set to a value lower than the value derived in the least-square regression, more grassland will be captured. A was set by examining the image histogram for the grass dominated areas and choosing a backscatter amplitude at the lowest range of the histogram. Since one canopy parameter was altered, the other canopy parameter B must be adjusted. By fixing A to avoid creating a negative value in the natural logarithm, canopy parameter B needed to be fit to this inverted form. The non-linear least squares regression was run on Equation 12 to solve for

parameter *B*. The new equation could be used to predict volumetric canopy moisture as a function of soil moisture and backscatter.

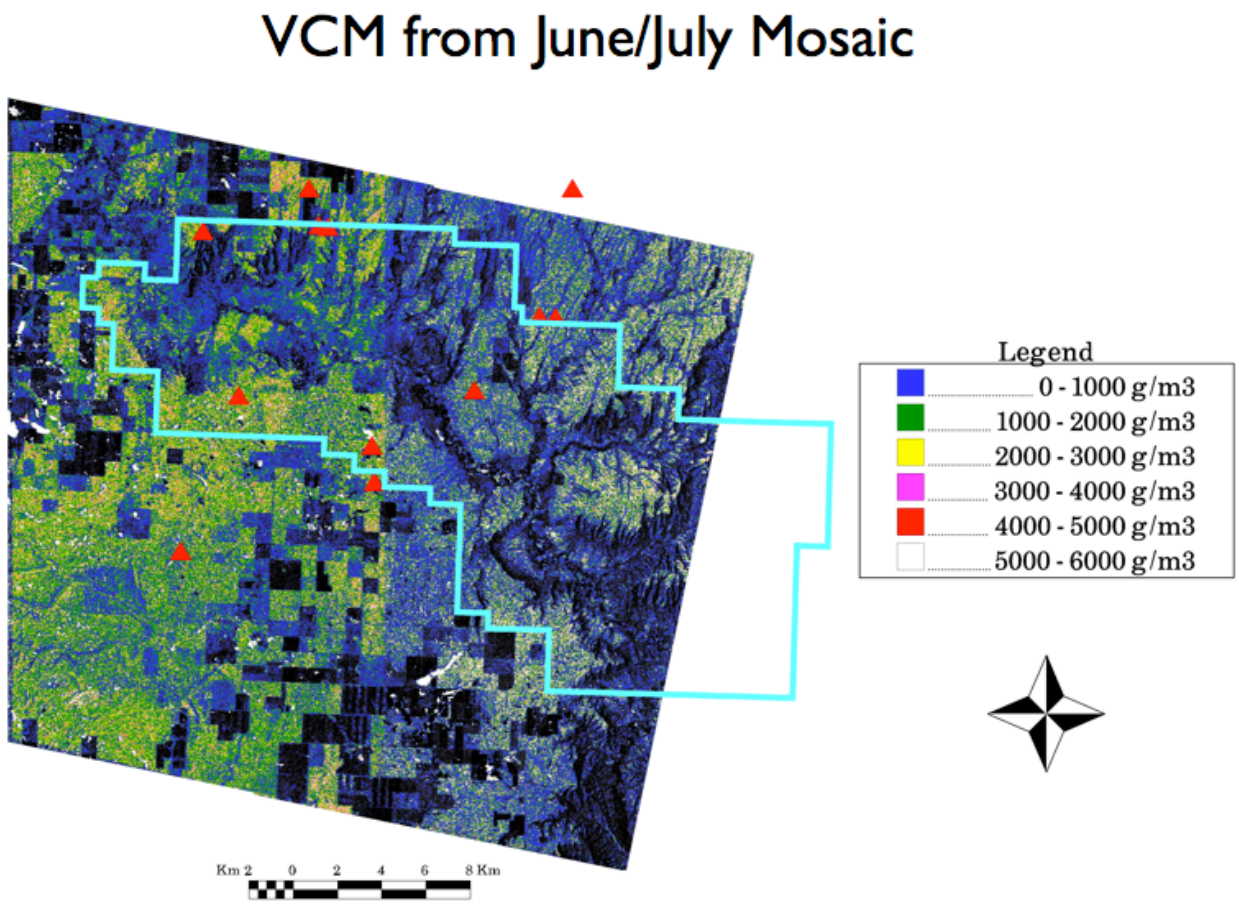

Figure 4-19: Results of the inverted model volumetric canopy moisture g/m³. A seam is again visible due to the much dryer July image.

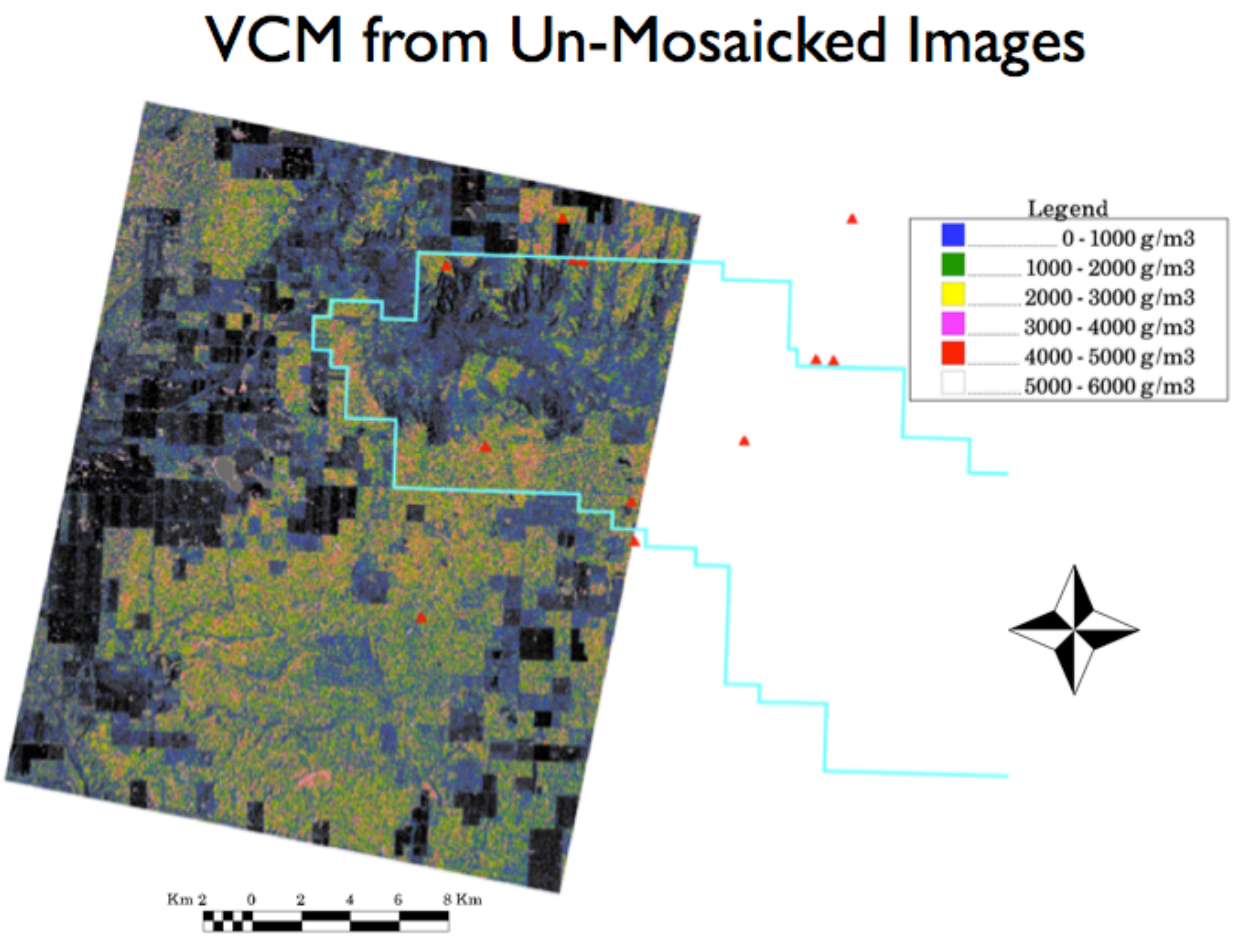

Figure 4-20 Results of the inverted model volumetric canopy moisture g/m³ for the un-mosaicked scene.

In order to apply the model to the imagery a measure of soil moisture was needed for every point in the image. Soil moisture derived from the Delta Index model was used for this purpose. The fitted general linear model (Equation 9) was used to convert the Delta Index to soil moisture values. The model results are illustrated in Figure 4-19. This full image has a visible seam from the combination of four different RADARSAT-2 images. For clarity the model results from the unmosaicked image are presented as well (Figure 4-20).

The canopy moisture image was sampled at every site and each pixel in a 100 m by 100 m area was averaged to retrieve a mean value for that site. This was compared to the canopy moisture

measured in the field (Figure 4-21). The dotted line represents a one to one correlation between the model and measured canopy moisture. For clarity, neither axis begins at zero canopy moisture. Canopy moisture measured in the field ranged from 500 - 3000 g/m^3 and the inverted water cloud model continuously over estimated the canopy moisture at the lower moisture levels. While the model estimations had more variation among the higher VCM levels, the model was able to explain 59% of the variation in volumetric canopy moisture. If a single image (no mosaicking and fewer data points) was used then the R^2 reaches 0.80 (See Figure 4-22), even though the unmosaicked images only cover seven ground sites. The mosaicking process introduces variation unaccounted for by the model. One point has undue leverage and was therefore removed; this left six ground points and a R^2 of 0.89 (See Figure 4-23). All models underestimated VCM. The regression line is plotted in blue while a one-to-one fit between the model and ground information is represented by the dotted line.

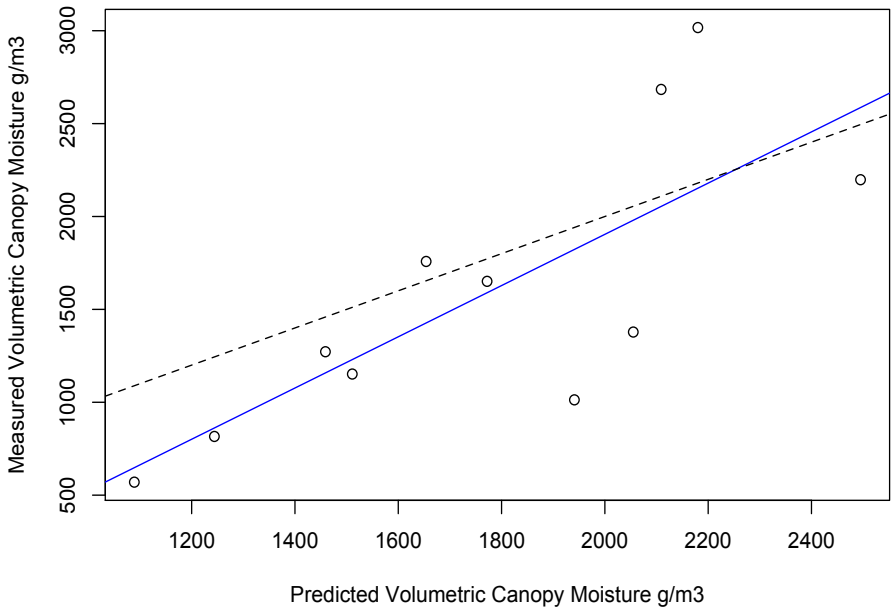

Figure 4-21 A comparison between the measured VCM and the VCM predicted by the inverted water cloud model.

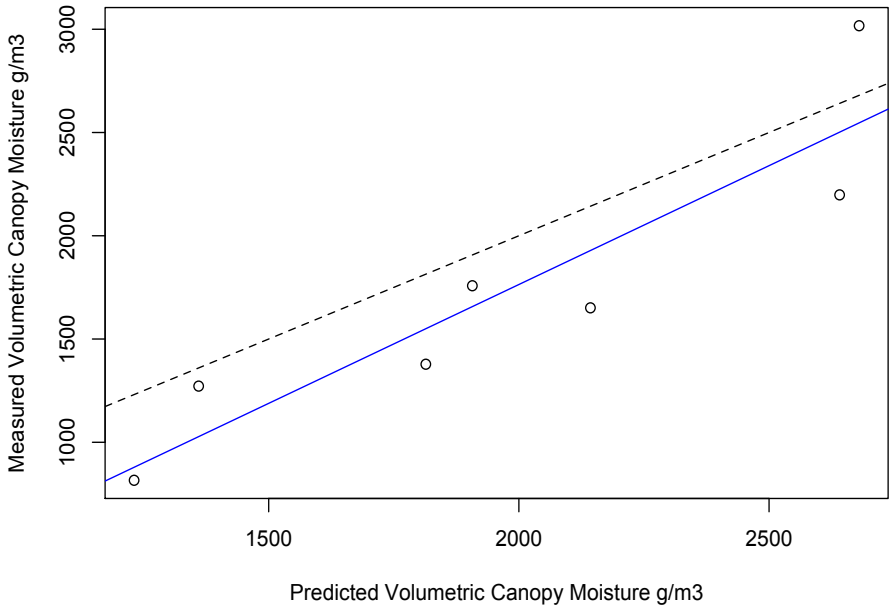

Figure 4-22 Comparing the Measured VCM versus the Predicted VCM for the unmosaicked image.

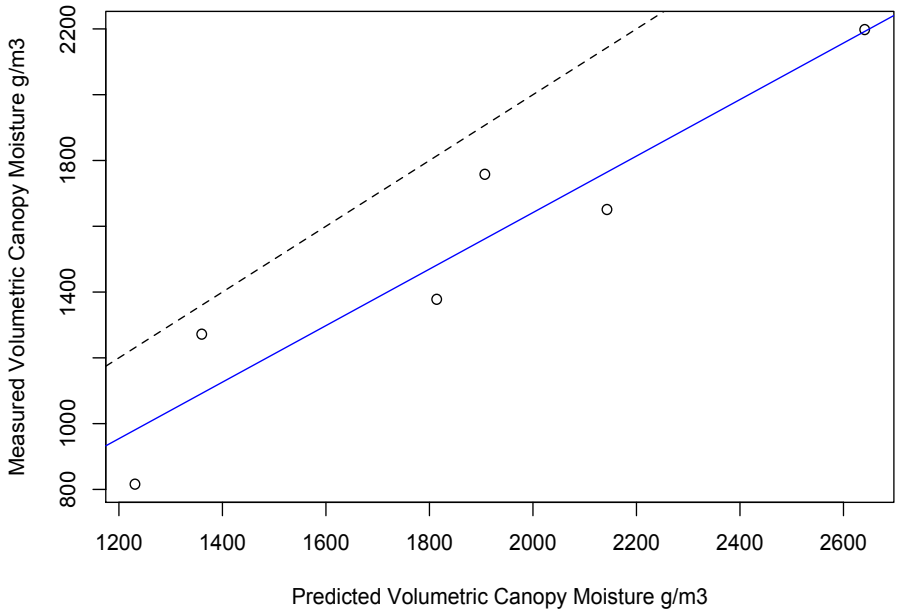

Figure 4-23 Predicted versus measured VCM with the high leverage point removed.

The model was trained in a grass dominated land cover. If soil moisture or backscatter value deviated greatly from those common to a grass dominated area, then the model would fail. Shrub dominated areas, and croplands both returned negative canopy moisture values, which are meaningless. Annual crops such as wheat, rye or barley would have similarities in structure to grasses, however these plants are much taller, and would have canopy moisture levels far in excess to anything sampled from the grassland. The model fails even for these superficially similar annual crops. These nonsensical results were simply ignored. Water bodies generally resulted in an undefined result; this occurred due to the equation inside the natural logarithm producing a value less than zero.

The Delta Index can be converted to soil moisture if the ground information existed. However, since the Delta Index is related to soil moisture it could be used directly in the place of soil moisture in the model. Following the same procedure described above, the water cloud model was recalibrated for the Delta Index. The Delta Index could be calculated for the May, June-July,

and July images. The August images could not be used, as these were the dry images used to formulate the Delta Index. To solve for the VCM in these other months it was necessary to make the assumption that parameters derived using the June image (the image with the accompanying ground data) remained constant throughout the growing season. The incident angle (θ) was slightly different in each image and that was accounted for in inverted water cloud model by substituting the new angle into Equation 12.

There is no ground information from May and July to verify the canopy moisture predictions. The results are presented here but no conclusion can be drawn. This method did not produce good results for sites U2, U3, and G3 (See Table 4-6). These sites were a part of the image that needed to be mosaicked. The mosaic process was error prone and those errors multiplied throughout the calculation of the volumetric canopy moisture. There was no pattern in VCM values for the period of May to July. The pattern that was expected from a consideration of a grass' phenological cycle would be an increasing trend in VCM from green up to peak green, followed by a decrease in VCM as the grasses senesce. This pattern was not found in the data. The assumption that the parameters do not change from month to month does not appear to be valid.

Table 4-6 Summary of the results from the inverted water cloud model for the months of May, June, and July: areas in purple have accumulated too many errors from the mosaicking process.

Site	May 14th and 17th Volumetric Canopy Moisture g/m³	June 24th and July 18th Volumetric Canopy Moisture g/m³	July 18th and July 21st Volumetric Canopy Moisture g/m³	June Volumetric Canopy Moisture g/m³ Measured from the Field
Site 01	1757	1911	1577	1272
Site 02	2411	2598	2593	2198
U0	1605	1617	1677	1758
U1	2557	1914	2318	1651
U2	582	460	402	570
U3	336	597	573	1013
U4	2152	2242	2296	1378
G0	1550	1705	1637	2684
G1	2274	2456	3089	3017
G3	404	607	481	1152
G4	1306	1453	1880	816

4.2.2 Biomass

The VCM is the density of water droplets distributed over a volume, while biomass in the mass of all plant material, without the moisture content, per unit area. VCM and biomass cannot be interchanged in the interpretation of the water cloud model. However, VCM is related to green grass biomass and negatively related to dead grass biomass. The more green grass present translates to greater VCM, conversely the more dead biomass that makes up the sample the smaller that VCM. Non-photosynthesizing biomass is dryer than the living photosynthesizing biomass. A general linear regression was employed to relate VCM to green biomass (Equation 13).

$$\text{Biomass} = 0.009\ \text{m} * \text{VCM} + 7.15\frac{g}{m^2} \quad (13)$$

Biomass is measured in units of grams per unit area and VCM is measured in units of grams per unit volume. The units can be matched by carefully choosing the units for the slope and intercept

fit by the general linear regression. This formula was applied using the EASI Modeler in PCI Geomatica. For each site, the biomass pixels were sampled from a 100 x 100 m area and averaged together to represent the site. Biomass values that were nonsensical due to a failure of the model were not counted. Plotting the predicted green grass biomass against the measured values revealed that the fit to the ground data is very poor (Figure 4-24). The regression line is plotted in blue while a one-to-one fit between the model and ground information is represented by the dotted line. The model is underestimating the amount of green grass biomass.

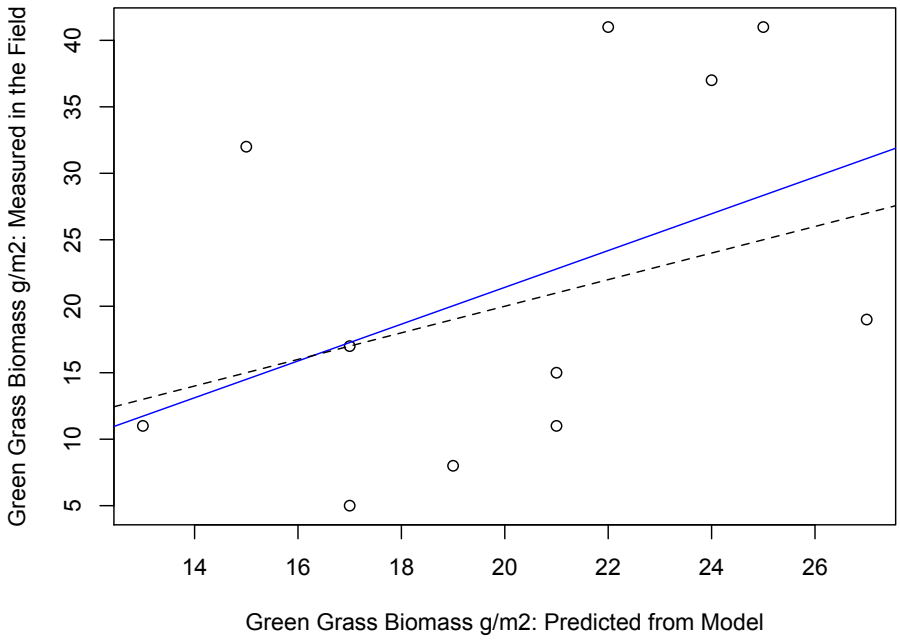

Figure 4-24 A comparison between the measured green grass biomass and predicted green grass biomass.

This model leaves most of the variation unexplained. All eleven data points are being used in this example. Using only one image may avoid errors caused by mosaicking, however there are not enough data to create a significant model between green grass biomass and volumetric canopy moisture.

4.2.3 Cross Polarization measures of Plant Form Diversity

Section 4.1.6 demonstrated that in a grass-dominated area, the greater the cross polarization ratio the higher the entropy as defined as plant form diversity. However a direct application of the result will not be useful. First, the regression is not significant and second, the cross polarization ratio will also increase when the dominant scattering process changes from surface to volume scattering, as it would in a shrub dominate riparian area of the Frenchman River. This increase in cross polarization ratio may not reflect an actual increase in entropy. When applying this relationship to the GNP, a threshold must be set in order to avoid applying this interpretation to non-grass dominated areas. Exploring the DN of grass-dominated areas, and locating an upper boundary could aid in setting a threshold. However the noise level in the cross polarization ratio image made such a simple procedure unworkable. Instead a simple land cover classification was performed, using the maximum likelihood supervised method, to isolate the grassland areas from other cover types. The maximum likelihood classification builds a probability model from user defined training data and employs this model to fit the other image pixels into each cover type. Once a grassland class was created a threshold was then applied only to the grassland areas, dividing these into areas of higher, moderate, and lower entropy. The resulting map is shown in Figure 4-25. The non-grassland classification mask is represented as the white areas. Areas of low plant form diversity are areas dominated by a single plant form; an example would be cultivated lands. Since cultivated areas are not grasslands they were removed by the non-grasslands mask; low diversity areas are not well represented in this map.

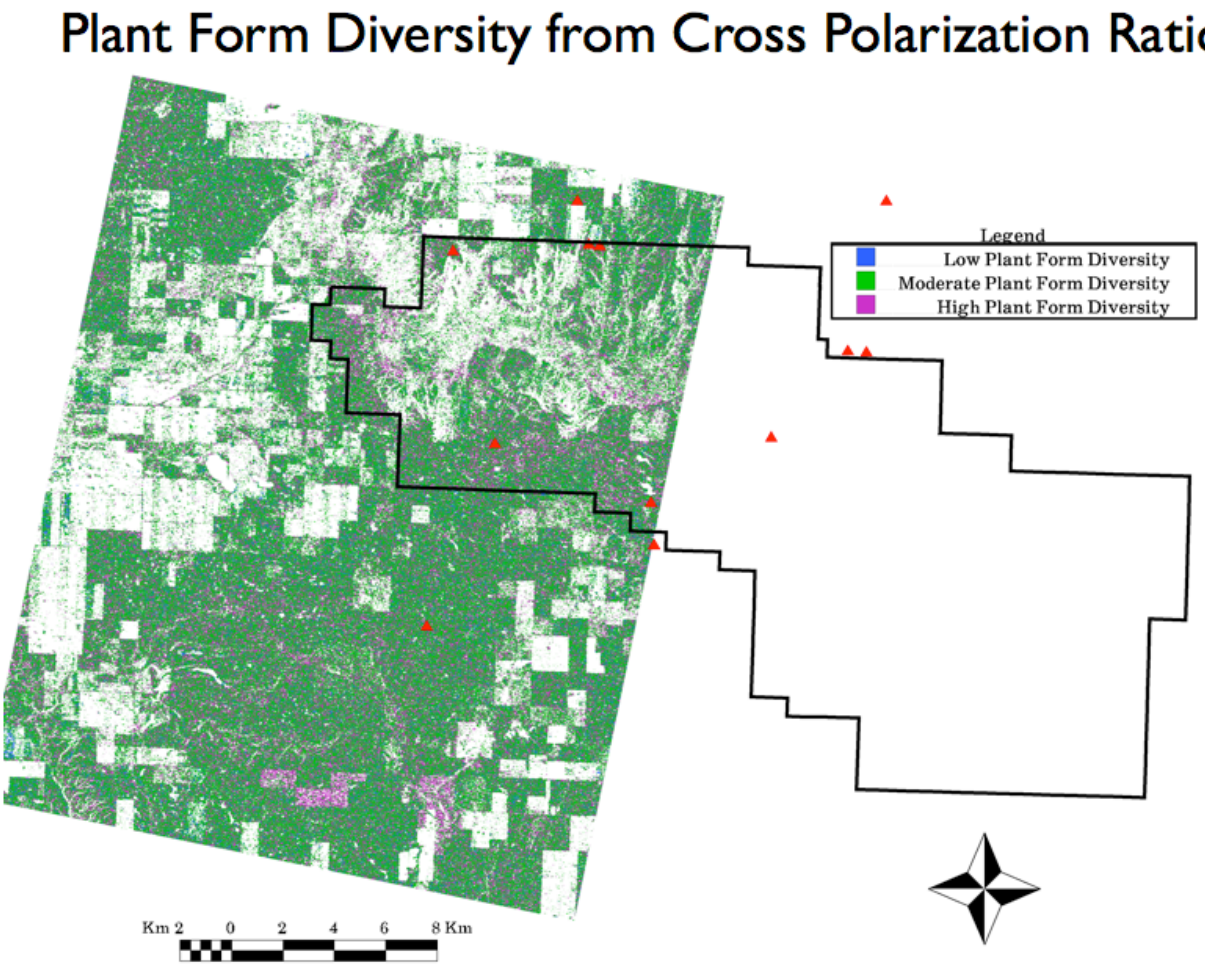

Figure 4-25 Higher and lower plant form entropy map derived from the cross polarization ratio. White areas non-grass dominated cover types.

4.2.4 Texture measures of Plant Form Diversity

Texture, in remote sensing, is defined as the spatial variation in pixel DNs. Texture measures derived from the cross-polarization ratio had a stronger with plant form diversity, than the cross-polarization ratio alone. A cutoff threshold was determined by first examining the plots of the texture measure plotted against the diversity indices. The principle of mediocrity suggests that a sample drawn at random from a population is more likely to represent an average rather than an extreme. The lower limits of diversity values sampled from the field were designated as low

plant form diversity, while values on the upper limit were delineated as high plant form diversity. These limits were again defined by the 11 sample sites. The lowest diversity point was considered the start of the low diversity range. The highest diversity site was considered the start of the high diversity range. The upper limits of both diversity indices are a function of their definitions. The rest of the image was considered moderate plant form diversity. Since texture features such as contrast and standard deviation are measures of variation, and are not dependent on the magnitude of the DNs, the relationships found in the grass dominated regions may also apply to shrub-dominated regions. This prediction cannot be tested with the limited ground data that has been collected, as these were constrained only to grass dominated areas. Given the nature of certain land cover types such as annual crops, one would expect these areas to be identified as low entropy, and they were in both maps (Figures 4-26 and 4-27).

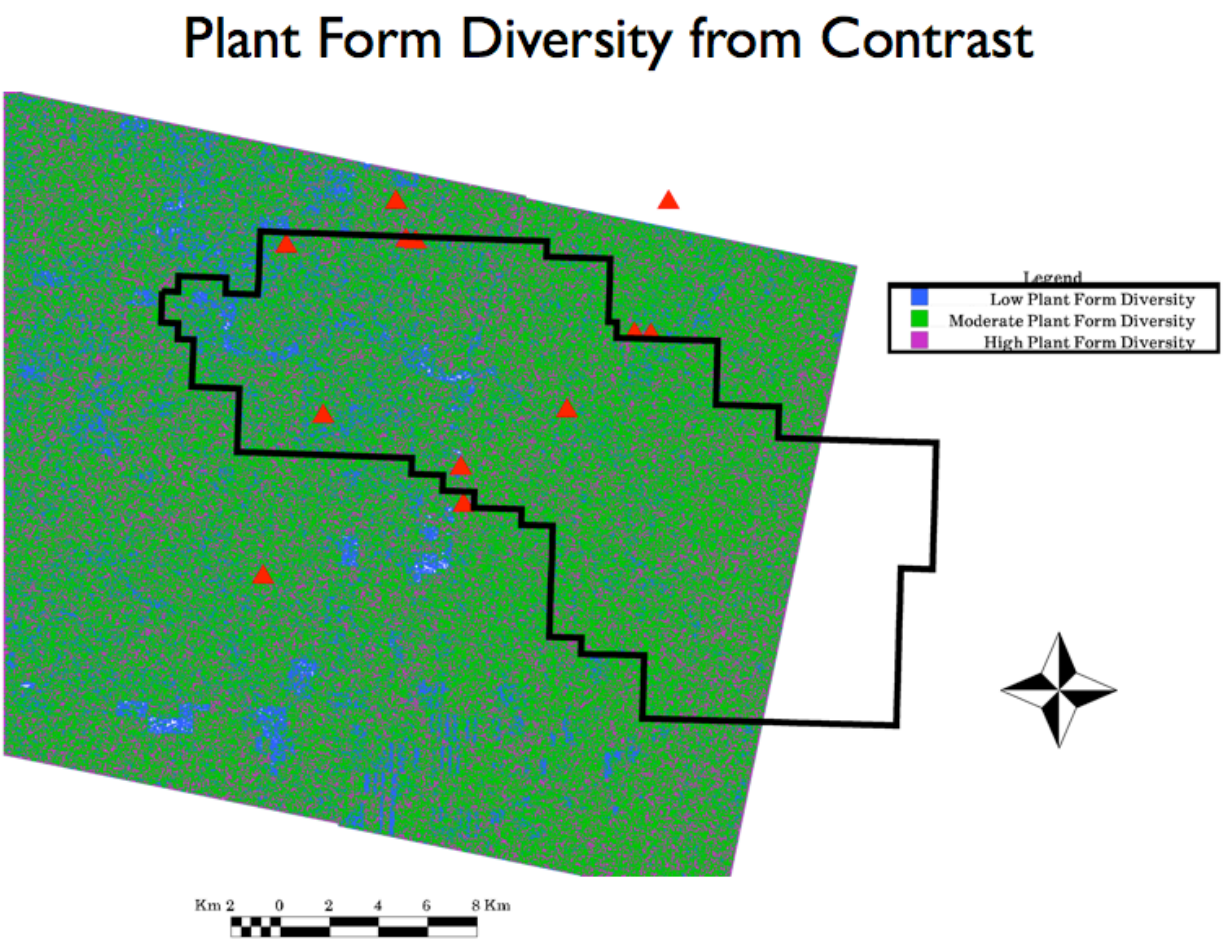

Figure 4-26 Higher and Lower plant form diversity map based on the contrast texture measure of the cross polarization ratio. Low plant form diversity cover types such as annual croplands have been properly delineated.

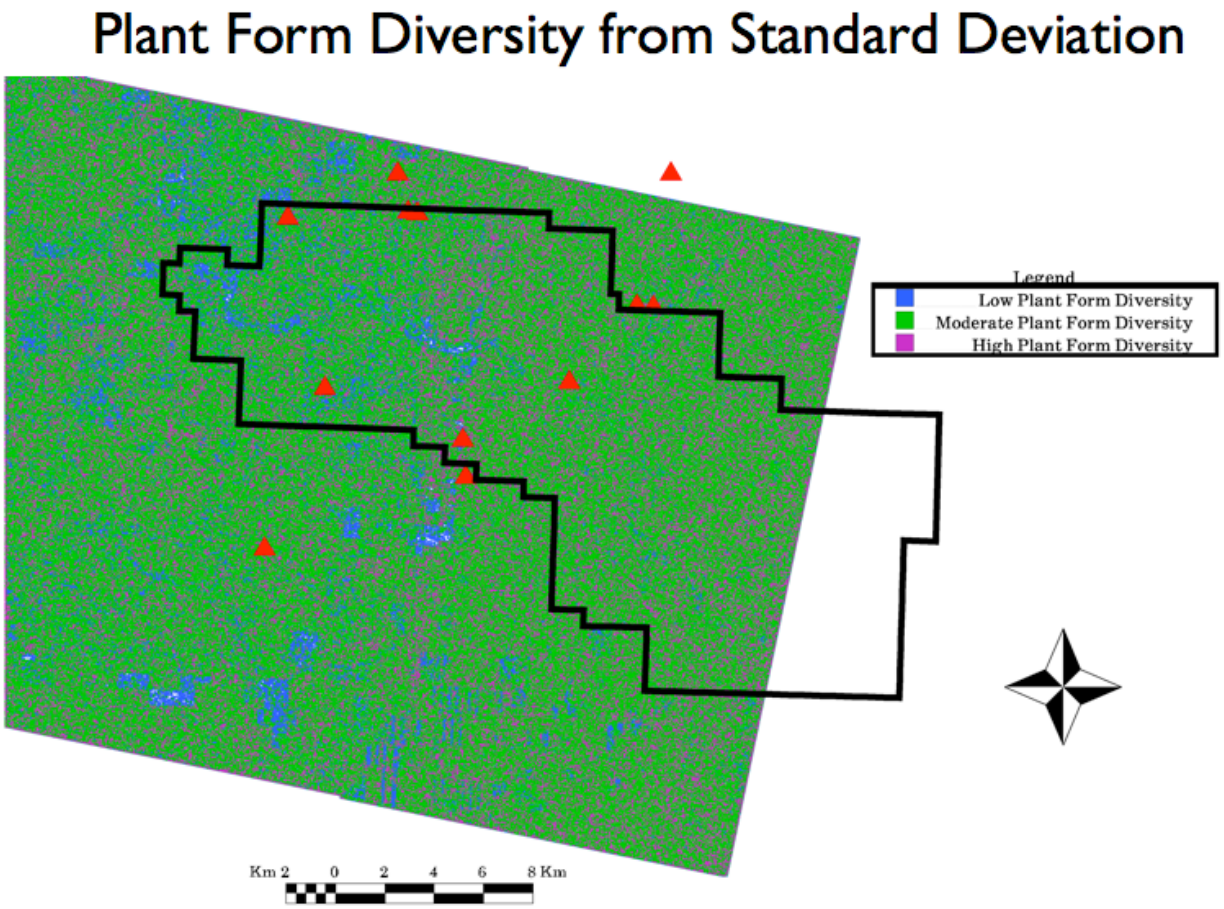

Figure 4-27 Higher and lower entropy maps based on the Standard Deviation texture measure of the Cross Polarization ratio. Low plant form diversity areas have been properly isolated.

4.3 Contributions from the Optical Sensors

4.3.1 Landsat-5 and Green and Dead biomass and canopy cover

In this study area there was very little relationship between the Landsat-5 reflectance and biophysical parameters such as biomass. The normalized difference vegetation index (NDVI) is known to be sensitive to the presence of chlorophyll, however this did not translate into a significant relationship between NDVI and green biomass, nor to any biomass type in general (Table 4-7 and Figure 4-28).

Table 4-7 Coefficient of Determination (R^2) between biomass type and NDVI.

Biomass Type	R^2	p-value
Green	0.04	0.52
Dead	0.20	0.17
Total	0.01	0.80

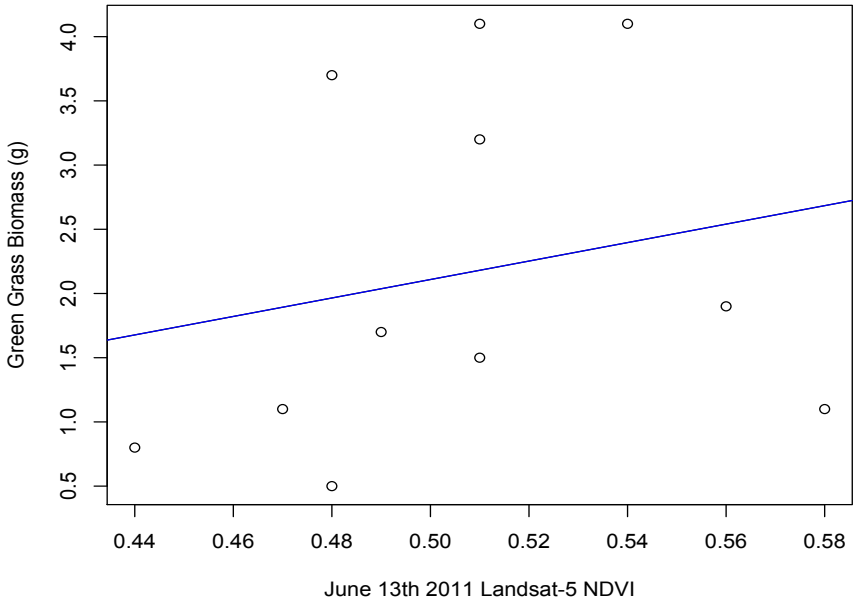

Figure 4-28 Green Grass Biomass and NDVI: the relationship is not strong.

Not long after the completion of the data collection phase of this research the Landsat-5 suffered

degradation in data quality resulting in its imaging processes being suspended while repairs were attempted. If the poor correlation were the result of sensor malfunction then other data sources would report better correlations. Since the ground data collection campaign was the result of the combined effort of several researchers, data was also collected for remote sensing research projects that relied on optical data sources. One of the instruments used in the field was an ASD Spectroradiometer with a spectral range of 300 – 2500 nm (Figure iv in Appendix A) and a bandwidth of one nm. This gives the instrument 2200 image bands; such an instrument is also referred to as a hyperspectral sensor. The spectroradiometer was calibrated to a white reference and operated only under clear sky conditions. A hyperspectral NDVI index was calculated after the formula presented in He & Guo, 2006a (Equation 14).

$$NDVI = \frac{\rho_{800} - \rho_{670}}{\rho_{800} + \rho_{670}} \quad (14)$$

where ρ_{800} is the reflectance at 800 nm and ρ_{670} is the reflectance at 670 nm. There is no correlation between the ground-based hyperspectral NDVI and green grass biomass (Table 4-8 and Figure 4-29).

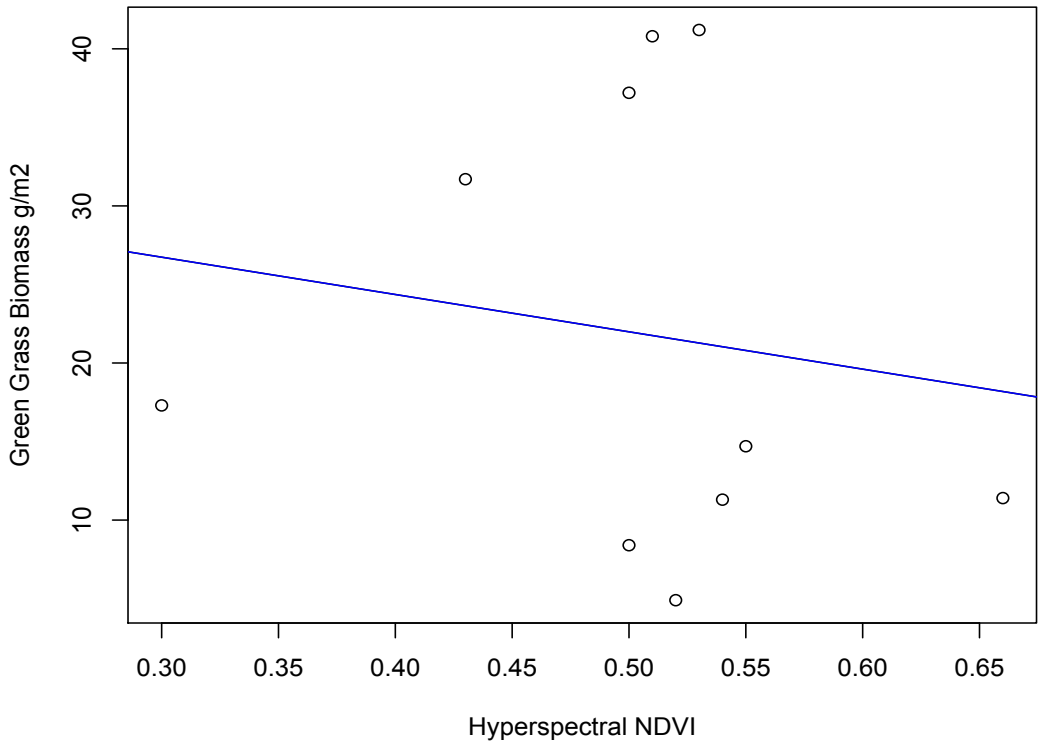

Figure 4-29 The Hyperspectral NDVI values do not have the expected relationship with Green Grass biomass.

Averaging the hyperspectral data to represent the Landsat-5 bandwidths also did not result in any improvement (Table 4-8).

Table 4-8 Coefficient of Determination (R^2) for Green Biomass and Hyperspectral NDVI.

Biomass Type	R^2	p-value
Green Grass	0.02	0.67
Forbs	0.05	0.53
Total Green Biomass	0.02	0.71

Comparing the space-borne NDVI values and ground hyperspectral data reveals that the Landsat-5 NDVI slightly underestimates the ground NDVI values (See Figure 4-30). The regression line derived from the two data sets is shown in blue while a one-to-one relationship is represented by the dotted line. Much of the variation in the ground-based measurements of NDVI is left unexplained by the Landsat-5 data.

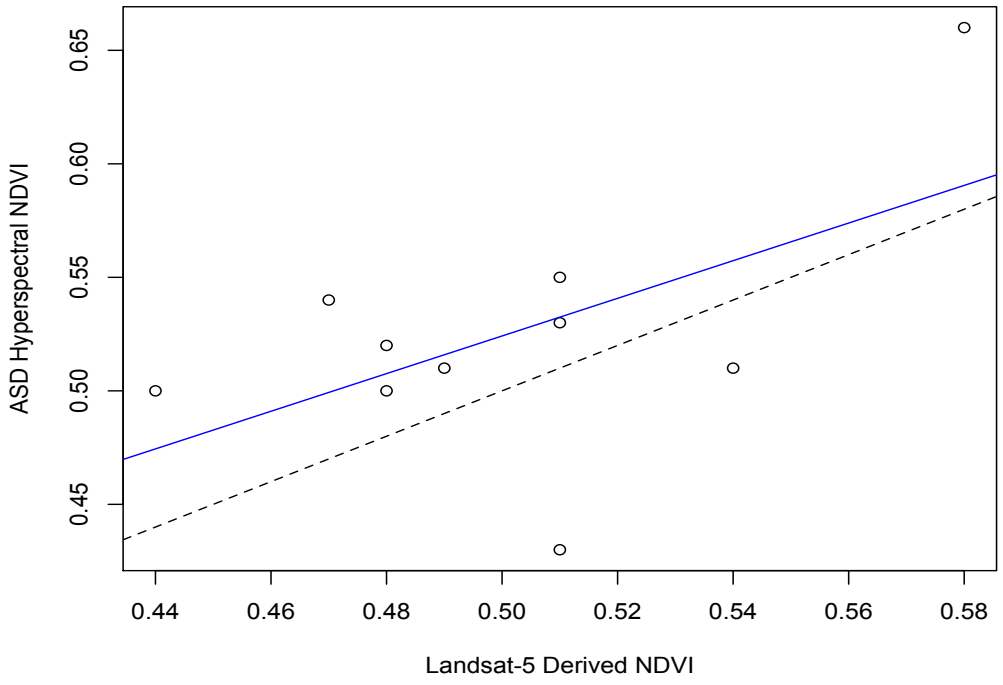

Figure 4-30 A comparison between the Landsat-5 NDVI and the ground base hyperspectral data (R^2 = 0.32).

Data was also acquired from the SPOT satellite, unfortunately not during the month of June. The image acquired closest to the ground data campaign was a July image. This scene was radiometrically and atmospherically corrected using the ATCOR 2 algorithm in PCI Geomatica. The July NDVI values were higher than the ones recorded in June and had no relationship with green grass biomass. As two independent optical data sources both point to a poor relationship with green grass biomass and NDVI, the cause of this issue is likely not the Landsat-5 data.

As previously discussed NDVI is not the best vegetation indices for grasslands due to the presence of dead biomass, and bare soil. Dead biomass is a major component of the grasslands in the GNP. Some hyperspectral indices have been developed to compensate for the presence of litter such as the L-ATSAVI (He et al., 2006a). Unfortunately the optical sensors used in this study are not suitable for the application of L-ATSAVI; instead soil-adjusted vegetation indices

were employed. Soil adjusted vegetation indices have proved superior to NDVI in other studies (He et al., 2006b). Two soil-adjusted indices were explored in this analysis: the ATSAVI and SATVI. ATSAVI is the adjusted transformed soil adjusted vegetation index, and is defined as follows (Equation 15):

$$ATSAVI = \frac{a(NIR - aRED - b)}{aNIR + RED + ab + X(1 + a^2)} \quad (15)$$

where *a* and *b* are slope and intercept values derived from the soil line and *X* is constant inserted into the equation to minimize soil effects, *X* is set to 0.08 (He and Guo, 2006b)

SATVI is the soil adjusted total vegetation index; it has a similar form to the soil adjusted vegetation index (SAVI), but it employs the middle infrared (MIR) band rather than the NIR band. Landsat-5 has two bands in the middle infrared region, band 5 and band 7; these will be referred to as MIR and MIRII respectively. SATVI is defined as follows (Equation 16):

$$SATVI = \frac{MIR - RED}{MIR + RED + L} * \left(1 + L_g\right) - \frac{MIRII}{2} \quad (16)$$

where L_g represent the proportion of green cover, in the GNP this would be approximately 0.5. Although ATSAVI and SATVI have been used in previous studies to improve biomass retrieval in grasslands areas (He et al., 2009), there was no improvement in biomass retrieval with either index (Table 4-9).

Table 4-9 A comparison of regression models for the prediction of green or dead biomass.

Model	R^2	p-value
Green Biomass ~ ATSAVI	0.00	0.92
Green Biomass ~ SATVI	0.00	0.89
Dead Biomass ~ ATSAVI	0.04	0.55
Dead Biomass ~ SATVI	0.17	0.21

4.3.2 Landsat-5 and Soil and Canopy Moisture

The Landsat-5 imagery was insensitive to volumetric canopy moisture and soil moisture in this study. The Normalized Difference Moisture Index (NDMI) is calculated using the middle infrared band (MIR) and the near infrared band. The structure of the formula is identical to that of the NDVI (Equation 3), with the NIR and MIR bands substituting for Red and NIR bands of the NDVI equation. The middle infrared band in located near a water absorption region of the electromagnetic spectrum making this band sensitive to the presence of water. This index has been used in forest studies to detect subtle deforestation processes such as partial cuts and insect damage (Wunderle et al., 2007). There was no significant relationship between NDMI and canopy or soil moisture in the GNP (Figure 4-31 and Table 4-10).

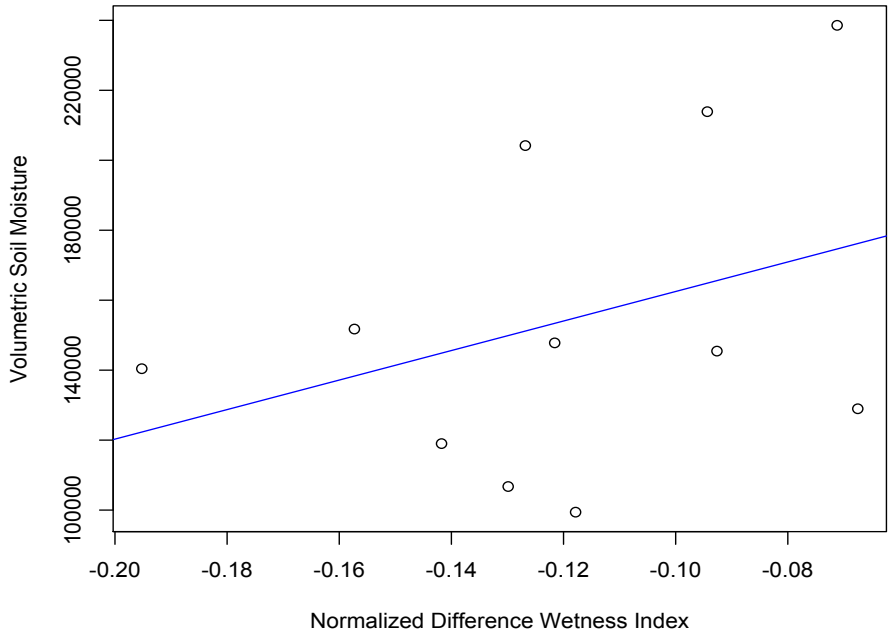

Figure 4-31 NDMI and Volumetric Soil Moisture: the fit is not very strong.

Table 4-10 A comparison of linear regression models for NDMI and Tasseled Cap Wetness for the prediction of soil and canopy moisture.

Model	R^2	p-value
Soil Moisture ~ NDMI	0.12	0.29
Canopy Moisture ~ NDMI	0.02	0.72
Soil Moisture ~ Wetness	0.17	0.21
Canopy Moisture ~ Wetness	0.01	0.74

The Tasseled Cap wetness index also exploits the middle infrared band's sensitivity to moisture. The Tasseled Cap transformation removes redundant information in Landsat-5 six bands and compressing the remaining variation into three bands that represent brightness, greenness, and wetness (Crist and Cicone, 1984). The Wetness index was positively correlated to canopy and soil moisture, however the relationship was not significant (Table 4-10). These indices have been used successively in other studies; the lack of significance here could be due to the dry climate and low amounts of vegetation, both green and dead, present in the study area.

4.3.3 Percentage Canopy Cover

Percentage canopy cover was estimated for each site for the different plant forms; for the analysis all green biomass cover types were aggregated into a class called "Green Cover"; dead cover was a combination of standing dead and litter. The vegetation indices were far more sensitive to percentage coverage of green plant materials than they were to biomass itself. ATSAVI is superior to either the SATVI or NDVI (Table 4-11).

Table 4-11 Model results from using vegetation indices to predict percentage canopy coverage.

Model	R^2	p-value
NDVI ~ Green Cover	0.11	0.33
ATSAVI ~ Green Cover *	0.53	0.01
SATVI ~ Green Cover	0.19	0.19
NDVI ~ Dead Cover	0.01	0.82
ATSAVI ~ Dead Cover	0.18	0.19
SATVI ~ Dead Cover	0.00	0.97

where a "*" represents a significant relationship at the $p < 0.05$ level.

4.3.4 Estimations of green biomass

Vegetation indices derived from optical satellites, such as the Landsat-5, have a well-understood correlation with the amount of green cover. The relationships described in Section 4.3.3 are consistent with the interpretation that the Landsat-5 is measuring percentage canopy cover, or more quantitatively, a property known as leaf area index (LAI). LAI is related to biomass, and can be used as a proxy for biomass (Butterfield and Malmstrom 2009). A combination of the two sensors brings together two different parameters related to biomass: the canopy moisture from the RADARSAT-2 and the percentage cover of green biomass from the Landsat-5. Of the published Landsat-5 vegetation indices the ATSAVI index performed the best.

Several model forms were explored, but the multi-linear regression of VCM and percentage canopy coverage (%Cov) outperformed the others. The multi-linear regression model created to estimate the biomass has the following form (Equation 17):

$$Biomass_{green} = a*VCM + b*\%\ Cov_{green} + c \quad (17)$$

where *a*, *b*, and *c* are derived parameters. Biomass is measured in units of $\frac{g}{m^2}$ and VCM is measured in units of $\frac{g}{m^3}$. In order to match the units on both sides of the equation the units for *a*,

b, and *c* need to be carefully chosen. The two-sensor model was more accurate in its estimation of green grass biomass than the RADARSAT-2 data alone. Comparing the green biomass predicted from the model to the biomass measured in the field reveals a significant relationship ($p < 0.05$, $R^2 = 0.54$). Further investigations into the fit revealed that a single point had undue leverage. When this point was removed the fit between the predicted and measured green biomass improved significantly ($p < 0.005$, $R^2 = 0.74$).

With the high leverage point removed the model explained 74% ($R^2 = 0.74$, Adjusted $R^2 = 0.71$) of the variation in the measured green biomass ($p < 0.005$). The blue line represents the regression model between the model and ground data, and the dotted line represents a one-to-one fit. It is clear from this graph that the model is underestimating green biomass. Using only the VCM information the slope of the fitted line is closer to one, see Figure 4-24, however the fit was poor. Incorporating the Landsat-5 information caused the slope to deviate from one, however the fit is much improved (See Figure 4-32).

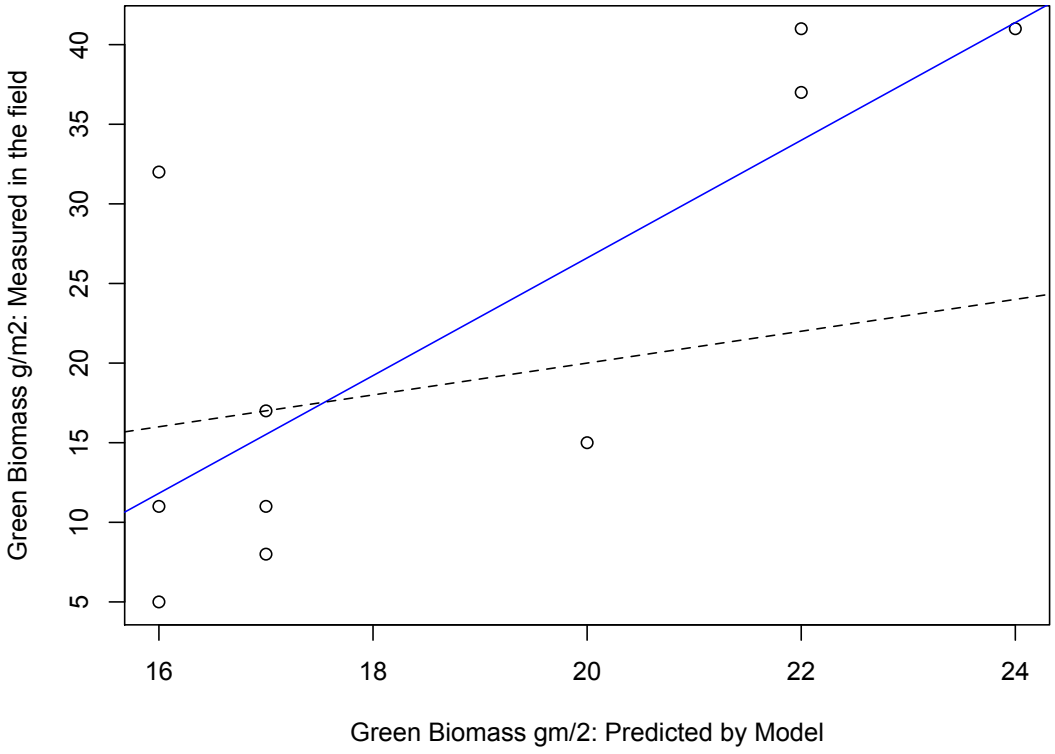

Figure 4-32 A comparison of the measured green biomass and the greed grass biomass predicted from the model. The model is deviating from the one-to-one relationship represented by the dotted line.

The model often produced nonsensical values for non-grass dominated land cover. This is the result of the VCM model failing to operate in croplands, shrubs, and water bodies. The green biomass map has a visible seam due to the mosaicking process. The percentage of no data pixels is higher in the eastern portion of the mosaic compared to the western portion (Figure 4-33). This feature is responsible for the different appearance of the two portions. If all ground data sites are all used then there are not enough data to build a model to predict green grass biomass. Only the June and July mosaic can be used for this analysis.

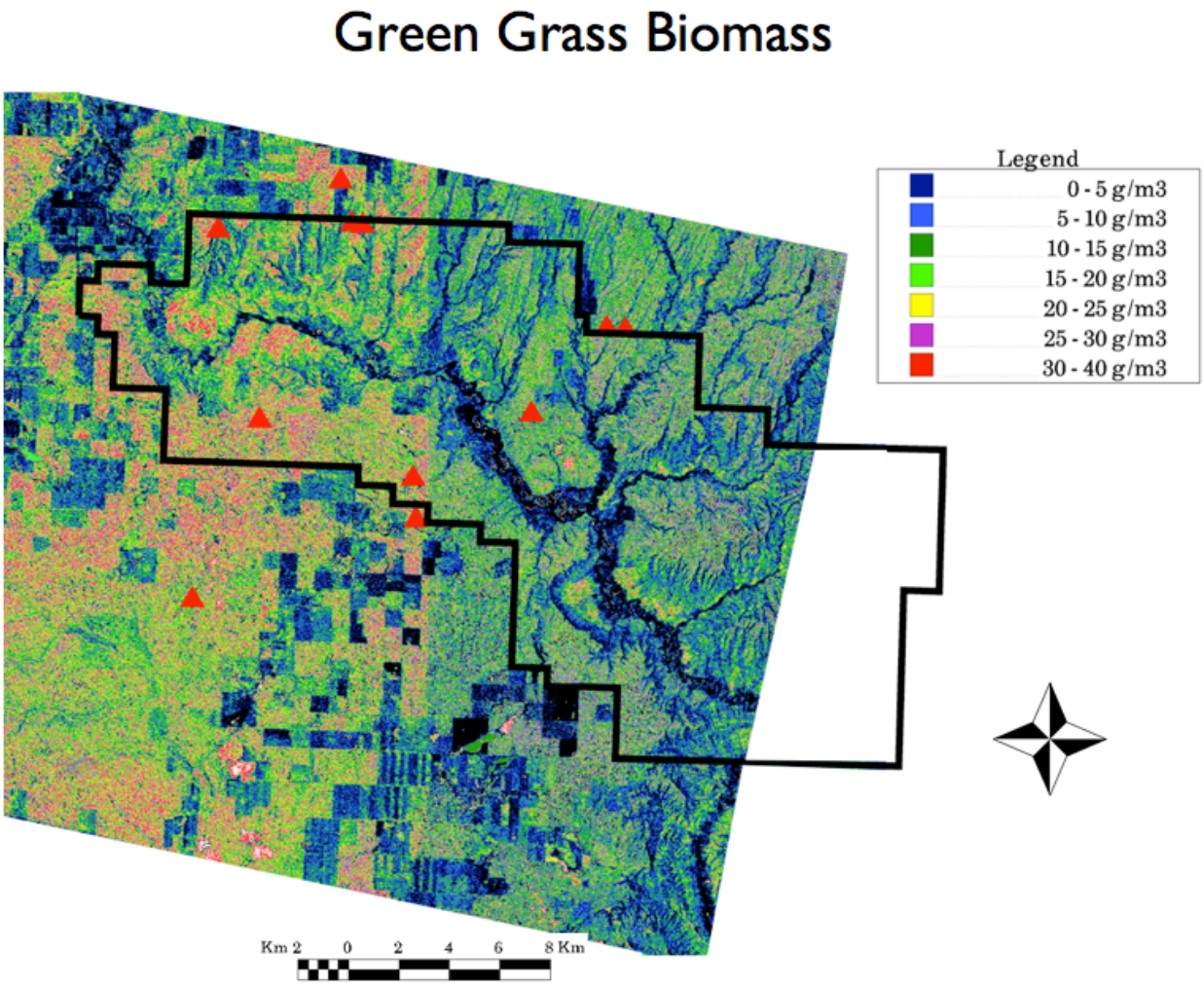

Figure 4-33 Green grass abundance in the GNP. This image combines data from both the RADARSAT-2 and the Landsat-5.

CHAPTER FIVE

CONCLUSION

5.1 Conclusion

The rationale for this study was to determine whether useful biophysical parameters could be derived from dual-polarimetric SAR data. Dual-polarimetric data will be available at no cost worldwide through the planned SAR constellations (ESA, 2009), and if accurate biophysical parameters could be derived, than ecologists would have a new monitoring tool, and one that is less dependent on cloud-free conditions.

Time series analysis of optical and SAR imagery demonstrate that the two images are sensitive to different independent landscape parameters. The time series of the corrected RADARSAT-2 images and the Landsat-5 images can be described as out of phase sinusoidal curves. The SAR backscatter amplitude reached a peak in June, and decreased rapidly in July and August complying with the trend in the moisture conditions. The NDVI, as derived from the Landsat-5, reached a peak in July, then began decreasing, showing the compliance with the greenness of the grassland that follows the changing moisture condition. Previous studies of optical time series have shown that NDVI time series are following plant phenology (Fesholt et al., 2012).

In this study, soil moisture was not collected to coincide with each RADARSAT-2 image, however previous research by Van Der Velde, and Su (2009) demonstrated that much of the variation in backscatter could be accounted for by soil moisture. This is a possible explanation of the appearance of the SAR time series, which had a peak in May and June when most of the precipitation fell. A single image acquired in June was positively correlated with soil moisture measured in the field, $R^2 = 0.41$.

This study investigated the relationship between the Delta Index, a combination of two scenes acquired at different times, (See Equation 2) and soil moisture. There was a stronger relationship with the Delta Index ($R^2 = 0.80$) than with the backscatter values of a single image ($R^2 = 0.41$). While these results are not as strong as the results reported by Thoma et al. (2006) ($R^2 = 0.91$) they are still reasonable. The linear relationship between the Delta Index and soil moisture was robust even though the mosaicking added considerable noise to the model.

The cross polarization ratio had the expected sign for correlation coefficients (R) for the Shannon and Simpson diversity indices, if the definitions of the diversity indices were restricted to vegetation cover types only. Using all of the land covers measured in the field (including plant forms, and non plant forms such as bare ground, and rock) the relationship between the cross-polarization ratio the diversity indices did not have the expected sign in the correlation coefficient. A stronger relationship was found between texture measures derived from the cross polarization ratio ($p < 0.05$) than the cross-polarization alone; in particular, the Contrast and Standard Deviation texture filters. Contrast and Standard Deviation were both positively correlated with the Shannon Index and can explain 50% and 55% of the variation in the Shannon Index respectively (R^2 of 0.50 and 0.55). Contrast and Standard Deviation were negatively correlated with the Simpson Index with a R^2 of 0.59 and 0.37 respectively. The sign of correlation coefficient matches the definition of both diversity indices; the Shannon Index is a measure of heterogeneity as are Contrast and Standard Deviation, therefore there should exist a positive correlation. The reverse is true for the Simpson Index, which is a measure of homogeneity. From the definitions of the Shannon and Simpson Indices it was possible to predict the sign of the correlation coefficient between the cross-polarization ratio and each diversity

index. The relationships that were found were consistent with those predictions. The texture measures were far superior to the cross polarization ratio alone.

The relationships found between the cross-polarization ratio and the diversity of plant forms that were discovered in this study were used to create maps of high, moderate, and low plant form diversity. Areas of low diversity were shown to be mainly areas of annual crops and bare ground.

Using the Delta Index as an indicator for soil moisture, the water cloud model can be inverted to extract volumetric canopy moisture. The inverted water cloud model derived in this study was able to explain 59% of the variation in canopy moisture as measured on the ground. When using a single scene the fit to the ground data was improved ($R^2 = 0.80$). This study suggests that a successful inversion of the water cloud model relies on good ground measurement collected as close as possible to the SAR image acquisition date.

The Delta Index could be derived for months for which there were no ground data (May and July). This index could be used as a proxy for soil moisture for those months. Using the June parameters to invert the water cloud model for May and July did not result in any recognizable trends. The volumetric canopy moisture, derived by this method, did not vary much in the period of May to July. This does not represent a failure of canopy model, rather it suggests that model parameters determined for one month cannot be extrapolated to other months.

Volumetric canopy moisture is positively correlated with the amount of green grass biomass ($R^2 = 0.38$). When a general linear model was employed to derive an equation to transform canopy moisture to green grass biomass it resulted in much unexplained variation in the measured ground information. It is possible that the relationship is not linear, however it would be difficult defend a non-linear relationship with only 11 data points. Only by using the mosaicked image that there are enough ground samples points to define a relationship with green grass biomass.

Reducing the sample sites to 7 results is not enough sample points to reveal any relationship with green grass biomass.

The results from optical imagery analysis demonstrated that for this area soil adjusted vegetation indices performed better than NDVI in predicting the percentage canopy coverage of green grass biomass. Of the soil-adjusted indices ATSAVI was superior. None of the moisture sensitive indices have a strong correlation with either canopy or soil moisture. This is likely due to the semi-arid nature of the mixed-grassland ecosystem.

This study using a multi-linear regression model of SAR and optical images was able to explain 74% of the variation in the measured green biomass, although it does underestimate green biomass, in areas of higher biomass. The volumetric canopy moisture is related to the mass of green grass biomass (Section 4.4), however there are many additional variables that will affect the amount of moisture within the canopy. Employing the percentage canopy coverage estimates from the ATSAVI was an attempt to explain some of the variation. The addition of the Landsat-5 data reduced the variance between the predicted and measured biomass. With the RADARSAT-2 alone, the model could explain about 40% of the variation green grass biomass, with the addition of the Landsat-5 imagery, a model was developed that could explain 74% of the variation in green grass biomass. The Landsat-5 optical information aided the analysis even though the vegetation indices derived were uncorrelated with green grass biomass. A regression model that consists of information from both types of images was superior to the ones using either image type alone.

5.2 Contribution

This study demonstrated that a simple linear regression derived from the Delta index could be used to represent soil moisture in this dry mixed grassland area. This relationship could be used

in this case in place of complex physical model.

The water cloud model will only return sensible values for landscapes similar to the ones used to fit the model. This landscape specificity could be an advantage as a monitoring tool as the model will break down the image into areas that do not match the general landscape conditions and ones that do. Non-grassland land covers will be eliminated from the analysis.

While not explored in this study, the volumetric canopy moisture maps can be used in fire modeling, which are used to predict fire behavior and can mitigate the risk of prescribed burning, or aid in combatting a wildfire. Live Fuel Moisture Content (LFMC) is a critical parameter for assessing fire risk (Dasgupta et al., 2007).

This study demonstrates that estimates of green grass biomass from a SAR platform can be improved through the inclusion of an optical image into the analysis.

This research also demonstrated that textures measures derived from the cross-polarization ratio are more sensitive to plant diversity measures than the cross polarization ratio alone. Plant form diversity is far coarser than species diversity, however the higher entropy areas may indicate diversity hot spots.

5.3 Limitations

Limitations are divided into two categories: limitations imposed by the imagery and imagery processing, and those imposed by the ground data collection.

5.3.1 Imagery Limitations

One limitation was the areal extent of the standard quad images. The image footprints were not large enough to cover the entire study area. This will be an unavoidable problem given the extent of many grasslands areas. Mosaicking multiple scenes together was a given, therefore it was

important to acquire two scenes close in time, otherwise the backscatter amplitude will begin to decrease (See Figure 4-2). Two scenes were acquired for each month except for the month of June. The second June acquisition must have been lost due to a technical error. This meant it was necessary to mosaic a June and July image for complete coverage of all sites. The Empirical Line Calibration method that was employed did not work as well for these widely temporally spaced scenes. This left a visible seam in the final product and caused unexplained variation in the soil moisture, VCM, and biomass models. This was seen as a difference in coefficient of determination (R^2) between models based on the mosaicked scene and the ones based on a single scene.

For large area applications this mosaicking issue must be solved. The satellites must be configured to acquire scenes with the same incident angle and closer in time. The proposed ESA Sentinel SAR mission will collect data at a fixed incident angle, meaning the viewing geometry will be consistent for each image. This will greatly improve the chance of a successful mosaic.

5.3.2 Ground Data Limitations

In this study, vegetation indices derived from Landsat-5 had little to no relationship with total biomass, green biomass, and dead biomass. This result may be due to the wet spring the GNP had been experiencing. Grasslands in the park normally have reached their peak green in June when the ground data collection normally occurs. The wet spring delayed the peak green to July as evidenced by the Landsat-5 time series. The ground data collection campaign occurred while the grasslands were still greening up.

The fitted inverted water cloud model is restricted to land covers similar to the one it was trained on. The model could not be applied to forb or shrub dominated areas since there is no ground information to train the model. This feature of the water cloud model was not known when the

ground data campaign was created.

Of the twelve quadrants per site only four were set aside for biomass measurements. In retrospect this limited amount of sampling may not be sufficient to represent the site. This amount of sampling was chosen to minimize the impact to the park. The sites chosen were mainly homogenous grass dominated areas and four quadrants were thought to be enough. However if there were more heterogeneity in the site, then four samples may be inadequate.

Sites were restricted to flat areas, meaning the results of the model in the highly sloped badland area will have more unexplained variation, however these areas are mainly bare. An advantage of restricting the model to flat areas is that topographical correction is not necessary. When interpreting the model it is important to recall that it is restricted to flat terrain. This is the dominant terrain structure in the park with the notable exception being the Frenchman River Valley.

5.4 Future Research

Further study is needed to expand this analysis is both areal extent and cover types. Grasslands have large spatial extents; so a monitoring tool should be able process these large areas. There are numerous questions to explore, such as the following three; how many ground points are necessary to invert the model for a larger study? What time of year will give the most accurate results? Could this technique also be used to measure production, i.e. the accumulation of biomass over a year? Had soil moisture and volumetric canopy moisture been sampled for each month the water cloud model could have been inverted for each month. This information would have been used to track changes in moisture content over each month. Since this VCM is related to biomass, it may have been possible to relate the trend in VCM over time to production. The water cloud model presented here was restricted to grass dominated areas. Could it be expanded

to areas with significant shrub or forb content? The possibility of using VCM to add in fire risk assessment is another avenue to explore. It is likely that the volumetric canopy maps could be adapted to measure LFMC, an important parameter in fire models.

Soil moisture models require a measure of surface roughness; this type of data was not collected during this study. Had it been collected then multiple methods of estimated soil moisture could have been compared for the GNP.

Continuing this investigation and addressing these questions would require more field data rather than the development of new analytical techniques.

The question of the plant diversity is not fully addressed. What do the high entropy areas identified in this research represent in the ecosystem? Are they areas of high biodiversity, or the signs of an invasive species? The same questions can be asked for the low entropy areas. Further research into those questions also requires more time in the field to understand what the higher entropy areas flagged in the map truly represent. Again, this question can be answered through additional field data.

This research demonstrates that useful biophysical parameters can be derived from the RADARSAT-2 dual polarimetric SAR imagery in a dry mixed grass dominated area. The Delta Index has not been tested in all the plant communities in park so its full applicability is unknown. Thoma et al. (2006) applied their model in semi-arid grassland with considerable more gravel content than the environment of the GNP. The model does work in both types of environments and is likely applicable over more areas.

The derived parameters include green grass biomass, canopy moisture, and soil moisture and plant form diversity. The main research questions for further research is how applicable are the techniques to different types of terrain and plant form composition.

REFERENCES

Atema, E., and Ulaby, F., 1978. Vegetation modeled as a water cloud, *Radio Science*, 13(2): 357-364

Butterfield, H., and Malmstrom, C., 2009. The effects on phenology on indirect measures of aboveground biomass in annual grasses, *International Journal of Remote Sensing*, 30(12): 3133-3146

Chander, G., Markham, B., and Barsi, J., 2007. Revised Landsat 5 Thematic Mapper Radiometric Calibration, *IEEE Geoscience and Remote Sensing Letters*, 2007(July): 1 - 10

Chen, C., Quilang, E., Alosnos, E., and Finnigan, J., 2011. Rice area mapping, yield, and production forecast for the province of Nueva Ecija using RADARSAT imagery, *Canadian Journal of Remote Sensing*, 37(1): 1-16

Chust, G., Ducrot, D., and Pretus, J., 2004. Land cover discrimination Potential of radar multitemporal series and optical multispectral images in a Mediterranean cultural landscape, *International Journal of Remote Sensing*, 25(17): 3513 - 3528

Crist, E., and Cicone, R., 1984. A Physically-Based Transformation of Thematic Mapper Data – The TM Tasseled Cap, *IEEE Transactions on Geoscience and Remote Sensing*, 22(2): 256-263

Critchley, C., Adamson, H., McLean, B., and Davies, O., 2008. Vegetation dynamics and livestock performance in system-scale studies of sheep and cattle grazing on degraded upland wet heath, *Agriculture, Ecosystems and Environment*, 128(2008): 59-61

Dabrowska-Zielinska, K., Inoue, Y., Kowalik, W., and Gruszczynska, M., 2007. Inferring the effect of plant and soil variables on C- and L-band SAR backscatter over agricultural fields, based on model analysis, *Advances in Space Research*, 39(1): 139-148

Dasgupta, S., Qu, J., Hao, X., and Bhoi, S., 2007. Evaluating remotely sensed live fuel moisture estimations for fire behavior predictions in Georgia, USA, *Remote Sensing of Environmen*t, 108(2): 138-150

Debinski, D., Kindscher, K., and Jakubauskas, M., 1999. A remote sensing and GIS-based model of habitats and biodiversity in the Greater Yellowstone Ecosystem, *International Journal of Remote Sensing*, 20(17): 3281- 3291

Duro, D., Coops, N., Wulder, M., and Han, T., 2007. Development of a large area biodiversity monitoring system driven by remote sensing, *Progress in Physical Geography*, 31(3): 235-260

ESA. 2009. www.esa.int/Our_Activities/Observing_the_Earth/ESA_Member_States_approve_full_ and _open_Sentinel_data_policy_principles

Evans, T., Costa, M., Telmer, K., and Silva, T., 2010. Using ALOS/PALSAR and RADARSAT-2 to Map Land Cover and Seasonal Inundation in the Brazilian Pantanal, *IEEE Journal of Selected Topics in Applied Earth Observations and Remote Sensing*, 3(4): 560-575

Fensholt, R., Langanke, T., Rasmussen, K., Reenberg, A., Prince, S., Tucker, C., Scholes, R., Le, Q., Bondeau, A., Eastman, Epstein, H., Gaughan, A., Hellden, U., Mbow, C., Olsson, L., Paruelo, J., Schweitzer, C., Seaquist, J., and Wessels, K., 2012. Greenness in semi-arid areas across the globe 1981–2007 — an Earth Observing Satellite based analysis of trends and drivers, *Remote Sensing of Environment*, 121(June 2012): 144-158

Franklin, S., 2010. Remote Sensing for Biodiversity and Wildlife Management: Synthesis and Applications, McGraw-Hill

Fujisada, H., Bailey, G., Kelly, G., Hara, S., and Abrams, M., 2005. ASTER DEM Performance, *IEEE Transactions on Geoscience and Remote Sensing*, 43(12): 2707-2714

Gao, S., Niu, Z., Huang, N., and Hou, X., 2013. Estimating the Leaf Area Index, height and biomass of maize using HJ-1 and RADARSAT-2, *International Journal of Applied Earth Observation and GeoInformation,* 24: 1-8

Graham, A., and Harris, R., 2002. Estimating crop and waveband specific water cloud model parameters using a theoretical backscatter model, *International Journal of Remote Sensing,* 23(23): 5129-5133

Graham, A., and Harris, R., 2003. Extracting biophysical parameters from remotely sensed radar data: a review of the water cloud model, *Progress in Physical Geography*, 27(2): 217-229

Griffiths, G., and Lee, J., 2000. Landscape pattern and species richness; regional scale analysis from remote sensing, *International Journal of Remote Sensing*, 21(13): 2685 – 2704

Hawkins, B., Field, R., Cornell, H., and Currie, D., 2003. Energy, water, and broad-scale geographic patterns of species richness, *Ecology*, 84(12): 3105-3117

He, Y., and Guo, X., 2006a. Studying mixed grassland ecosystems I: suitable hyperspectral vegetation indices, *Canadian Journal of Remote Sensing*, 32(2): 98-107

He, Y., and Guo, X., 2006b. Leaf Area Index Estimation Using Remotely Sensed Data for Grasslands National Park, *Prairie Perspectives: Geographical Essays*, 9(1): 105-117

He, Y., Guo, X., and Wilmshurst, J., 2009. Reflectance measures of grassland biophysical structure, *International Journal of Remote Sensing*, 30(10): 2509 - 2521

Hill, M., Donald, G., and Vickery, P., 1999. Relating Radar Backscatter to Biophysical Properties of Temperate Perennial Grassland, *Remote Sensing of Environment*, 67(1): 15-31

Hill, M., Ticehurst, C., Lee, J., Grunes, M., Donald, G., and Henry, D., 2005. Integration of optical and radar classification for mapping pasture types in Western Australia, *IEEE Transactions on Geoscience and Remote Sensing*, 43(7): 1665-1681

Hinse, M., Gwyn, Q., and Bonn, F., 1988. Radiometric Correction of C-Band Imagery for Topographic Effects in Regions of Moderate Relief, *IEEE Transactions on Geoscience and Remote Sensing*, 26(2): 122-132

Loveland, T., Reed, B., Brown, J., Ohlen, D., Zhu, Z., Yang, L., and Merchant, J., 1998. Development of a Global Land Cover Characteristics Database and IGBP DISCover from 1-km AVHRR Data, *International Journal of Remote Sensing,* 21(6-7): 1303-1330

Jensen, J., 2007. Remote Sensing of the Environment: An Earth Resource Perspective, Pearson Prentice Hall

McDermid, G., Franklin, S., and LeDrew, E., 2005. Remote sensing for large-area habitat mapping, *Progress in Physical Geography*, 29(4): 449-474

McNairn, H., and Brisco, B., 2004. The application of C-band polarimetric SAR for agriculture : a review, *Canadian Journal of Remote Sensing*, 30(3): 525-542

McNairn, H., Champagne, C., Shang, J., Holmstrom, D., and Reichert, G., 2009. Integration of optical and Synthetic Aperture Radar (SAR) imagery for delivering operational annual crop inventories, *ISPRS Journal of Photogrammetry and Remote Sensing*, 64(5): 434-449

Miller, H., Sexton, N., Koontz, L., Loomis, S., and Hermans, C., 2011. The Users, Uses, and Value of Landsat and Other Moderate-Resolution Satellite Imagery in the United States - Executive Report, Open-File Report 2011-1031, U.S. Department of the Interior, and the U.S. Geological Survey, http://pubs.usgs.gov/of/2011/1031/pdf/OF11-1031.pdf

Moran, M., Hymer, D., Qi, J., and Sano, E., 2000. Soil moisture evaluation using multi-temporal synthetic aperture radar (SAR) in semiarid rangeland, *Agricultural and Forest Meteorology*, 105(1): 69-80

Natali, S., Pellegrini, L., Rossi, G., Giordano, L., Iannetta, M., Schino, G., Marini, A., and Nabil, G., 2009. Estimating Soil Moisture Using Optical and Radar Satellite Remote Sensing Data in *Desertification and Risk Analysis Using High and Medium Resolution Satellite Data* [Springer Netherlands]: 105–116

Oh, Y., 2004. Quantitative Retrieval of Soil Moisture Content and Surface Roughness From Multipolarized Radar Observations of Bare Soil Surfaces, *IEEE Transactions on Geoscience and Remote Sensing*, 42(3): 596-601

Parks Canada, 2010. Grassland's National Park of Canada: Management Plan

Peake, W., and Oliver, T., 1971. Response of Terrestrial Surfaces at Microwave Frequencies, Airforce Avionics Lab Report #TR-70-301, Columbus: Ohio State University

Peterson, G., Allen, C., and Hollin, C., 1998. Ecological Resilience, Biodiversity, and Scale, *Ecosystems,* 1: 6-18

Price, K., Guo, X., and Stiles, J., 2002. Comparison of Landsat TM and ERS-2 SAR data for discriminating among grassland types and treatments in eastern Kansas, *Computers and Electronics in Agriculture*, 37(1-3): 157-171

Porcello, L., Massey, N., Innes, R., and Marks, J., 1976. Speckle reduction in synthetic-aperture radars, Journal of Optics Society of America 66: 1305-1311

Seaquist, J., 2003. A remote sensing-based primary production model for grassland biomes, *Ecological Modelling,* 169(1): 131-155

Shang, J., McNairn, H., Champagne, C., and Jiao, X., 2008. Contribution of Multi-Frequency, Multi-Sensor, and Multi-Temporal Radar Data to Operational Annual Crop Mapping, *Geoscience and Remote Sensing Symposium, 2008. IGARSS 2008. IEEE International :* 3(7-11 July 2008)**:** III - 378 - III - 381

Shannon, C., 1948. A mathematical theory of communication, *The Bell System Technical Journal*, 27, 379-423 and 623-656

Simpson, E., 1949. Measurement of diversity, *Nature*, 163: 688

Svoray, T., and Shoshany, M., 2002. SAR-based estimation of areal aboveground biomass (AAB) of herbaceous vegetation in the semi-arid zone: a modification of the water-cloud model, *International Journal of Remote Sensing*, 23(19): 4089-4100

Svoray, T., and Shoshany, M., 2003. Herbaceous Biomass Retrieval in Habitats of Complex Composition: A Model Merging SAR Images With Unmixed Landsat TM Data, *IEEE Transaction on Geoscience and Remote Sensing*, 41(7): 1592-1601

Tilman, D., and Downing, J., 1994. Biodiversity and stability in grasslands, *Nature (London)*, 367: 363–365

Thoma, D., Moran, M., Bryant, R., Rahman, M., Holifield-Collins, C., Skirvin, S., Sano, E., and Slocum, K., 2006. Comparison of four models to determine surface soil moisture from C-band radar imagery in a sparsely vegetated semiarid landscape, *Water Resources Research* 42(1): 1-12

Tucker, C., and Sellers, P., 1986. Satellite remote sensing of primary production, *International Journal of Remote Sensing*, 7(11): 1395 – 1416

Van Der Velde, R., and Su, Z., 2009. Dynamics in land-surface conditions on the Tibetan Plateau observed by Advanced Synthetic Aperture Radar (ASAR), *Hydrological Sciences Journal*, 54(6): 1079-1093

Wang, K., Franklin, S., Guo, X., He, Y., and McDermid, G., 2009. Problems in remote sensing of landscapes and habitats**,** *Progress in Physical Geography,* 33(6): 747-768

Whittaker, R., 1972. Evolution and Measurement of Species Diversity, *Taxon*, 21(2-3): 213-251

Wunderle, A., Franklin, S., and Guo, X., 2007. Regenerating boreal forest structure estimation using SPOT5 pansharpened imagery, *International Journal of Remote Sensing*, 28(19): 4351-4364

Yonezawa, C., Negishi, M., Azuma, K., Watanabe, M., Ishitsuka, N., Ogawa, S., and Saito, G., 2012. Growth Monitoring and Classification of Rice Field Using Multitemporal RADARSAT-2 Fully Polarimetric Data, *International Journal of Remote Sensing*, 33(18): 5696-5711

Zhang, C., Guo, X., Wilmhurst, J., and Sissons, R., 2006. Application of RADARSAT imagery to grassland heterogeneity assessment, *Canadian Journal of Remote Sensing*, 32(4): 281-287

Appendix A

Figure i Quadrant for Above Ground Biomass Removal.

Figure ii LiCor LAI 2000.

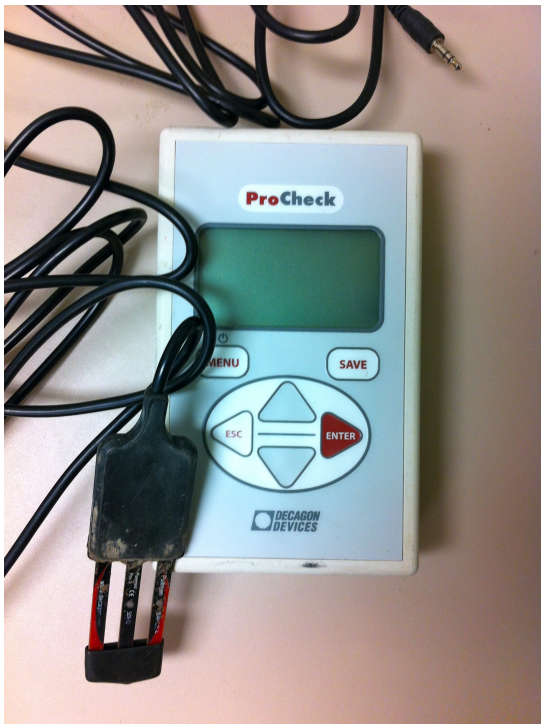

Figure iii ProCheck Soil Moisture Probe.

Figure iv ASD Spectroradiometer.